Durham E-Theses

The suitability of polymerised microemulsions as stationary phases for capillary electrochromatography

Flook, Kelly Joanne

How to cite:

Use policy

The Suitability Of Polymerised Microemulsions As

Stationary Phases For Capillary Electrochromatography

A thesis submitted to the University of Durham in accordance with the

regulations governing the award of Doctor of Philosophy

Kelly Joanne Flook

Department of Chemistry
University of Durham
Durham

1 0 NOV 2003

March 2003

Abstract

The Suitability Of Polymerised Microemulsions As Stationary Phases For Capillary Electrochromatography

Kelly Flook

Submitted for Ph.D. March 2003

Capillary electrochromatography (CEC) is an analytical separation technique, coupling the electroosmotic flow principles of capillary electrophoresis (CE) with the stationary phase separation principles of high performance liquid chromatography (HPLC). The development of this technique has been slowed due to technical problems with packing capillary columns. Alteration of the stationary phase to a solid monolithic support enables ease of filling and reduces bubble formation. Polymerisation of bicontinuous microemulsions can yield porous structures that are potentially suitable for use as a stationary phase for this technique. Polymerising bicontinuous microemulsions with different compositions produces monoliths of varying pore sizes. The microemulsions consist of a hydrophobic phase and an aqueous phase. The hydrophobic phase is typically methyl or butyl methacrylate, and a cross-linker, ethylene glycol dimethacrylate. The aqueous phase consists of water and a surfactant, typically sodium dodecyl sulfate. A short chain alcohol (C3-C5) is added as a porogen which also acts as a co-surfactant to aid with the stabilisation of the microemulsion. AMPS (2-acrylamido-2-methyl-1-propane sulfonic acid), added to the aqueous phase provides a charge along the polymer backbone essential for electroosmotic flow mechanism in electrochromatography. SEM analysis shows that polymerisation in-situ yields a structure with a porous topography. Materials prepared were assessed for suitability with a variety of microemulsion compositions.

Declaration

The material contained within this thesis has not previously been submitted for a degree at the University of Durham or any other University. The author has conducted the research reported within this thesis unless indicated otherwise.

Kelly Joanne Flook
March 2003

There is a theory which states that if ever anybody discovers exactly what the Universe is for and why it is here, it will instantly disappear and be replaced by something even more bizarre and inexplicable. There is another theory which states that this has already happened.

Douglas Adams

Acknowledgments

AIBN   α,α'-azobis isobutyronitrile

AMPS   2-acrylamido-2-methyl-1-propane sulfonic acid

APS   Ammonium persulfate

AUDMAB   (acryloyloxy)undecyltrimethylammonium bromide

BMA   Butyl methacrylate

BPPGSE   Bipolar pulsed field-gradient spin echo

BSE   Backscattered electrons

CEC   Capillary Electrochromatography

c.m.c.   Critical Micelle Concentration

CZE   Capillary Zone Electrophoresis

DEAEMA   2-(Diethylamino) ethyl methacrylate

DTAB   Dodecyltrimethylammonium bromide

DDAB   Didecyldimethylammonium bromide

DOSY   Diffusion-ordered spectroscopy

DVB   Divinylbenzene

EGDMA   Ethyleneglycol dimethacrylate

EOF   Electroosmotic Flow

ESEM   Environmental scanning electron microscopy

HETP   Height Equivalent to one Theoretical Plate

HEMA   2-hydroxyethyl methacrylate

Abbreviations

HPLC	High Performance Liquid Chromatography
MEKC	Micellar ElectroKinetic Chromatography
MeCN	Acetonitrile
MMA	Methyl methacrylate
Na11-EAAU	Sodium 11(*N*-ethylacrylamido)undecanoate
NMR	Nuclear magnetic resonance
ODS	Octadodecyl silane
o/w	Oil-in-water
PFG	Pulsed field gradient
PMMA	Poly(methyl methacrylate)
SE	Secondary electrons
SEM	Scanning electron microscopy
SDS	Sodium Dodecyl Sulfate
TEM	Transmission electron microscopy
TEOS	Tetraethoxysilane
THF	Tetrahydrofuran
TMEDA	Tertramethylethylenediamine
VP	4-vinylpyridine
w/o	Water-in-oil

Table of Contents

Table of Contents

Table of Contents

List of Figures

List of Figures

List of Tables

Liquid Phase Separation

Techniques

1 Liquid Phase Separation Techniques

1.1 Introduction

Analytical separation techniques are continuously being developed to achieve improved performances such as greater efficiency, shorter analysis times and enhanced selectivity. The importance of these techniques is heightened by the growing number of substances requiring analysis, especially of biological importance. Three analytical techniques which have been developed over the years are High Performance Liquid Chromatography (HLPC), Capillary Electrophoresis (CE) and Capillary Electrochromatography (CEC). They have been applied to a range of areas and thousands of instruments are now in use for the analysis of a wide variety pharmaceuticals, samples of biological importance, forensic samples, agrochemicals and fine chemicals. HPLC is the most commonly used liquid separation technique and is well established in industry. There is much interest worldwide in improving these techniques and expanding their versatility.

1.2 High Performance Liquid Chromatography

Chromatography can be defined as a separation process in which a sample mixture is distributed between two phases.

1.2.1 History

HPLC is capable of resolving a wide range of both neutral and charged analytes. At present hundreds of thousands of HPLC systems are running all over the world, carrying out thousands of different analyses. There has been a huge increase in stationary phase development since the early 1970's. Multiple phases with widely differing chemistries are now available in a range of particle sizes. Furthermore, non-

particulate stationary phases have been developed including monolithic silica [1-5] and polymeric rods [6-9]. Stationary phase development also includes imprinted polymer packing [10]. Recent developments in synthetic column packing are reviewed [11].

1.2.2 Operation
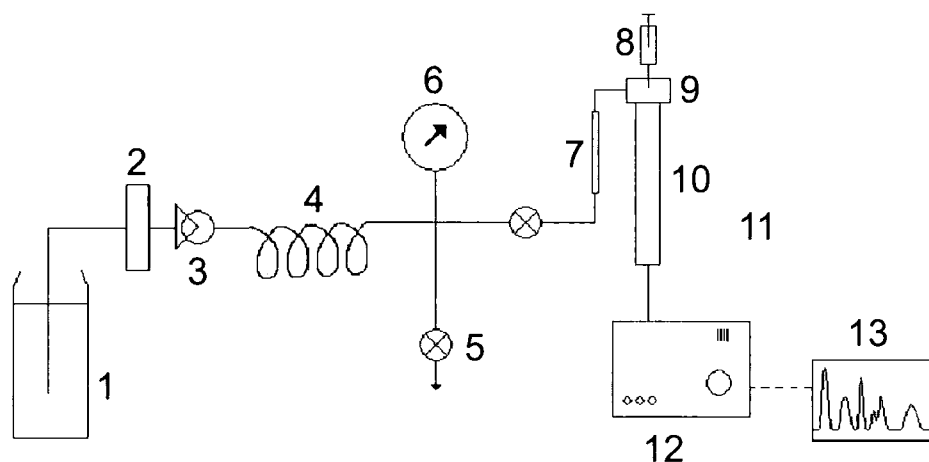
Figure 1.1 **Schematic diagram of an HPLC system. 1 = solvent reservoir; 2 = sintered frit; 3 = high pressure pump; 4 = pulse damper; 5 = drain valve; 6 = manometer; 7 = optional precolumn; 8 = injection syringe; 9 = injection valve; 10 = column; 11 = thermostat oven (optional); 12 = detector; 13 = data acquisition.**

The mobile phase flow in HPLC is provided by a high pressure pump attached to the solvent reservoir, which may consist of a single solvent or multiple solvents in multiple reservoirs. From the reservoir the mobile phase is pumped through a sintered frit to filter the solvent prior to entering the oven. The HPLC column may be situated in a thermostatically controlled oven. If this is the case the mobile phase will pass into the oven prior to entering the column. The sample is injected onto the column typically by syringe or an automated injection system into a loop valve. On

elution from the column the sample peaks will pass into a detector, typically a UV detector or mass spectrometer. The data acquisition will be computer controlled.

1.2.3 Separation Principles

A mixture of compounds is separated by partitioning between two phases; a mobile phase and a stationary phase. In the case of HPLC the stationary phase is a solid, porous surface active material or a coating on a non surface active support or column wall. Typically the stationary phase is in the form of small particulates. The phase presence can be expressed by either the distribution coefficient, K:

$$K_x = \frac{c_{stat}}{c_{mob}}$$

Equation 1.1

where c_{stat} is the concentration of compound x in the stationary phase and c_{mob} is the concentration of x in the mobile phase, or the capacity factor, k.

$$k_x = \frac{n_{stat}}{n_{mob}}$$

Equation 1.2

where n_{stat} is the number of moles of x in the stationary phase and n_{mob} is the number of moles of x in the mobile phase.

If the components present have different distribution coefficients, and hence different capacity factors in the chromatographic system, they can be separated. On introduction of the mixture to the column the components will equilibrate between the mobile and stationary phases. As a flow through the column is established and fresh eluent is introduced, the sample molecules in the mobile phase will be partly adsorbed by the stationary phase and those already adsorbed will move into the mobile phase; a new equilibrium is reached. On repeating this process many times the individual components with different distribution coefficients will eventually

become separated. Where a component has a preference for the mobile phase it will migrate through the column more rapidly than one with a higher affinity for the stationary phase. The capacity factor for individual components can be calculated from the experimental data using the retention time (time taken from injection to elution from the column), t_R and the retention of an unretained marker, t_0.

$$k = \frac{t_R - t_0}{t_0}$$

Equation 1.3

1.2.4 Column Efficiency

The distance along the column where the new balance is found represents a *theoretical plate* or *plate height, H.* The longer the column the more theoretical plates it contains and the better the separation will be. The column efficiency of each separation can be expressed as the number of theoretical plates, N (plate number) or the HETP, height equivalent to one theoretical plate (also known as plate height). Both the plate height and the plate number can be calculated using the standard deviation, σ, of the peak in time, length, or volume and the length, L of the column in metres or centimetres.

$$N = (L/\sigma)^2$$

Equation 1.4

where the population standard deviation is defined as the square root of the sample population variance, the amount of dispersion in the data where $\overline{x} - x_i$ is the difference between the value and the mean and n is the number of terms.

$$\sigma = \sqrt{\frac{\sum_{i-n}^{n}(\overline{x} - x_i)^2}{n-1}}$$

Equation 1.5

As the standard deviation is dependent on the peak width the plate number can be calculated experimentally using the peak retention time and the width of the peak at half its height, $w_{1/2}$.

$$N = 5.54(t_R / w_{1/2})^2$$

Equation 1.6

$$H = \sigma^2 / L$$

Equation 1.7

The narrower the peak or the lower the standard deviation of the peak in question the higher the number of theoretical plates there are for that column. It follows that as the height equivalent to one theoretical plate is inversely proportional to the number of theoretical plates then the better the column, the lower the HETP.

It should also be noted that in order to compare column efficiencies directly, calculations should be carried out on the same analytes.

The typical way to assess the efficiency of a column is by generating a Van Deemter curve. This assesses the effect of flow velocity, v, on efficiency. Equation 1.8 shows this relationship where A is the eddy diffusion and flow distribution component (a function of packing quality), B is the longitudinal diffusion and C is the mass transfer component.

$$H = Av^{0.33} + \frac{B}{v} + Cv$$

Equation 1.8

The shape of the plot of H against v is shown in Figure 1.2.

A main indication of poor column performance is the issue of band broadening. There are many causes of this and it is important that these are kept to a minimum so the number of theoretical plates is high.

$$H = A + B/v + Cv$$
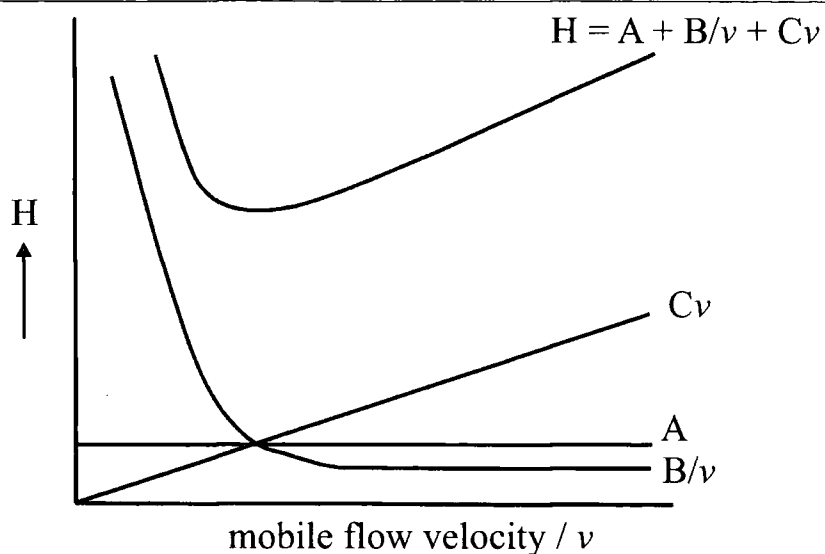
Figure 1.2   A general plot of the van Deemter equation showing the effects of A, B, and C on H.

1.2.4.1   Eddy Diffusion

The column is packed with small stationary phase particles. The mobile phase passes through and transports the sample molecules with it. Some molecules are 'fortunate' and leave the column before most of the others, after having travelled by chance in roughly a straight line through the chromatographic bed. Other molecules leave later having undergone several diversions on the way.
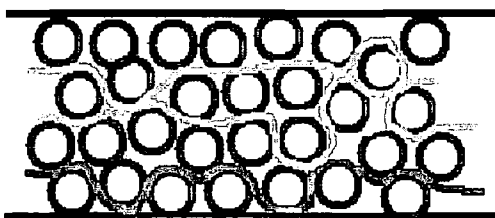
Figure 1.3   Schematic representation of eddy diffusion through particulate packing material.

1.2.4.2   Flow Distribution

In pumped systems the mobile phase passes in a laminar flow between the stationary phase particles (Figure 1.4). The flow is faster in the centre of the channel than near the particle. This effect is reduced by the use of an electroosmotically driven flow system.

Using particles with a narrow size distribution can reduce effects of eddy diffusion and flow distribution. The ratio between the largest and smallest particle diameters should not exceed 2.

The band broadening due to eddy diffusion and flow distribution is little affected by the mobile phase velocity.
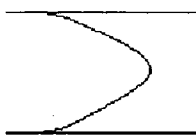
Figure 1.4   Laminar flow profile in pumped systems

1.2.4.3   Sample diffusion in the mobile phase.

Sample molecules spread out in the solvent without any external influence (Figure 1.5). This is an important effect in gas chromatography yet can often be ignored in liquid chromatography especially when particle diameters exceed 30μm. Longitudinal diffusion has a disadvantageous effect on plate height if there is a combination of particle diameters less than 10μm, a low mobile phase velocity and a relatively large sample diffusion coefficient.

The mobile phase flow velocity should also be chosen so that longitudinal diffusion has no adverse effect. This occurs when $v > 2D_m/d_p$, where v is the linear flow velocity of the mobile phase, D_m is the diffusion coefficient of the sample in the mobile phase and d_p is the particle diameter.
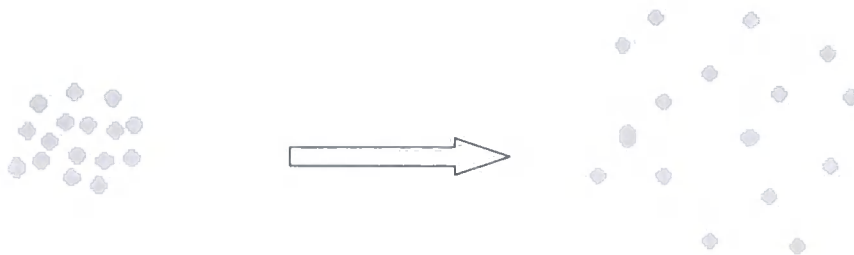
Figure 1.5   Sample diffusion in the mobile phase.

1.2.4.4   Mass transfer between mobile, 'stagnant mobile', and stationary phases

Within a stationary phase particle there are both narrow and wide pores, some pass straight through the whole particle and others are closed off (Figure 1.6). The pores are filled with stagnant mobile phase. A sample molecule entering a pore ceases to be transported by the solvent flux and changes its position by means of diffusion only. Two possibilities present themselves:

(a) The molecule diffuses back in to the mobile phase flux. This process takes time and the molecules that have not been retained in pores have moved further down the column. This results in band broadening. The shorter the pores the smaller the resulting band broadening. Also, the diffusion rate of the sample molecules in a solvent is larger in a lower viscosity medium.

(b) The molecule interacts with the stationary phase itself and is adsorbed. It remains 'stuck' for a while to the stationary phase and then passes on once more. Again this mass transfer takes time.

In both cases band broadening increases with increasing mobile phase velocity. The sample molecules remaining in the moving solvent are further removed from those trapped in the stagnant pools of mobile phase.
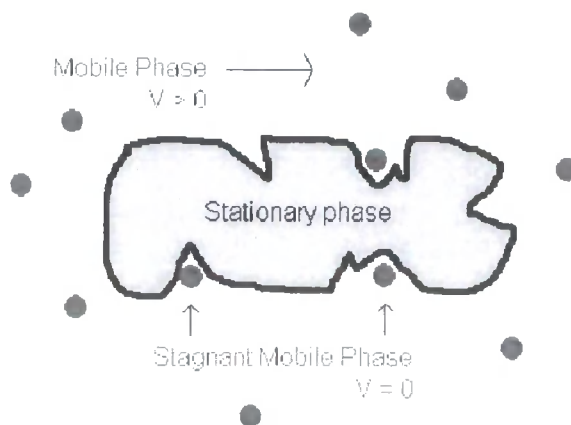
Figure 1.6 Mass transfer between mobile, 'stagnant mobile' and stationary phases.

Plate numbers of popular conventional HPLC columns have been around 10,000-30,000 plates per column for the last few decades.

1.2.5 Limitations

The correct storage of columns is vital to ensure their longevity. Due to the nature of the stationary phase the columns should be stored sealed containing a suitable solvent to prevent the material drying out. Upon drying the stationary phase packing is likely to crack, producing gaps along the column length which are detrimental to the separation.

HPLC analysis, along with all analytical techniques, is subject to detection limits dependent on the detection system used. Where separations are achievable with high efficiencies the detection limits will be much lower. One should always strive to develop methods to increase efficiency without compromising the resolution of the resulting separation. New column technologies are being developed to improve column efficiency and hence improve separation efficiencies.

1.3 Capillary Electrophoresis

1.3.1 History

Electrophoresis, as a separation technique, was introduced by Arne Tiselius in 1937 [12] who was awarded a Nobel Prize in 1948 "for his research on electrophoresis and adsorption analysis, especially for his discoveries concerning the complex nature of the serum proteins". 1967 saw initial work on open tube electrophoresis by Hjertén [13] who rotated the millimetre-bore capillaries to minimise convection effects. As narrower bore capillaries became available the rate of development of the technique increased. The number of publications on capillary electrophoresis rose dramatically in a few years, from about 80 in 1989 to about 1000 in 1994 and the increased interest can be seen from Figure 1.7. Even though CE is a much developed technique widely used in the pharmaceutical industry, sales of instruments are still much lower than those of high performance liquid chromatography (HPLC).
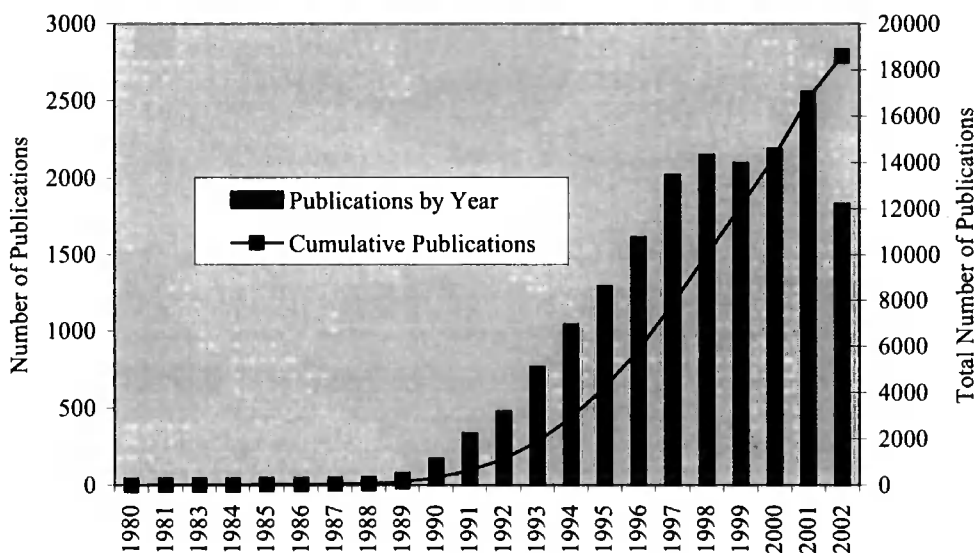
Figure 1.7 Records from Scifinder show an increase in capillary electrophoresis research through the early 1990s.

The reason for this is probably due to the number of established methods already carried out with HPLC, transferring these methods to CE takes time and resources. CE methods principally involve the separation of charged species that are irresolvable by HPLC.

There has been a wide range of HPLC stationary phases available for several years allowing the technique to be tailored to specific separations to maximum efficiency with little effort. The recent history of the development of CE is reviewed by Issaq [14].

1.3.2 Operation
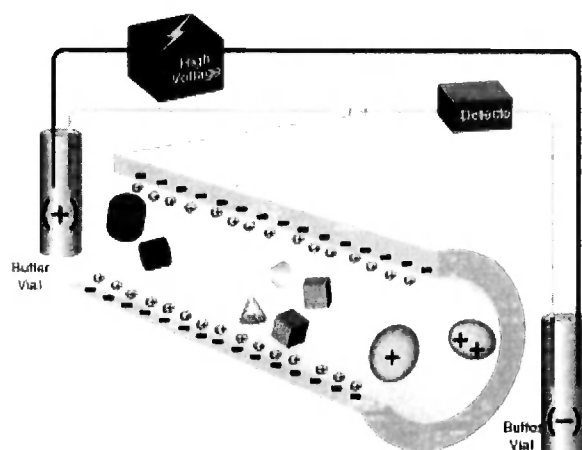
Figure 1.8 Schematic of capillary electrophoresis operation and separation.

Capillary electrophoresis (CE) employs coated fused silica tubing in which the electrophoretic separation occurs. It utilises very high electric field strengths, often higher than 500V/cm. Detection is on-capillary via an optical detection window in line with typically a single wavelength or diode array UV detector. The ends of the capillary are placed in the buffer reservoirs which act as the mobile phase. A third reservoir contains the analytes, often dissolved in buffer solution. The sample is introduced by placing the inlet of the capillary into this reservoir and either an electric field is applied causing electrophoretic migration of the charged species (electrokinetic injection) or a pressure difference is created. This was traditionally

achieved by elevating the inlet reservoir above the outlet reservoir. Newer systems allow pressurisation of either one or both reservoirs in preparation for separation.

1.3.3 Separation Principles

One fundamental process that drives CE is electroosmosis. This is a consequence of the surface charge on the capillary wall. The silanol groups of the fused silica are ionisable in contact with the buffer solution contained within the capillary. The isoelectric point (pI) of fused silica is about 1.5 and can be controlled mainly by the pH of the buffer. The electroosmotic flow, μ_{eo}, is proportional to the applied electric field, E and defined by Equation 1.9 where $\in$ is the dielectric constant, η is the viscosity of the buffer and ζ is the zeta potential measured at the shear plane close to the liquid-solid interface.

$$\mu_{eo} = \frac{\in \zeta}{4\pi\eta} E$$

Equation 1.9
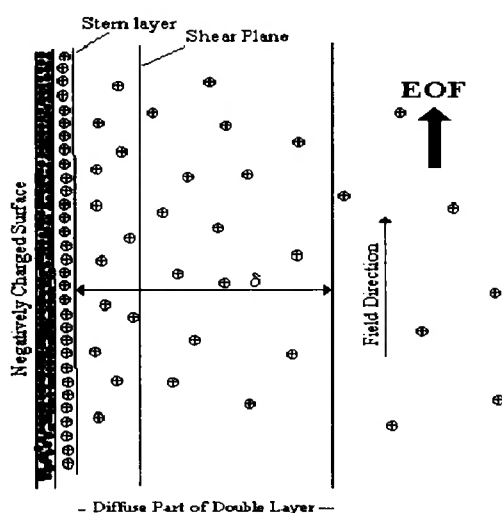
Figure 1.9   The electrical double layer.

The negatively charged wall attracts the positively charged ions from the buffer creating an electrical double layer. Upon application of a voltage across the capillary the cations in the diffuse layer migrate towards the negative electrode, carrying water

with them. The result is a net migration towards the cathode. The EOF increases at higher pH for a constant buffer concentration.

The zeta potential is inversely proportional to the charge per unit surface area (the number of valence electrons) and the square root concentration of the electrolyte. This means that increasing the buffer concentration decreases the EOF.

In the case of CE the EOF is measured simply by introducing a neutral species and measuring the time it takes to reach the detector.

1.3.4 Electroosmosis

In an electric field charged species will migrate depending on their charge and mass. This is known as their electrophoretic mobility (μ_{ep}) and is dependent on the field applied. The applied field is calculated by dividing the applied volts, V by the total column length, L_t.

$$\mu_{ep} = \frac{\upsilon_{ep}}{E} = \frac{L_d / t_m}{V / L_t}$$

Equation 1.10

As velocities (υ) are measured terms they can be calculated by dividing the migration time (t_m) by the length of time taken to get to the detector (L_d). Apparent mobilities are then determined by dividing the velocity (υ_{ep}) by the field strength, E. To calculate the actual mobility, electrophoretic effects must be accounted for.

Imagine the separation of a mixture containing a zwitter ion, such as a peptide, at different pHs. At low pH the peptide will be positively charged and the EOF is low, thus the electrophoretic migration is towards the cathode. The peptide will be detected prior to a neutral EOF marker. At high pH EOF is large and the peptide is negatively charged. Even though the electrophoretic migration is towards the anode

14

the EOF is overwhelming and the net migration is towards the cathode, the peptide migrating behind the neutral marker.

1.3.5 Limitations

Due to the mode of separation mixtures containing more than one neutral molecule cannot be analysed effectively due to the lack of charge difference. The addition of surfactants (micellar electrokinetic chromatography, MEKC) may be employed to separate electrically similar or neutral analytes with different partition coefficients in and out of the micelle. The migration times of electrically neutral molecules are between t_0 and t_{mc}, the migration time of the micelle. Separation of neutral species is only by partitioning in and out of the micelle. Varying the nature of the surfactant in the micelle can dramatically change selectivity.

1.4 Capillary Electrochromatography

1.4.1 A hybrid technique

Capillary electrochromatography is an analytical separation technique combining the separation principles of HPLC and the electroosmotically driven mobile phase flow of capillary electrophoresis. Over the past few years it has been the subject of general reviews by several authors [15-18].

1.4.2 History

The advantages of combining electroosmotic flow (EOF) with thin layer and column chromatography were recognised as early as 1974 [19] but the first electro-chromatographic separations were not demonstrated until the early 1980's [20]. Technical difficulties slowed development, mainly due to the availability of packing materials that are easily packed into μm scale capillaries and bubble formation at the frits required to hold the packing material in place. Most groups have been

implementing HPLC particle technology in CEC [21-33], which is difficult on the capillary scale. CEC has been used for a variety of separations [34] including chiral separations of amino acids [35], dyes [36] and toxins. In recent years several groups have moved development towards monolithic stationary phases where a solution is polymerised inside the capillary to produce a porous stationary phase through which separation can be carried out. These monolithic columns have also been the subject of several reviews [37-39].
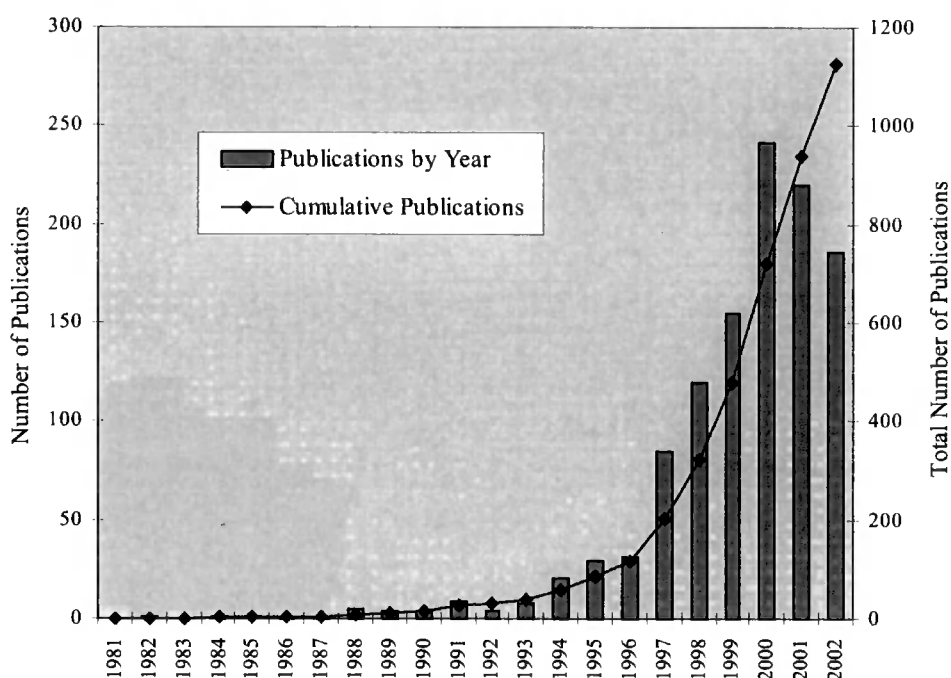
Figure 1.10 Records from Web of Science show an increase in Electro-chromatography with a decline after 2000.

1.4.3 Operation

The operation of the instruments is similar to that of CE described earlier in this chapter. Mobile phase flow is induced by the application of a potential difference across the capillary. Migration of analytes is again caused by the generated EOF and separation of neutral species is by partitioning with the mobile phase. Separation of

charged analytes is a combination of partitioning between the mobile and stationary phases and electromigration.

Until six years ago CEC was performed on modified standard CE equipment. The requirement of vial pressurisation has lead to instruments being manufactured by Hewlett Packard (HP^{3D}CEC), Thermoseparations (Ultra) and Beckman (P/ACE MDQ). These instruments are similar in operation to that of standard CE with the option to regulate the pressure of one or both buffer vials during separation. A review by Steiner describes the development of column technology and the adaptation of commercial CE instruments for electrochromatography [40].

1.4.4 Applications

In the last few years there has been a steady flow of publications describing the use of CEC for the analysis of neutral and ion suppressed pharmaceuticals [41-45] due to its ability to provide highly efficient, rapid analysis with increased peak capacity. CEC has also been employed in the analysis of natural products such as triglycerides and fatty acids and their derivatives. A review of specific applications by Krull [46] covers the analysis of biopolymers such as proteins, nucleic acids, peptides and antibodies.

1.4.5 Monolithic Columns

Columns for CEC have been developed using a variety of procedures to eliminate the need for frit fabrication. Monolithic columns, where the bed is microfabricated in an inorganic material by ablation [47] is one option. Several methods have been employed using modified silica to produce continuous beds [3,18,48-52]. Sintered octadecylsilica columns have been prepared from traditionally packed CEC columns and the retaining frit was then cut off to remove the inhomogeneities [50]. ODS-

modified silica gels [48] and silica particles embedded in a sol-gel column [53] have been used for the separation of enantiomers (amino acids).

Hydrophobic hydrogels have been used for the separation of polyaromatic hydrocarbons and steroids, on beds prepared from acrylamides [49] as well as monoliths based on water soluble monomers [54-56].

Solid monoliths have extensively been prepared from butyl methacrylate and ethyleneglycol dimethacrylate [57-61] for the separation of basic pharmaceuticals [57], polycyclic aromatic hydrocarbons [58] and benzene derivatives [59-61].

Poly(styrene-divinylbenzene) supports have also proven to be suitable for CEC [62-65]. The development of stationary phases has also developed in the area of enanteomeric separations [35,66-69] with a monolithic chiral ligand-exchange phase for the chiral separation of underivatized amino acids [70]. Josic et al. have reviewed the use of monoliths for the separation of proteins and polynucleotides [71].

The analysis of plant extracts has been successfully transferred from HPLC to CEC using monolithic macroporous polyacrylamide columns [72]. Continuous beds have also been used for the analysis of basic pharmaceuticals.

Fused silica tubing with a coating to produce open tubular capillary electrochromatography [73-75], including the use of quaternary ammonium-bearing latex particles, was used as the stationary phase in open tubular and CEC separations in order to combine the separation mechanisms from both capillary electrophoresis and ion-exchange chromatography [76].

1.4.6 Limitations

The analysis of basic analytes is problematic due to the presence of the acidic silanol groups vital for EOF generation. Peak tailing occurs due to the mixed mode of operation. The capillaries available commercially are prepared using traditional

HPLC packing materials. In HPLC analysis basic compounds are incorporated into the packing to minimise interactions with basic analytes. This has been shown also to be a successful technique when applied to CEC [77].

The development of CEC has been slowed due to technical problems associated with packing capillary columns with traditional materials. Packing small diameter silica beads involves the use of very high pressures and an experienced chromatographer to produce columns with a high batch-to-batch reproducibility. As with HPLC it is recommended either to purchase professionally-packed columns or to invest a large amount of time in packing columns in-house. Colón et al.[78] have discussed packing methods for CEC columns, and have identified problems associated with the frits required to hold the packing material in the capillary. These can be formed using a heating filament at 450°C to sinter locally a narrow band of the packing material [79]; this can alter the characteristics of the material, creating a non-homogeneous section through which passage of the mobile phase can lead to bubble formation at the frit-open column boundary.

1.5 References

1. Cabrera, K.; Lubda, D.; Eggenweiler, H. M.; Minakuchi, H. N., K *HRC - J. High Resolut. Chromatog.* **2000**, *23*, 93-99.

2. Nakanishi, K.; Shikata, H.; Ishizuka, N.; Koheiya, N.; Soga, N. *HRC - J. High Resolut. Chromatog.* **2000**, *23*, 106-110.

3. Tanaka, N.; Nagayama, H.; Kobayashi, H.; Ikegami, T.; Hosoya, K.; Ishizuka, N.; Minakuchi, H.; Nakanishi, K.; Cabrera, K.; Lubda, D. *HRC-J. High Resolut. Chromatogr.* **2000**, *23*, 111-116.

4. Ishizuka, N.; Minakuchi, H.; Nakanishi, K.; Hirao, K.; Tanaka, N. *Colloid Surf. A-Physicochem. Eng. Asp.* **2001**, *187*, 273-279.

5. Ishizuka, N.; Kobayashi, H.; Minakuchi, H.; Nakanishi, K.; Hirao, K.; Hosoya, K.; Ikegami, T.; Tanaka, N. *J. Chrom. A* **2002**, 85-96.

6. Yoshizako, K.; Hosoya, K.; Iwakoshi, Y.; Kimata, K.; Tanaka, N. *Anal. Chem.* **1998**, *70*, 386-389.

7. Chirica, G. S.; Remcho, V. T. *Anal. Chem.* **2000**, *72*, 3605-3610.

8. Premstaller, A.; Oberacher, H.; Walcher, W.; Timperio, A. M.; Zolla, L.; Chervet, J.; Cavusoglu, N.; van Dorsselaer, A.; Huber, C. *Anal. Chem.* **2001**, *73*.

9. Janco, M.; Xie, S.; Peterson, D.; Allington, R.; Svec, F.; Frechet, J. *J. Sep. Sci.* **2002**, *25*, 909-916.

10. Baggini, C.; Giraudi, G.; Vanni, A. *Bioseparation* **2001**, *10*, 389-394.

11. Buchmeiser, M. *J. Chrom. A* **2001**, *918*, 233-266.

12. Tiselius, A. *Biochem. J.* **1937**, *31*, 1464-77.

13. Hjerten, S. *Chrom. Rev.* **1967**, *9*, 122-219.

14. Issaq, H. J. *Electrophoresis* **2000**, *21*, 1921-1939.

15. Dittmann, M. M.; Rozing, G. P. *J. Chrom. A* **1996**, *744*, 63-74.

16. Stevenson, R.; Mistry, K.; Krull, I. *American Laboratory* **1988**, *30*, A16.

17. Altria, K. D. *J. Chrom. A* **1999**, *856*, 443-463.

18. Fujimoto, C. *TrAC: Trends Anal. Chem.* **1999**, *18*, 291-301.

19. Pretorius, V.; Hopkins, B. J.; Schieke, J. D. *J. Chrom. A* **1974**, *99*, 23-30.

20. Jorgenson, J. W.; Lukacs, K. D. *J. Chromarog. A* **1981**, *218*, 209-216.

21. Behnke, B.; Grom, E.; Bayer, E. *J. Chromarog. A* **1995**, *716*, 207-13.

22. Boughtflower, R. J.; Underwood, T.; Paterson, C. J. *Chromatographia* **1995**, *40*, 329-335.

23. Dittmann, M. M.; Wienand, K.; Bek, F.; Rozing, G. P. *Lc-Gc* **1995**, *13*, 800-814.

24. Walhagen, K.; Unger, K. K.; Olsson, A. M.; Hearn, M. T. W. *J. Chromarog. A* **1999**, *853*, 263-275.

25. Flanagan, R. J.; Harvey, E. J.; Spencer, E. P. *Forensic Science International* **2001**, *121*, 97-102.

26. McKeown, A. P.; Euerby, M. R.; Lomax, H. *J. Sep. Sci.* **2002**, *25*, 1257-1268.

27. Lumley, B.; Khong, T. M.; Perrett, D. *Chromatographia* **2001**, *54*, 625-628.

28. McKeown, A. P.; Euerby, M. R.; Johnson, C. M.; Koeberle, M.; Lomax, H.; Ritchie, H.; Ross, P. *Chromatographia* **2000**, *52*, 777-786.

29. Walhagen, K.; Unger, K. K.; Hearn, M. T. W. *J. Chromarog. A* **2000**, *894*, 35-43.

30. Walhagen, K.; Unger, K. K.; Hearn, M. T. W. *J. Chromarog. A* **2000**, *893*, 401-409.

31. Gucek, M.; Gaspari, M.; Walhagen, K.; Vreeken, R. J.; Verheij, E. R.; Van der Greef, J. *Rapid Commun. Mass Spec.* **2000**, *14*, 1448-1454.

32.   Hilhorst, M. J.; Somsen, G. W.; De Jong, G. J. *J. Chromarog. A* **2000**, *872*,

315-321.

33.   Walhagen, K.; Unger, K. K.; Hearn, M. T. W. *Anal. Chem.* **2001**, *73*, 4924-

4936.

34.   Altria, K. D. *Journal of Chromatography A* **1999**, *856*, 443-463.

35.   Lammerhofer, M.; Svec, F.; Frechet, J. M. J.; Lindner, W. *J. Microcolumn*

Sep. **2000**, *12*, 597-602.

36.   Lord, G. A.; Gordon, D. B.; Tetler, L. W.; Carr, C. M. *J. Chromarog. A* **1995**,

700, 27-33.

37.   Svec, F.; Peters, E. C.; Sykora, D.; Yu, C.; Frechet, J. M. J. *HRC-J. High*

Resolut. Chromatogr. **2000**, *23*, 3-18.

38.   Svec, F.; Peters, E. C.; Sykora, D.; Frechet, J. M. J. *J. Chromarog. A* **2000**,

887, 3-29.

39.   Pursch, M.; Sander, L. C. *J. Chromarog. A* **2000**, *887*, 313-326.

40.   Steiner, F.; Scherer, B. *J. Chromarog. A* **2000**, *887*, 55-83.

41.   Adam, T.; Kramer, M. *Chromatographia* **1999**, *49*, S35-S40.

42.   Angus, P. D. A.; Victorino, E.; Payne, K. M.; Demarest, C. W.; Catalano, T.;

Stobaugh, J. F. *Electrophoresis* **1998**, *19*, 2073-2082.

43.   Debowski, J. K. *J. Liquid Chromatog. Rel. Tech.* **2002**, *25*, 1875-1917.

44.   Euerby, M. R.; Gilligan, D.; Johnson, C. M.; Roulin, S. C. P.; Myers, P.;

Bartle, K. D. *J. Microcolumn Sep.* **1997**, *9*, 373-387.

45.   Wistuba, D.; Schurig, V. *J. Chromarog. A* **2000**, *875*, 255-276.

46.   Krull, I. S.; Sebag, A.; Stevenson, R. *J. Chromarog. A* **2000**, *887*, 137-163.

47.   Regnier, F. E. *HRC-J. High Resolut. Chromatogr.* **2000**, *23*, 19-26.

48.   Tang, Q.; Lee, M. L. *HRC-J. High Resolut. Chromatogr.* **2000**, *23*, 73-80.

49.   Fujimoto, C.; Fujise, Y.; Matsuzawa, E. *Anal. Chem.* **1996**, *68*, 2753-2757.

50.   Asiaie, R.; Huang, X.; Farnan, D.; Horvath, C. *J. Chromarog. A* **1998**, *806*, 251-263.

51.   Zimina, T. M.; Smith, R. M.; Myers, P. *J. Chromarog. A* **1997**, *758*, 191-197.

52.   Fujimoto, C. *HRC-J. High Resolut. Chromatogr.* **2000**, *23*, 89-92.

53.   Kato, M.; Dulay, M. T.; Bennett, B.; Chen, J.-r.; Zare, R. N. *Electrophoresis* **2000**, *21*, 3145-3151.

54.   Palm, A.; Novotny, M. V. *Anal. Chem.* **1997**, *69*, 4499-4507.

55.   Maruska, A.; Ericson, C.; Vegvari, A.; Hjerten, S. *J.Chromatog. A* **1999**, *837*, 25-33.

56.   Hjerten, S. *Ind. Eng. Chem. Res.* **1999**, *38*, 1205-1214.

57.   Hindocha, D.; Smith, N. W. *Chromatographia* **2002**, *55*, 203-209.

58.   Liao, J. L.; Chen, N.; Ericson, C.; Hjerten, S. *Anal. Chem.* **1996**, *68*, 3468-3472.

59.   Peters, E. C.; Petro, M.; Svec, F.; Frechet, J. M. J. *Anal. Chem.* **1997**, *69*, 3646-3649.

60.   Peters, E. C.; Petro, M.; Svec, F.; Frechet, J. M. J. *Anal. Chem.* **1998**, *70*, 2288-2295.

61.   Peters, E. C.; Petro, M.; Svec, F.; Frechet, J. M. J. *Anal. Chem.* **1998**, *70*, 2296-2302.

62.   Gusev, I.; Huang, X.; Horvath, C. *J. Chromatog. A* **1999**, *855*, 273-290.

63.   Zhang, G. D.; Xu, B. J. *J. Chromatog. A* **2001**, *912*, 335-342.

64.   Xiong, B.; Zhang, L.; Zhang, Y.; Zou, H.; Wang, J. HRC-*J. High Resolut. Chromatogr.* **2000**, *23*, 67-72.

65. Huang, X. A.; Zhang, S.; Schltz, G. A.; Henion, J. *Anal. Chem.* **2002**, *74*, 2336-2344.

66. Haginaka, J. *J. Chromatog. A* **2000**, *875*, 235-254.

67. Lammerhofer, M.; Lindner, W. *J. Chromatog. A* **1998**, *829*, 115-125.

68. Takeuchi, T.; Matsui, J. HRC-*J. High Resolut. Chromatogr.* **2000**, *23*, 44-46.

69. Lammerhofer, M.; Svec, F.; Frechet, J. M. J.; Lindner, W. *Trac-Trends in Anal. Chem.* **2000**, *19*, 676-698.

70. Schmid, M. G.; Grobuschek, N.; Tuscher, C.; Gubitz, G.; Vegvari, A.; Machtejevas, E.; Maruska, A.; Hjerten, S. *Electrophoresis* **2000**, *21*, 3141-3144.

71. Josic, D.; Buchacher, A.; Jungbauer, A. *J. Chromatog. B* **2001**, *752*, 191-205.

72. Kvasnickova, L.; Glatz, Z.; Sterbova, H.; Kahle, V.; Slanina, J.; Musil, P. *J. Chromatog. A* **2001**, *916*, 265-271.

73. Huang, X.; Horvath, C. *J. Chromatog. A* **1997**, *788*, 155-164.

74. Kapnissi, C. P.; Akbay, C.; Schlenoff, J. B.; Warner, I. M. *Anal. Chem.* **2002**, *74*, 2328-2335.

75. Konig, S.; Welsch, T. *J. Chromatog. A* **2000**, *894*, 79-88.

76. Breadmore, M. C.; Boyce, M.; Macka, M.; Avdalovic, N.; Haddad, P. R. *J. Chromatog. A* **2000**, *892*, 303-313.

77. Gillott, N. C.; Barrett, D. A.; Nicholas Shaw, P.; Euerby, M. R.; Johnson, C. M. *Anal. Commun.* **1998**, *35*, 217-220.

78. Colon, L. A.; Maloney, T. D.; Fermier, A. M. *J. Chromatog. A* **2000**, *887*, 43-53.

79. van den Bosch, S. E.; Heemstra, S.; Kraak, J. C.; Poppe, H. *J. Chromatog. A* **1996**, *755*, 165-177.

Colloidal Systems

2 Colloidal Systems

2.1 Introduction

2.1.1 Emulsions

An emulsion is a system of two liquid phases where one phase is dispersed in the other with varying stability. In the usual type of emulsion (macroemulsions), the globules of dispersed liquid are usually between 0.1μm and 10μm in diameter. Microemulsions may have droplet diameters of up to 0.01 μm. The droplet size influences the visual appearance of the emulsion due to an influence on the degree of light scattering. Large particles give a milky-white-opaque appearance whereas smaller droplets give a grey-translucent-transparent appearance.

Emulsions are typically classed as oil-in-water (o/w) or water-in-oil (w/o) depending on which phase is the dispersed phase and which is the dispersing medium.

2.1.2 Emulsion Stability

When an emulsion is prepared by homogenising two liquid phases, separation will occur quickly. To stabilise the prepared emulsion an emulsifying agent or amphiphile is required. Surface-active agents (surfactants) are one type of these. They form an adsorbed film around the droplets to help prevent coagulation and coalescence.

2.2 Surfactants

Surface-active agents (or surfactants) are amphiphilic molecules, *i.e.* they possess hydrophobic and hydrophilic groups. They are used as stabilising (emulsifying) agents in emulsion preparation. Due to the nature of the surfactant molecule it tends to form aggregates in solution with properties that change with concentration. The Debye equation (Equation 2.1) relates the surfactant concentration, c, to the turbidity,

τ, of the system to determine the molecular weights, M, of the aggregates formed above the CMC (critical micelle concentration). K is the optical constant and A_2 is the osmotic pressure. The effect of concentration is shown schematically in Figure 2.1 where a change in the physical properties is observed around the CMC. The osmotic pressure is proportional to the total concentration of micelles and monomers. Above the CMC added surfactant forms micelles and the increase in the total number of 'particles' is small. The turbidity is proportional to the concentration of micelles. Larger aggregates will have a greater scattering intensity and contribute more to the turbidity.

$$\frac{K(c - CMC)}{\tau} = \frac{1}{M} + 2A_2(c - CMC)$$

Equation 2.1
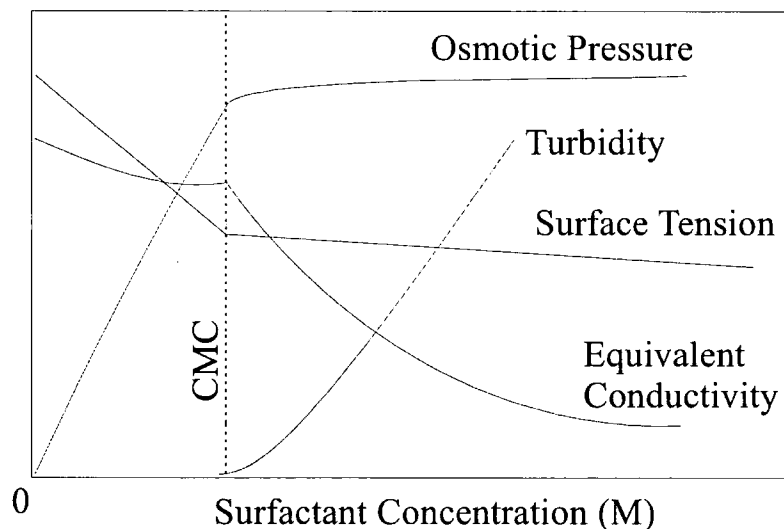
Figure 2.1 The effect of surfactant concentration on osmotic pressure, turbidity, surface tension and conductivity.

2.2.1 Interfacial Tension

Surfactant molecules spontaneously adsorb at the liquid interface; either liquid – air or liquid – liquid. At the interface between two liquids, there is an imbalance of

intermolecular forces. The molecules located in the bulk of the liquid are, on average, subjected to equal forces of attraction in all directions. Those located at the surface (liquid-air interface) or interface (liquid-liquid interface) experience unbalanced attractive forces resulting in a net inward pull. This is represented schematically in Figure 2.2.
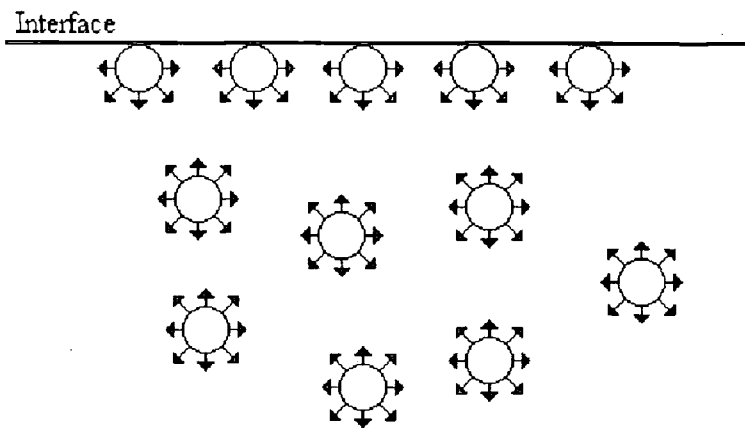
Interface

Figure 2.2   Forces exerted on molecules in bulk solution and near the interface.

Phase A

Interface

Head group

Tail group
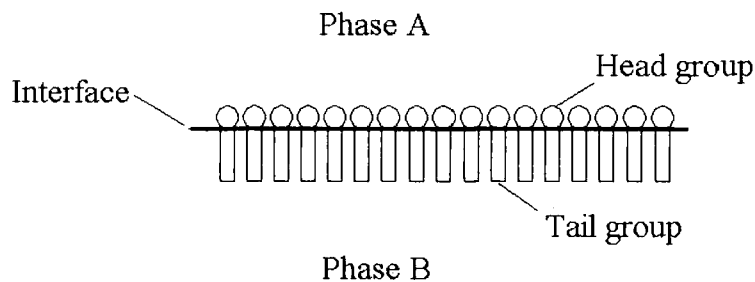
Phase B

Figure 2.3   Surfactant packing at the interface.

When the solubility of the surfactant is low in either of the two phases (aqueous and/or organic) the molecules concentrate at the interface forming a two-dimensional monolayer, Figure 2.3. If the surface area of a liquid is increased, more molecules are at the surface and work must be done. A surface therefore has an excess Gibbs energy, relative to the interior of the liquid. The force required to stretch the surface film of length 1 is proportional to 2l. The proportionality constant, γ is known as the

surface tension. It has SI units of N m^{-1} therefore is the surface energy per unit area, f. The surface pressure, Π is the lowering of surface tension due to the monolayer; the expanding pressure exerted by the monolayer which opposes the normal contracting tension of the 'clean' interface, γ_0. Any spontaneous process results in a lowering of free energy and associated with a lowering of the surface tension.

$$\gamma = \gamma_0 - \Pi$$

Equation 2.2

$$\gamma_{min} = \gamma_{\Pi} = \gamma_0 - \Pi_{max}$$

Equation 2.3

γ_0 and γ are the surface tensions before and after adsorption respectively. If the surfactant molecules are more soluble in either of the two phases, a monolayer is still formed at the interface but it will exchange between the monolayer and the bulk phases. The interfacial tension at the liquid-air interface will never be very small as the surfactant chains will orientate to form an 'organic' layer in direct contact with the air.

The surface pressure will be dependent on concentration. Its maximum concentration will correspond to a maximum chain coverage (Equation 2.3) where γ_H is the hydrocarbon liquid surface tension. The interfacial tension of an oil/water mixture can be very low and possibly zero when the hydrophobic and hydrophilic parts of the surfactant completely balance the interactions between the oil and the water. This happens when the interface is saturated at a particular value of area per surfactant molecule, a*. A precise value of a* can be determined [1]. The surface free energy can be written:

$$f = \gamma_0 A + n_s G_{(a)}$$

Equation 2.4

where A is the total surface area, which is the product of the area per surfactant molecule, a, and the number of surfactant molecules in the layer, n_s and G is the free energy per molecule describing surfactant – surfactant repulsions. The system will adjust its surface concentration to minimise f so that the surface pressure is equal to the surface tension.

In the case of an interface between two phases, the amount of substance adsorbed per unit area of the interface can be described as the surface excess concentration, Γ. The general form of the Gibbs equation (Equation 2.5) can be applied to adsorption processes where the chemical potential of the component, μ of component i is related to its activity (and concentration for dilute systems).

$$d\gamma = -\Sigma \Gamma_i d\mu_i$$

Equation 2.5

where the chemical potential can be expressed in terms of standards potential, μ_i^{ϕ} in relation to the surfactant activity, a.

$$\mu_i = \mu_i^{\phi} + RT \ln a$$

Equation 2.6

In region A, Figure 2.4, as the surfactant concentration increases, as does the surface excess concentration, Γ as surfactant molecules spontaneously adsorb at the surface. Upon adding more surfactant region B is approached. The surface excess remains constant as the interface is 'saturated' by surfactant. However, the surface tension still reduces. At a constant surface excess concentration the area per surfactant molecule can be calculated. As the concentration increases to region C micelles are

formed. The monomer concentration will remain at a constant level dependant on its solubility in the appropriate phases.
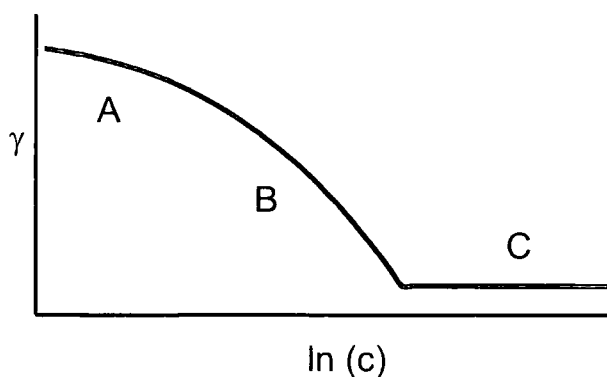
Figure 2.4 The effect of surfactant concentration on surface tension.

2.2.1.1   Electrical double layer repulsion.

When ionic emulsifying agents are used, double layer repulsion may prevent the formation of a close-packed film. This effect can be minimised by using mixed ionic/nonionic surfactants and/or increasing the electrolyte concentration in the aqueous phase to balance the repulsive charges.

2.3 Microemulsions

2.3.1 Initial Development

Becher defines an emulsion as an unstable heterogeneous system in which the diameters of the dispersed droplets exceed 1000 Å [2]. The term 'microemulsion', introduced in 1959 by Schulman, refers to a thermodynamically stable, fluid oil-water-surfactant mixture in which contain tiny ordered oil or water droplets. By staining the oil phase with osmium tetroxide oil droplets can be observed by electron microscopy [3]. This was again defined by Lindman in 1981 as 'a system of water,

oil and amphiphile which is a single optically isotropic and thermodynamically stable liquid solution' [4]. It was Schulman, in 1943, who noticed that the addition of an alcohol, amine, fatty acid or another non-ionised amphiphilic substance to a course emulsion could be used to form an optically transparent, thermodynamically stable solution [5]. He suggested that, upon addition of an amphiphilic species, the dispersed phase then consisted of sub-microscopic micelles having a core of surfactant in water and surface of surfactant ion pairs with the hydrocarbon chains pointing outwards into the dispersed phase. The oil/water interface would contain non-ionised amphiphilic molecules sufficiently separating the surfactant ion pairs to prevent repulsion between them that would normally occur, therefore, increasing the stabilising power of the interface.

2.3.2 Types of Microemulsion

Winsor observed that mixtures containing oil and brine in equivalent amounts which contain small amounts of ionic surfactant and co-surfactant often demix into two or three phases. At low salinity an oil-in-water microemulsion co-exists with an excess oil phase. At high salinity the inverse is observed, a water-in-oil microemulsion co-exists with an excess oil phase. A third phase is also observed where the equilibrium is at an intermediate where the oil and aqueous domains are interdispersed. Klier et al. discuss the properties and applications of different types of microemulsion [6].

2.3.3 Physical Properties

The physical properties of a microemulsion can be identified using a variety of methods such as identification by the naked eye, light scattering, small angle x-ray scattering, nuclear magnetic resonance spectroscopy and microscopy.

2.3.3.1   Light scattering

Macroemulsions, where droplet sizes are in the range of 100-10,000nm, will scatter visible light and will appear white and opaque. As the droplet diameter is decreased to about ¼ wavelength of visible light (ca 1400 Å), white light is not scattered and passes straight through. The microemulsion will then appear translucent or opalescent. At about 100 Å the systems are no longer translucent but transparent.

2.3.3.2   Nuclear Magnetic Resonance

NMR diffusion studies can be used to measure the obstruction effects resulting from systems in various conformations. Initial experiments were carried out by Schulman and work has expanded to the development of pulsed field gradient methods for the investigation of microemulsion structure. In recent years microemulsions have been characterised using NMR [7-11] including their potential use as transdermal drug delivery agents [12].

2.3.3.3   Electron Microscopy

Early methods of microemulsion investigation carried out by Schulman [3] involving the staining of organic materials in the oil phase by exposure to osmium tetroxide vapour enabling one to take a picture of the organic phase. With the development of microscopic techniques, transmission electron microscopy (TEM) is now the most important technique for the visual study of microstructures. It has the ability to produce high resolution images of the captured microstructures. Due to the low operating pressures of TEM being incompatible with the high vapour pressures of the microemulsions, the ability of electrons to induce chemical reactions in organic systems and the lack of contrast between the microstructures and their surroundings various preparation techniques have been developed. Cryo-TEM is the technique of

choice to produce the best images of microemulsion microstructures. The technique is covered well by Bellare et al [13].

2.3.3.4   Conductivity

Ions in an applied electric field will migrate, generating a current. The current generated by a system will be dependent on the resistance of the liquid to which the electric field is applied. As the ions in a system containing an ionic surfactant are 'bound' at the interface and exist in the aqueous fraction their movement in an electric field will be dependent on the total electrolyte concentration, the surface charge density of the microemulsion droplet and its size, among other factors. Lam and Schechter [14] studied the effects of diffusion and electrical conductivity in microemulsions. When the system consists of an aqueous phase dispersed in an oil continuous phase the conductivity of the system will be closer to that of the oil phase. As the oil fraction is decreased and the system inverts to a water continuous state the conductivity will increase. Unlike macroemulsions there is a gradual change in conductivity rather than a sharp change associated with phase inversion. This suggests an intermediate microstructure different to oil in water or water in oil. The preparation of polymer latexes formed from acrylamide containing microemulsions was monitored by conductivity and shows a rapid fall in conductivity as the polymerisation progresses [15].

2.3.4   Microemulsion Formation

In contrast to conventional emulsions, microemulsions have a droplet size below $0.1 \mu m$ and form spontaneously. Spontaneous formation and stability of small droplet sized dispersions is thought to be due to zero interfacial tension. If the surface pressures measured are in excess of the o/w surface tension then a negative interfacial tension will result as there would be energy ($-\gamma_o dA$) available to increase

the interfacial area. Microemulsions may be formed with low surfactant levels and may involve the introduction of an alcohol as a co-surfactant or salt to alter the surface tension, which has been reported to be close to zero. Flexible films can be obtained using an anionic surfactant or an ionic surfactant with the addition of an alcohol or amine as a co-surfactant. As most microemulsions form when the co-surfactant is oil soluble, the co-surfactant distributes itself between the oil phase and the interface. The negative surface tension is not necessarily a result of an increase in surface pressure but a depression of $\gamma_{o/w}$ by the co-surfactant.

The structure of the microemulsion can vary widely with composition and will resemble swollen micelles at small fractions of water-in-oil (w/o) or oil-in-water (o/w). Scriven suggested a bicontinuous structure at larger fractions of oil and water [16] where the oil and water phases form interconnecting domains separated by a surfactant film. The bicontinuous candidate will be an optically isotropic and light scattering microemulsion containing comparable amounts of oil and water where one predominates. An illustration is shown in Figure 2.5.

Surfactants have the ability to stabilise oil and water due to their amphiphilic nature and form a variety of stable phases. The phases exhibited in water–SDS–alcohol systems have previously been documented [17]. The water–SDS–1-pentanol system at 25°C has been shown to exhibit four one-phase regions. Three of them are mesophases: the lamellar phase; the hexagonal phase; and the rectangular phase [18]. Regions of these systems have the ability to stabilise volumes of oil. When volumes of oil and water are comparable a random bicontinuous structure is formed.

There has been much debate as to whether microemulsions should be considered as swollen micelles or small droplet emulsions, as they represent the intermediate stage between micelles and ordinary emulsions. Their droplet size can still be large enough

to classify them as emulsions but their thermodynamic stability and reproducibility is uncharacteristic of ordinary emulsions.
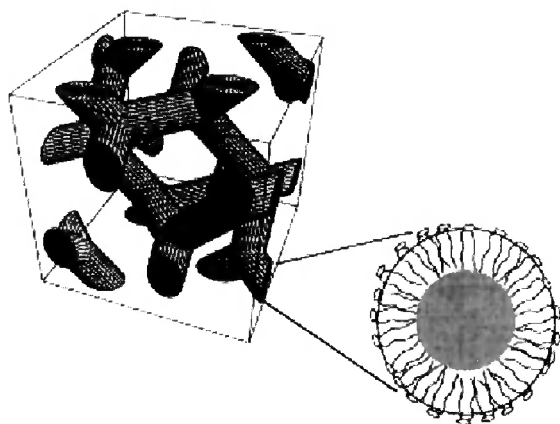
Figure 2.5   Representation of a bicontinuous microemulsion structure [9]

2.3.4.1   Co-surfactants

Microemulsions can be formed either using high levels of a non-ionic surfactant or an ionic surfactant with the addition of a co-surfactant. Certain surfactants are not capable of lowering the surface tension enough to form microemulsions without the addition of another amphiphilic species known as a co-surfactant. The addition of high levels of a non ionic surfactant are sufficient to lower the surface tension and increase the interfacial area enough to form a microemulsion. The addition of a co-surfactant acts to shield the repulsion of the head groups allowing closer packing and a lowering of the surface tension.

2.3.5   Microscopic surface tension

In the case of microemulsions the surface is sometimes assumed to be zero [19] and has been shown to be zero by electrical birefringence [20]. This means that if the area per surfactant molecule stays constant the microstructural entities are deforming. Inelastic neutron scattering [21] suggests that the shape fluctuations are governed by the bending elasticity.

2.3.6 Reactions in Microemulsions

Nanosized ceramic powders such as hydroxyapatite, ZrO_2, ferrites, $PbTiO_3$, and $PbZrO_3$ powders were prepared via reactions in bicontinuous microemulsions and inverse microemulsions [22-24]. Colloidal silica particles ranging from about 10 to 20 nm in diameter have been synthesised by the controlled hydrolysis and polymerisation of sodium metasilicate in bicontinuous microemulsions at room temperature [25].

2.3.7 Microemulsion Polymerisation

Pioneering work in the early 1980's by Stoffer and Bone revealed the concept of microemulsion polymerisation [26] expanding the research previously carried out to the polymerisation of methyl acrylate and methyl methacrylate in a microemulsion system containing 1-pentanol, water and sodium dodecyl sulfate. It was shown that the molecular weight of the resulting polymers is a function of the 1-pentanol concentration, as expected when the solvent acts as a chain transfer agent. The phase separation observed on polymerisation was explained by Gan and co-workers as a space-restriction conformational problem due to the dramatic reduction in solubility of the dimer compared to the monomer [27,28].

It has been shown that the presence of polymers can have a profound effect on the stability of microemulsions [27-29]. Replacement of styrene with the dimer reduces the water solubility of the microemulsion by 80% and further with the addition of the oligomer. The resulting systems were then subject to phase separation during polymerisation as the growing polymer chain becomes less soluble in the co-surfactant and monomer.

Oil-in-water microemulsions have been polymerised to produce polystyrene [30,31] and PMMA [32-34] particles whose size distribution widens at increasing

conversions. The effect of microemulsion composition on the structure of PS particles has also been investigated [35,36].

Polymerisation of microemulsions in the bicontinuous region yields a monolithic structure with open pore characteristics suitable for transport of a solution. Subsequently, Gan and co-workers [33,37-40] observed that the pore sizes of the materials prepared from bicontinuous microemulsions could be varied by altering the nature of the monomer, surfactant and co-surfactant. The development of microporous polymer composites prepared from microemulsion polymerisation is reviewed by Gan and Chew [41].

2.3.8 Polymerisation of Bicontinuous Microemulsions

2.3.8.1 Acrylamide/Sodium Acrylate

Work by Candau et al. shows the polymerisation of acrylamide in inverse microemulsions, stabilised by Aerosol OT produces clear microlatices with diameters of approximately 50nm [42]. This work was then progressed to investigate the use of bicontinuous microemulsions that progress on polymerisation to form uniform, stable and clear latexes from acrylamide and sodium acrylate. A linear decrease in the radius of gyration from 890 and 296 Å was found with an increase in acrylate content. It was suggested that as the polymer is insoluble in the monomer the monomer consumption gives rise to a shift in the phase diagram producing temporarily a three phase Winsor III type system explaining why the random structure evolves towards a final globular configuration after polymerisation.

2.3.8.2 Acrylic Acid/Styrene

Antonietti et. al [43] showed the polymerisation of bicontinuous microemulsions prepared from styrene and acrylic acid formed using an ionic surfactant, cetyltrimethylammonium chloride and m-diisopropenylbenzene as a crosslinker.

Shear measurements were taken during the course of the reaction to measure the process of gelation and phase behaviour. Those samples containing a high and low water content showed a low and high modulus respectively. They attribute the viscosity increases upon polymerisation to an overlap of the behaviour of lyotropic structures and the onset of gelation. Polarisation microscopy was used to examine samples before and during polymerisation and shows the transition of the microemulsion from a bicontinuous phase to a lamellar phase. The final polymerised samples were observed by TEM and SEM and show a porous sponge like fractured surface where they found no influence of surfactant/water ratio on the pore size of the resulting monoliths.

2.3.8.3   *Methyl methacrylate*

Polymerisation of single-phase (Winsor IV) microemulsions containing methyl methacrylate and acrylic acid crosslinked with EGDMA has been shown by Raj *et. al* to yield porous solid materials and films with good mechanical properties [44]. The prepared microemulsion was spread as a film and polymerised. Solid porous structures were observed on polymerisation of microemulsions containing up to 80 wt% water, were transparent up to 60 wt% water and self supporting up to 70 wt% water. However, the transparency of the resulting monoliths was found to be dependent on the EGDMA level. SEM imaging showed a pore diameter of 2-4 μm. Incorporation of potassium undecanoic acid in place of the acrylic acid yielded microemulsion with a droplet size smaller than that of the acrylic acid system [45] with a typical pore size of 1-3 μm. Micrographs indicated that the microporous structure in the polymer was related to the water content of the precursor microemulsion.

The effect of surfactant concentration on the structure of microporous polymeric materials prepared from methyl methacrylate was investigated by Chieng et al. [38]. At 40 wt% monomer and a low surfactant/water ratio larger and less uniform globular structures were observed along with a dramatic decrease in channel diameter. Based on the fractured surfaces, 6 wt% DTAB (dodecyltimethyl-ammonium bromide) produced pore dimensions in the region of 1-3μm dropping to 0.1-0.3μm at 9 wt% and 0.05-0.2μm at 12 wt% due to the reduced stability of the interface at lower surfactant concentrations. On comparing the effect of anionic and cationic surfactants on the morphology, swelling and permeability of membranes prepared from microemulsions in the bicontinuous region it was found that the pore size could be decreased by increasing the DTAB concentration while the reverse was true for a system prepared using SDS [46]. Materials prepared using SDS exhibited larger pore sizes (in the range of 100nm to 3μm) than those prepared using DTAB (up to 100nm) but both suggest a loss of the bicontinuous structure of the precursor microemulsions on polymerisation. It was also reported that at SDS levels above 10 wt% phase separation occurs prior to gelation resulting in the formation of membranes with low mechanical strength. More DTAB than SDS was required to stabilise the system and increasing the concentration of cationic surfactant led to a decrease in opacity. It was also noted that there was little change in the equilibrium water content of membranes prepared with increasing SDS content whereas a decrease was observed with increasing DTAB.

Burban et al [47] investigated both hydrophilic and oleophilic monomers for the preparation of microporous materials from bicontinuous. They note that the use of hydrophobic monomers (MMA or BMA crosslinked with EGDMA and stryrene crosslinked with DVB) produce opaque monoliths possibly due to phase separation

on polymerisation whereas hydrophilic monomers (acrylic acid and methacrylic acid crosslinked with EGDMA) produce transparent monoliths. X-ray scattering data of the parent microemulsions and porosity analysis of the resulting monoliths show that upon polymerisation 90% of the potential surface area is lost suggesting the microemulsion structure is not captured in the final porous material.

2.3.8.4   Microemulsions using polymerisable surfactants.

Gan *et. al* have shown that transparent porous monoliths with channel diameters in the range of 20-50nm can be prepared from bicontinuous microemulsions containing methyl methacrylate with the incorporation of a polymerisable surfactant, sodium 11-(*N*-ethylacrylamido)undecanoate (Na11-EAAU) when the water content is above 20 wt% [37]. A combination of Na11-EAAU and SDS allows materials with an increased pore diameter of 1-2μm [39] where the glass transition temperature of the resulting monoliths was found the be proportional to the Na11-EAAU weight ratio in the total surfactant mix. Monoliths with channel sizes of up to 200nm have also been prepared using a polymerisable cationic surfactant, acryloyloxyundecyl trimethylammonium bromide (AUMAB) [48]. A difference observed between the sample surface and the fractured surface was suggested to be related to a possible change in the structure of the precursor microemulsion upon polymerisation.

The use of a zwitterionic polymerisable surfactant also produces transparent porous materials with up to 50 wt% MMA in the parent microemulsion [33]. The randomly distributed and intertwining water channels and polymer islands of the resulting monoliths was seen to be between 50 and 70 nm. Monoliths prepared in this manner using polymerisable surfactants have also been prepared for use as ultrafiltration membranes [40].

The use of a polymerisable surfactant showed no apparent phase separation of the microemulsion during polymerisation, unlike in previous studies [49].

Gan et al use a nonionic macromonomer (ω-methoxy poly(ethylene oxide)$_{40}$ undecyl-α-methacrylate) in the polymerisation of MMA and HEMA to yield materials with pore sizes in the range of 0.02-1 μm [50,51]. Nanofiltration membranes have also been produced by the same group in a similar manner using acrylonitrile as the monomer [52]. The effect of electrolyte concentration, water, HEMA and polymerisable surfactant was investigated [53] and showed that water content increases pore size, HEMA narrows the channels and increasing the NaCl concentration increases the pore size.

Bicontinuous microemulsions have also been synthesized containing ruthenium complexes to produce materials for practical applications such as the development of chemical sensors and biosensors [54].

2.3.8.5 Macroporous silica frameworks

Sims et. al [55] prepared macroporous frameworks from bicontinuous microemulsions prepared from tetraethoxysilane (TEOS) solubilised in alkanes. The prepared microemulsions were frozen prior to the hydrolysis and condensation of the TEOS. Mesoporous organic networks with well-defined nanostructure have also been obtained by polymerization within the interconnective pore system of a mesoporous silica monolith by two step nanocasting [56].

2.3.9 The potential use as stationary phases

Due to the ability to control successfully the structure and porosity of the monoliths prepared from bicontinuous microemulsions and their low viscosity prior to polymerisation it should be possible to produce continuous beds from microemulsions inside fused silica capillaries used for CEC.

2.4 References

1. De Gennes, P. G.; Taupin, C. *J. Phys. Chem.* **1982**, *86*, 2294-2304.

2. Becher, P. *Emulsions; Theory and Practice* New York, 1965.

3. Schulman, J. H.; Stoeckenius, W.; Price, L. M. *J. Phys. Chem.* **1959**, *63*, 1677-80.

4. Lindman, B.; Danielsson, I. *Colloids and Surfaces* **1981**, *3*, 391-2.

5. Schulman, J. H. *Nature (London)* **1943**, *152*, 102-103.

6. Klier, J.; Tucker, C. J.; Kalantar, T. H.; Green, D. P. *Adv. Mater.* **2000**, *12*, 1751-1757.

7. Chew, C. H.; Gan, L. M.; Ong, L. H.; Zhang, K.; Li, T. D.; Loh, T. P.; MacDonald, P. M. *Langmuir* **1997**, *13*, 2917-2921.

8. Lindman, B.; Olsson, U. *Phys. Chem. Chem. Phys.* **1996**, *100*, 344-363.

9. Soderman, O.; Nyden, M. *Colloid Surf. A-Physicochem. Eng. Asp.* **1999**, *158*, 273-280.

10. Groger, S.; Rittig, F.; Stallmach, F.; Almdal, K.; Stepanek, P.; Papadakis, C. M. *J. Chem. Phys.* **2002**, *117*, 396-406.

11. Kumar, C. *J. Phys. Chem.* **1980**, *84*, 1895-1899.

12. Kreilgaard, M.; Pedersen, E. J.; Jaroszewski, J. W. *J. Control. Release* **2000**, *69*, 421-433.

13. Bellare, J.; Haridas, M.; Li, X. In *Handbook of Microemulsion Science and Technology*; Mittal, K., Kashmiri, L., Eds.; Marcel Dekker: New York, 1999, p Chapter 13 p 411-436.

14. Lam, A. C.; Schechter, R. S. *J. Colloid Inter. Sci.* **1987**, *120*, 42-55.

15. Carver, M. T.; Hirsch, E.; Wittmann, J. C.; Fitch, R. M.; Candau, F. *J. Phys. Chem.* **1989**, *93*, 4867-4873.

16.   Scriven, L. E. *Nature (London)* **1976**, *263*, 123-5.

17.   Bellocq, A. In *Handbook of Microemulsion Science and Technology*; Mittal, K., Kashmiri, L., Eds.; Marcel Dekker: New York, 1999, p 139-184.

18.   Prince, L. M. *Microemulsions; Theory and Practice*; Academic Press, Inc.: New York, 1977.

19.   Safran, S. A.; Roux, D.; Cates, M. E.; Andelman, D. *Phys. Rev. Lett.* **1986**, *57*, 491-494.

20.   van der Linden, E.; Geiger, S.; Bedeaux, D. *Physica A* **1989**, *156*, 130-143.

21.   Huang, J. S.; Milner, S. T.; Farago, B.; Richter, D. *Phys. Rev. Lett.* **1987**, *59*, 2600-2603.

22.   Lim, G. K.; Wang, J.; Ng, S. C.; Chew, C. H.; Gan, L. M. *Biomaterials* **1997**, *18*, 1433-1439.

23.   Wang, J.; Lim, G. K.; Ong, C. L.; Ng, S. C.; Chew, C. H.; Gan, L. M. *Key Eng. Mater.* **1997**, *132-136*, 8-11.

24.   Lim, B. P.; Wang, J.; Ng, S. C.; Chew, C. H.; Gan, L. M. *Ceramics International* **1998**, *24*, 205-209.

25.   Zhang, K.; Gan, L. M.; Chew, C. H.; Gan, L. H. *Mater. Chem. Phys.* **1997**, *47*, 164-170.

26.   Stoffer, J. O.; Bone, T. *J. Polym. Sci., Polym. Chem. Ed.* **1980**, *18*, 2641-8.

27.   Gan, L. M.; Chew, C. H.; Friberg, S. E.; Higashimura, T. *J. Polym. Sci., Polym. Chem. Ed.* **1981**, *19*, 1585-7.

28.   Gan, L. M.; Chew, C. H.; Friberg, S. E. *J. Polym. Sci. Polym. Chem. Ed.* **1983**, *21*, 513-23.

29.   Friberg, S. E.; Liang, P. *J. Polym. Sci. Polym. Chem. Ed.* **1984**, *22*, 1699-705.

30. Guo, J. S.; Sudol, E. D.; Vanderhoff, J. W.; Elaasser, M. S. *J. Polym. Sci. Pol. Chem.* **1992**, *30*, 691-702.

31. Guo, J. S.; Sudol, E. D.; Vanderhoff, J. W.; Elaasser, M. S. *J. Polym. Sci. Pol. Chem.* **1992**, *30*, 703-712.

32. Bleger, F.; Murthy, A. K.; Pla, F.; Kaler, E. W. *Macromolecules* **1994**, *27*, 2559-2565.

33. Gan, L. M.; Li, T. D.; Chew, C. H.; Teo, W. K.; Gan, L. H. *Langmuir* **1995**, *11*, 3316-3320.

34. Loh, S. E.; Gan, L. M.; Chew, C. H.; Ng, S. C. *J. Macromol. Sci.-Pure Appl. Chem.* **1996**, *A33*, 371-384.

35. Full, A. P.; Kaler, E. W.; Arellano, J.; Puig, J. E. *Macromolecules* **1996**, *29*, 2764-2775.

36. Xu, X. J.; Chew, C. H.; Siow, K. S.; Wong, M. K.; Gan, L. M. *Langmuir* **1999**, *15*, 8067-8071.

37. Gan, L. M.; Chieng, T. H.; Chew, C. H.; Ng, S. C. *Langmuir* **1994**, *10*, 4022-4026.

38. Chieng, T. H.; Gan, L. M.; Chew, C. H.; Lee, L.; Ng, S. C.; Pey, K. L.; Grant, D. *Langmuir* **1995**, *11*, 3321-3326.

39. Chieng, T. H.; Gan, L. M.; Chew, C. H.; Ng, S. C.; Pey, K. L. *Langmuir* **1996**, *12*, 319-324.

40. Li, T. D.; Gan, L. M.; Chew, C. H.; Teo, W. K.; Gan, L. H. *Langmuir* **1996**, *12*, 5863-5868.

41. Gan, L.-M.; Chew, C.-H. *Colloid Surf. A-Physicochem. Eng. Asp.* **1997**, *123-124*, 681-693.

42.   Candau, F.; Leong, Y. S.; Fitch, R. M. *J. Polym. Sci. Pol. Chem.* **1985**, *23*, 193-214.

43.   Antonietti, M.; Hentze, H. P. *Colloid Polym. Sci.* **1996**, *274*, 696-702.

44.   Raj, W. R. P.; Sasthav, M.; Cheung, H. M. *Langmuir* **1991**, *7*, 2586-2591.

45.   Raj, W. R. P.; Sasthav, M.; Cheung, H. M. *Langmuir* **1992**, *8*, 1931-1936.

46.   Chieng, T. H.; Gan, L. M.; Chew, C. H.; Ng, S. C.; Pey, K. L. *Polymer* **1996**, *37*, 2801-2809.

47.   Burban, J. H.; He, M. T.; Cussler, E. L. *Aiche J.* **1995**, *41*, 907-914.

48.   Li, T. D.; Chew, C. H.; Ng, S. C.; Gan, L. M.; Teo, W. K.; Gu, J. Y.; Zhang, G. Y. *J. Macromol. Sci.-Pure Appl. Chem.* **1995**, *A32*, 969-980.

49.   Chew, C. H.; Gan, L. M. *J. Polym. Sci. Pol. Chem.* **1985**, *23*, 2225-2232.

50.   Gan, L. M.; Liu, J.; Poon, L. P.; Chew, C. H.; Gan, L. H. *Polymer* **1997**, *38*, 5339-5345.

51.   Liu, J.; Gan, L. M.; Chew, C. H.; Teo, W. K.; Gan, L. H. *Langmuir* **1997**, *13*, 6421-6426.

52.   Liu, J.; Teo, W. K.; Chew, C. H.; Gan, L. M. *J. Appl. Polym. Sci.* **2000**, *77*, 2785-2794.

53.   Chew, C. H.; Li, T. D.; Gan, L. H.; Quek, C. H.; Gan, L. M. *Langmuir* **1998**, *14*, 6068-6076.

54.   Moy, H. Y.; Chow, P. Y.; Yu, W. L.; Wong, K. M. C.; Yam, V. W. W.; Gan, L. M. *Chem. Commun.* **2002**, 982-983.

55.   Sims, S. D.; Walsh, D.; Mann, S. *Adv. Mater.* **1998**, *10*, 151-154.

56.   Goltner, C. G.; Weissenberger, M. C. *Acta Polym.* **1998**, *49*, 704-709.

General Experimental

3 General Experimental

3.1 Materials

The monomers methyl methacrylate, butyl methacrylate (99%), ethyleneglycol dimethacrylate (98%) and 2-hydroxyethyl methacrylate (98%), were purchased from Aldrich and the inhibitors were removed by passing through basic alumina in a sintered funnel. α,α'-azobis isobutyronitrile (AIBN) (99%) which was purchased from BDH. Methanol and ethanol were supplied by Fischer. Phosphoric acid (85%) dipropylphthalate, diphenylphthalate and thiourea were a gift from Astra Zeneca (Macclesfield, Cheshire). All other components were purchased from Sigma-Aldrich; 1-propanol (99%), 1-butanol (99.8%), 1-pentanol (99%), sodium dodecyl sulfate (97%), didecyldimethylammonium bromide (98%), ammonium persulfate (98%), sodium persulfate (98%), N, N'-tetramethylethylene diamine (TMEDA) (99%).

3.2 Equipment

3.2.1 Mercury Porosimetry

3.2.1.1 Instrumentation

Mercury porosimetry was carried out using a Micrometrics Autopore 9400 series porosimeter. This high pressure porosimeter allows sample pressurisation up to 60,000 psia and can be used to measure pore sizes accurately in the range of 360μm down to 0.003μm. Samples were analysed up to a pressure of 2000 psia in order to prevent sample collapse at higher pressures.

During analysis the sample is placed in a penetrometer, detailed in Figure 3.1. A nut and cap are placed around the sample cup and seal to ensure no leaks occur. The penetrometer is filled with mercury through the base of the capillary stem upon

application of pressure. Electrical contact between the stem coating and conductive plates on the porosimeter provides a means to measure the volume of mercury in the stem.
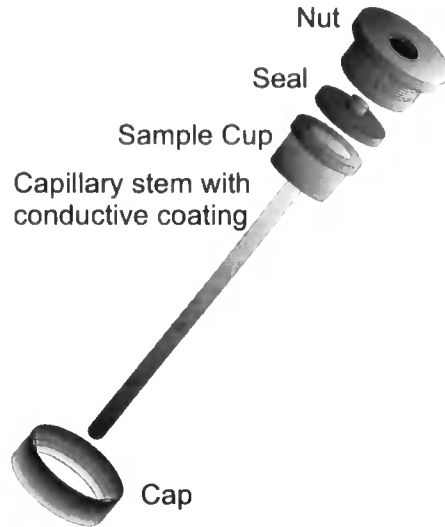
Figure 3.1   Penetrometer and closure components.

3.2.1.2   Theory

Mercury does not wet most surfaces and will not penetrate pores by capillary action. It must be forced to intrude pores. Liquid mercury has a high surface tension (485 dyne/cm) and contact angle, θ (130°C) with most solids. See Figure 3.2.
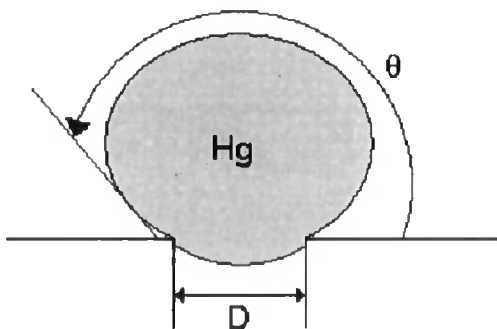
Figure 3.2   Mercury in contact with a pore.

When mercury is in contact with a circular pore opening the surface tension of the mercury acts along the circle of contact for a length equal to the perimeter of the

circle. The force, F_1, with which the mercury resists entering the pores is shown in Equation 3.1 where D is the diameter of the pore, θ is the contact angle and γ is the surface tension. (For values of $\theta > 90^\circ$ the term is intrinsically negative).

$$F_1 = -\pi D \gamma \cos \theta$$

Equation 3.1

The force, F_2, due to an externally applied pressure, P, acts over the area of the circle of contact and is expressed mathematically by Equation 3.2.

$$F_2 = \pi D^2 \, P/4$$

Equation 3.2

At equilibrium the opposing forces are equal ($F_1 = F_2$) and the pore diameter can be calculated at a given pressure using the Washburn equation (Equation 3.3)

$$D = \frac{-4\gamma \cos \theta}{P}$$

Equation 3.3

An over-simplification assumes that the pores are cylindrical but this is the best representation.

The volume of mercury forced into pores increases with pressure (up to 60,000 psi) producing a unique pressure-volume curve. As the pressure is reduced again a mercury extrusion curve will be produced. Where the extrusion curve does not overlay the intrusion curve suggests the presence of bottle-necked pores where the mercury is trapped. Incremental pore volumes can be related to some mean pore diameter. If the pores are taken to be cylinders, pore wall areas can be calculated from the pore volume data. Plots of differential intrusion versus diameter (dV/dD) and log differential intrusion (dV/d(logD) can be obtained where the peaks will be

plotted with equal areas on the logarithmic diameter axis when a sample has pores concentrated in distinct size ranges containing the same total volume.

3.2.2 SEM and ESEM

3.2.2.1 Instrumentation

Scanning electron microscopy was carried out at the University of Newcastle using a Hitachi S2400 electron microscope operating at 25kV. Samples were prepared for SEM by mounting on aluminium stubs using adhesive carbon disks to increase the conductivity. All samples were sputter-coated twice with a layer of gold, prior to collection of a secondary electron image, to enhance conductivity. A double coating was required to reduce charging phenomena.

In the latter part of this study SEM images were obtained using a Phillips XL30 electron microscope with environmental capabilities. Samples were prepared by mounting on aluminium stubs using carbon disks. Backscattered electron images were generated in ESEM, low vacuum mode which does not require electrically conducting samples. Operating conditions can be found on the individual images.

3.2.2.2 Theory

The SEM uses electrons rather than light to form an image (hence, the images are always rendered black and white). An electron gun emits a beam of high energy electrons which travels vertically downwards through a series of magnetic lenses designed to focus the electrons to a very fine spot. Near the bottom, a set of scanning coils moves the focused beam back and forth across the sample, row by row. As the electron beam hits each spot on the sample, electrons (secondary or backscattered) are ejected from its surface. Detectors count these electrons and send signals to an amplifier. The final image is built up from the number of electrons emitted from each spot on the sample.
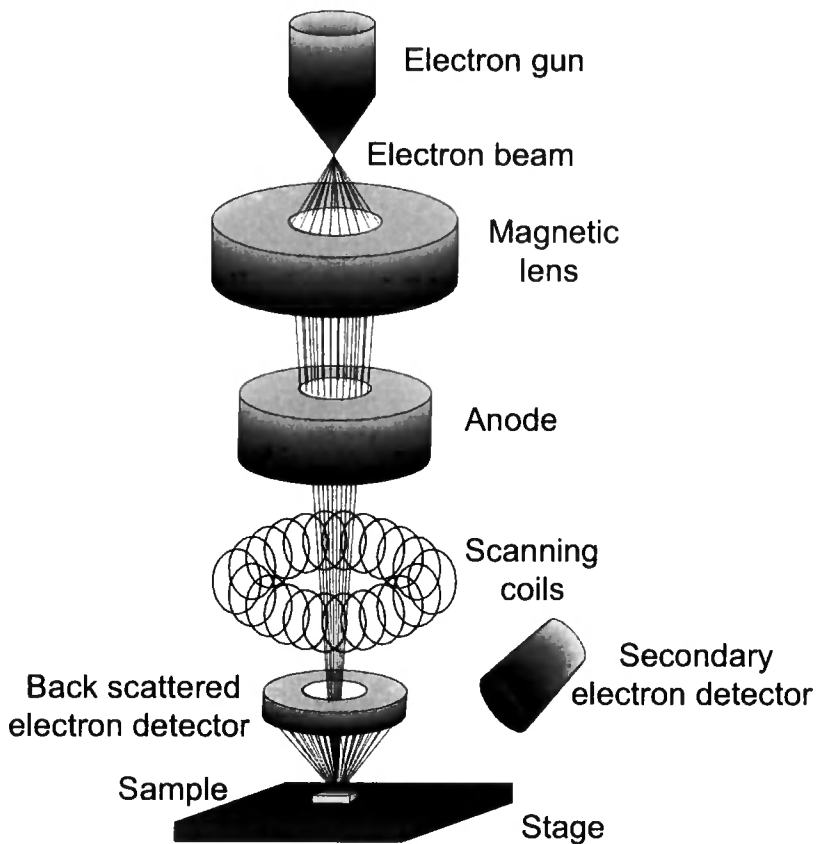
Figure 3.3   The scanning electron microscope

3.2.2.2.1   *Secondary Electrons (SE)*

When beam electrons approach the electrons in an atom they slow down as they repel the specimen electrons. This repulsion may be so great that the specimen electrons are ejected from the atom and exit the surface of the sample. These electrons are called secondary electrons. These electrons are moving very slowly when they leave the sample but due to their negative charge they can be attracted to a positively charged detector. Electrons are attracted from a wide area including around corners giving the ability to produce an apparent three dimensional image.
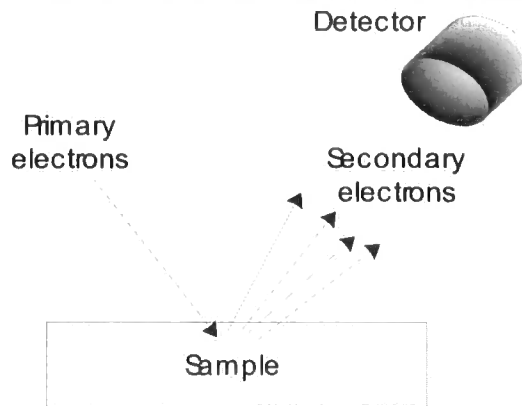
Figure 3.4   Secondary electron production

3.2.2.2.2   Backscattered electrons (BSE)

When the electron beam strikes the sample some of the electrons will interact with the nucleus. The electrons will be attracted to the positive charged nucleus but the correct incident angle will result in the electrons being caught in the 'gravitational pull' of the nucleus and ejected back from the sample. These high velocity backscattered electrons travel in straight lines therefore a detector must be placed directly in their path. This type of imaging can be used to enhance different elements of a sample as the number of BSE increases with nuclear size.

3.2.2.2.3   Environmental Scanning Electron Microscopy (ESEM)

The development of ESEM now allows specimens to be viewed in their natural state surrounded by a gaseous environment meaning that samples need not be coated with a conductive material.

As electrons travel through the gaseous environment collisions occur between an electron and a gas particle resulting in the emission of more electrons and an ionisation of the gas molecules. This increase in the amount of electrons effectively amplifies the electron signal. The positively charged gas ions are attracted to the negatively biased specimen offsetting charging effects.
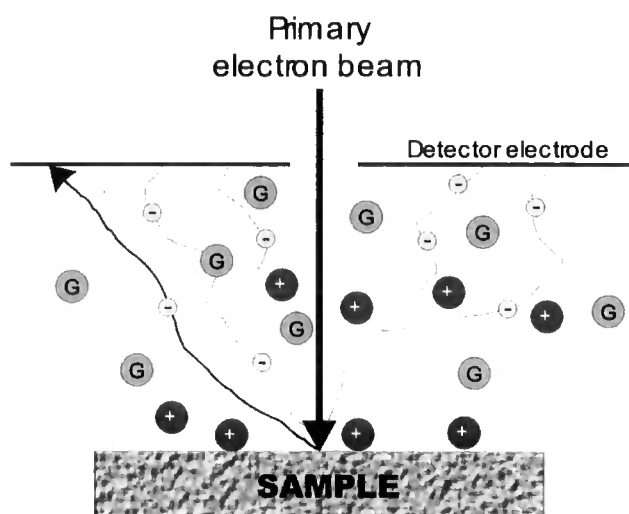
Figure 3.5   Electron interactions in ESEM

3.3   Capillary Electrochromatograph

Figure 3.6   The Beckman P/ACE MDQ method development system.

CEC analysis was carried out using the Beckman P/ACE Method Development System which is a CE-based analytical system configured for methods development. The system is configured with both a photo diode array and selectable-wavelength UV/Vis (200, 214, 254 and 280 nm filters included) detector, UV source optics, temperature-controlled sample storage module and 32 Karat™ Software.

3.3.1 Sample Introduction

Automated sample introduction is achieved directly from 96 well plates which hold 2ml vials and 0.5 ml tubes. Sample can be introduced by three injection modes; electrokinetic, pressure and vacuum with variable control of each parameter.

3.3.2 Sample Tray Temperature Control

The sample tray storage area within the unit is also temperature controlled independently from the electrophoresis buffers. Sample temperature may be maintained from 4° to 60° C in order to minimise degradation of temperature-labile compounds and controlling reaction rates when looking at enzyme kinetics.

3.3.3 36 Position Buffer Array

A 36 position buffer pair array independent from sampling vials enables method development to be optimised to determine successful separation conditions.

3.3.4 Multiple Separation Modes

This system allows several modes of operation including voltage, current, power, pressure and vacuum. All electrophoretic separations allow the programming of both step and linear gradients along with the simultaneous application of pressure or vacuum on both ends of the capillary necessary for CEC. The application of voltage gradient programming can be beneficial for separations over a wide range of fragment sizes particularly for the separation of nucleic acids. The application of simultaneous voltage and pressure is beneficial for detecting material not migrated off the capillary.

3.3.5 Detectors

A high sensitivity selectable wavelength UV detector is available complete with up to seven filters which can be changed during a run. Detector sensitivity in CE is

critical due to the small mass loads introduced and small detection path lengths. Fixed wavelength detection in a filter wheel assembly maximizes detector sensitivity yet still allows wavelength changes during a run. Additionally the system employs fibre-optic technology bypassing the necessity of an optical bench and lowering the noise on the detection system. A diode array detector is also available and essential for method development work which allows a real time display, collection and analysis of electropherograms from up to four different wavelengths simultaneously.

Methyl Methacrylate

Systems

4 Methyl Methacrylate Systems

4.1 Introduction

Polymerising microemulsions in the bicontinuous region has been shown to yield porous structures with a variety of pore sizes. Initial studies investigated systems to assess their suitability for the preparation of stationary phases for use in CEC and included the introduction of a charged species required to support an EOF. A system reported by Gan *et al.* [1] was investigated initially to study the effect of HEMA and EGDMA on microemulsion formation and pore size. In order to assess the suitability of polymerised microemulsions as stationary phases, capillaries were filled and the filling technique was developed to produce homogeneously packed capillaries. An alteration of the microemulsion composition has also been investigated to assess the effect of the weight fraction of each component on the topography and pore size.

4.2 Experimental

4.2.1 Standard Procedures

4.2.1.1 Microemulsion Preparation

Each microemulsion composition detailed in appendix A was prepared by adding the components to a glass vial and manually shaking. To ensure stability, each composition was allowed to equilibrate by standing at room temperature for a minimum of 15 minutes.

4.2.1.2 Microemulsion Polymerisation

The prepared microemulsion was purged with nitrogen for 10 minutes and sealed with a rubber seal. Polymerisation was carried out at the temperature detailed in appendix A either in an oven (above 40°C) or a water bath (up to 40°C). The monoliths were cleaned by Soxhlet extraction in the appropriate solvent.

4.2.2   Capillary filling

The microemulsions detailed in appendix A4 were prepared according to the procedure in 4.2.1.1 and purged with nitrogen for 10 minutes. The microemulsion was injected into six 30cm lengths of fused silica capillary (75 μm i.d.) using a syringe and adapter. A further six lengths were filled by drawing the microemulsion up into the capillary. These lengths were sealed with rubber and polymerised in an oven at 70°C overnight. Three lengths of each set were placed in the oven horizontally and the remaining three placed in the oven vertically.

A further six lengths were filled using the apparatus in Figure 4.1 which involves a glass tube with a side arm. The microemulsion is placed in the bottom of the tube and lengths of capillary are passed through a rubber septum and into the microemulsion using a syringe needle. Upon pressurising the tube the microemulsion is driven up the capillary to the desired level. The filled capillaries were then sealed with rubber and suspended vertically from the outlet end in an oven 70°C overnight.

The homogeneity of the packing inside the capillary was determined using a light microscope.

Subsequent capillaries were filled using the apparatus in Figure 4.1.

4.2.3   Solubility of Surfactants

SDS and DDAB (20-40mg) were added to glass vials containing 2 ml of either water, methanol, ethanol, chloroform, THF or dichloromethane.

Syringe needle (removed)

Septum

Pressure Gas

Capillary

Side Arm

Microemulsion
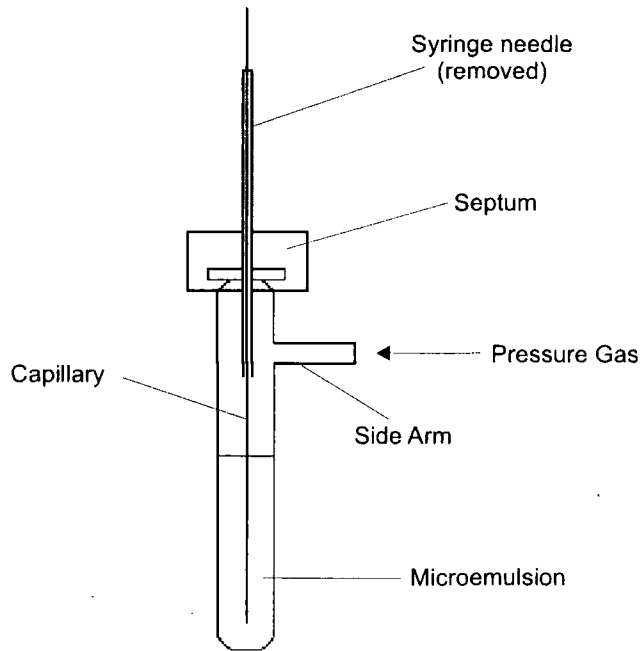
Figure 4.1 Pressurised glass capillary filler.

4.2.4 Capillary Cleaning.

Each capillary prepared in all the previous experiments were attached to an HPLC pump after fracturing 5mm from each end of the capillary. Deionised water and acetonitrile were applied successively up to a pressure of 60 bar.

The capillary prepared in 4.2.2 was broken into 4cm lengths and immersed in different solvents for 24 hours; ethanol, THF and water. They were then dried on a vacuum line for 24 hours alongside an untreated capillary. Each capillary was then halved and each end was examined by SEM.

4.2.5 Effect of a Liquid Interface

In order to assess whether the surface morphology of the polymerised microemulsion can be altered a layer of heptane was carefully placed on top of the microemulsion, which was then polymerised.The microemulsion composition in appendix A9 was used for this.

4.2.6   *Application to HPLC*

The microemulsion prepared according to appendix A9 was filled into a 25cm, 5mm i.d. HPLC column, polymerised and flushed with 80 % acetonitrile and 20 % water (v/v). A plastic disk was placed at each end to prevent the microemulsion running out prior to polymerisation.

4.3 Results and Discussion

4.3.1 The Effect of EGDMA and HEMA

The microemulsion formulation in appendix A1 was prepared, following work by Gan *et al.* [1] who reported pore sizes of up to 800nm. The reported recipe included 42wt% 2-hydroxyethyl methacrylate (HEMA). As the initial stationary phase to be investigated was to be reverse-phase, the HEMA was omitted and replaced with MMA. The introduction of polar components results in a normal-phase packing. Upon preparation the resulting emulsion was slightly opaque in appearance suggesting the droplet size was not small enough to be classified as a microemulsion. In this case phase separation occurred during the first 30 minutes of polymerisation. When the HEMA was then added to replace some of the MMA a stable optically transparent system was formed. The addition of HEMA may act to stabilise the microemulsion by acting as a type of co-surfactant due to it being similar amphiphilic in nature. The hydroxyl groups will act as the hydrophilic head and the acrylate group will act as the end of the hydrophobic tail. Its effect as a surfactant will be weak due to its short hydrocarbon chain length. The addition of HEMA has been found to enlarge the microemulsion region by increasing the flexibility of the oil-water interface [2] and also to reduce the pore size of the resulting monolith [2-4]. The fractured surface of the monolith prepared without the addition of HEMA exhibits an aggregate and channel structure (Figure 4.2). The channels appear to be wider than those observed with the inclusion of HEMA (Figure 4.3i). The addition of a co-surfactant will reduce the surface tension and the size of the bicontinuous channels in the microemulsion and hence the channels in the resulting monolith. As it had been previously reported that a higher concentration of EGDMA causes phase separation [5], the preparation with MMA was repeated with less EGDMA, however

phase separation still occurred prior to gelling. Coalescence of the oil phase occurs as the microemulsion is allowed to stand without agitation. As a microemulsion is thermodynamically stable and does not separate, it is concluded that the systems initially prepared are not microemulsions. The addition of HEMA to the system at the expense of methyl methacrylate results in an optically transparent and homogeneous microemulsion which remained stable throughout the polymerisation.
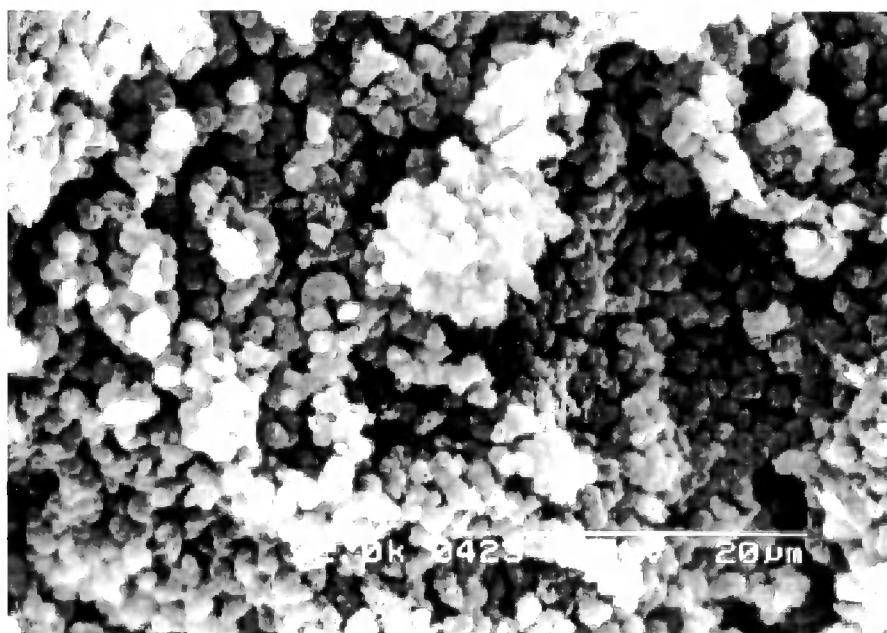
Figure 4.2 Monolith prepared from 28 wt% water, 9 wt% SDS, 54 wt% MMA and 9 wt% EGDMA. Appendix A1.

The addition of EGDMA to a microemulsion accelerates gelation and hence aids the preservation of the microemulsion structure upon polymerisation [5]. It can also reduce the extent of physical changes (e.g. shrinkage) on drying and increase the mechanical strength of the resulting foam [2].

From the first set of experiments the need to include a co-surfactant in order to form a microemulsion when using an ionic surfactant such as SDS has been confirmed.

4.3.2 Capillary Preparation

Attempts to fill capillaries homogenously with the microemulsion in appendix A4 were unsuccessful due to the high polymerisation rate using the redox system of initiators, ammonium persulfate and. TMEDA. SEM images of a fractured section of a polymerised capillary can be seen in Figure 4.3ii. The porous structure observed in the fractured surface of the monolith is not observed here. This is possibly due either to phase separation of the microemulsion prior to polymerisation or the channels being blocked with surfactant. Attempts to flush the capillary with both water then ethanol were unsuccessful.

The microemulsion polymerisation in appendix A4 uses an oil soluble initiator, AIBN, which is initiated above room temperature to enable the filling of a capillary to occur before polymerisation. Filling was difficult using a syringe and adapter. It was found to be more effective to draw the microemulsion up into the capillary from the preparation vial. A constant pressure was required to achieve a uniformly filled section of capillary. During polymerisation of the capillaries it was found that a higher success rate of homogeneously packed capillaries was achieved when both ends of the capillary were sealed and they were placed in the oven vertically with the unfilled end to the top.

Later experiments employed a capillary filler (Figure 4.1). Filling at a constant pressure enabled the production of homogeneously filled capillaries.

The effect of polymerisation position was assessed by polymerising microemulsion filled capillaries in various positions. It was difficult to assess the polymer inside the capillary due to the polyamide coating on the capillary. Dark gaps along the capillary length were assumed to be gaps in the monolith. All the capillaries appeared to contain air bubbles, the ones polymerised vertically had larger homogeneous sections

than those laid horizontally. It was concluded that the filling technique requires care and the polymerisation technique may need improving. The microemulsion structure has been shown to alter over a range of temperatures [6]. If this is the case and the bicontinuous structure is lost, a non homogeneous packing will result.

(i)

(ii)
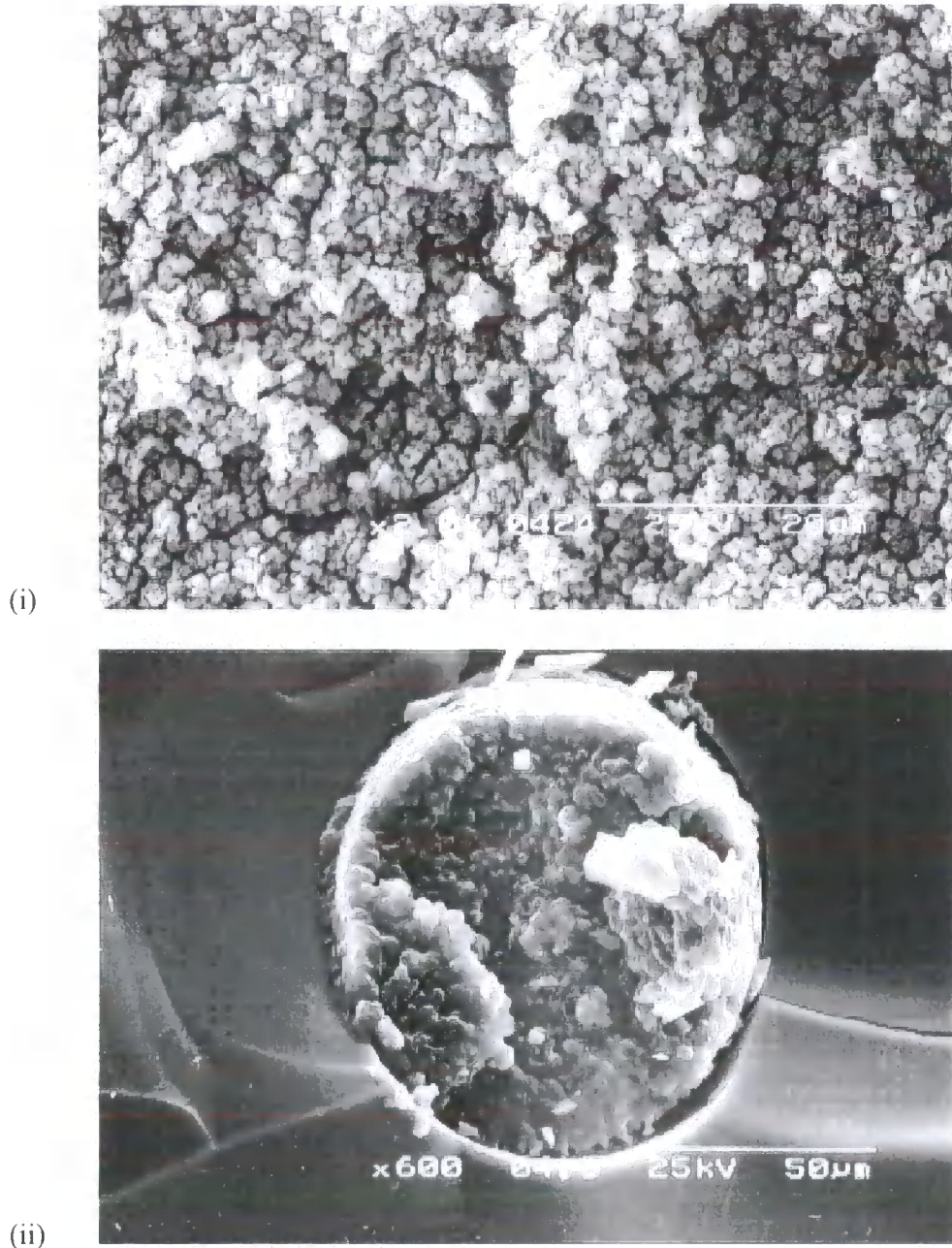
Figure 4.3   SEM images of the fractured surface of (i) a monolith prepared from MMA, EGDMA, DDAB and water and (ii) the resulting filled capillary (appendix A4)

4.3.3 Introduction of Charged Species

The next stage was the introduction of a potentially charged species to a microemulsion (appendix A5). In order to support an electroosmotic flow through the capillary, a species needs to be introduced that will enable the support of an electrical double layer to provide the flow of ions required for electroosmosis. A redox initiator was used; the microemulsion formed easily but polymerisation was too rapid to enable capillary filling. The polymerisation was repeated with a fresh monomer mixture. It was now found that gelling did not begin until a few minutes after the addition of the aqueous phase to the oil. This could simply be a result of the change in ambient temperature. This enabled capillary filling until gelling started. SEMs of the polymerised microemulsions show elongated aggregates (Figure 4.4(i)). These elongated particles could be due to the fast polymerisation rate and the preservation of the microemulsion structure within the monolith.
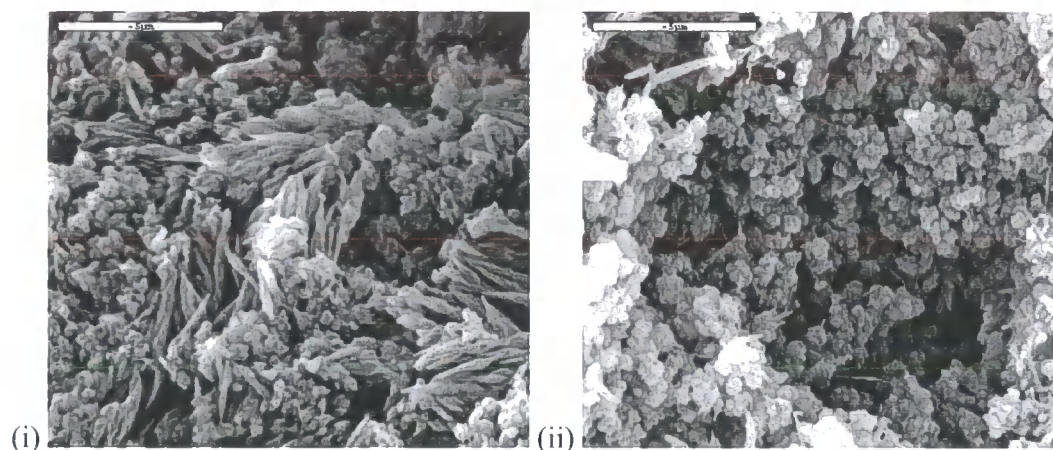
Figure 4.4   SEM image monolith prepared form a microemulsion containing (i) 4-vinylpyridine; (ii) DEAEMA.

Altering the potentially charged species to DEAEMA seems to give a reduction of these elongated aggregates and a structure similar to that observed for the composition containing no charged species (Figure 4.4(ii)). The occurrence of these elongated aggregates could be due to the use of a water soluble initiator where

polymerisation will be with radicals at the interface, however, in previous experiments using a water soluble initiator spherical aggregates were observed (Figure 4.2).
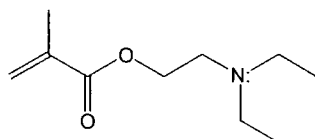
Figure 4.5 The structure of 2-(Diethylamino)ethyl methacrylate

Again polymerisation is rapid and the microemulsion had begun to gel before it could be removed from the filler.

As polymerisation is still too rapid at room temperature with redox initiation AIBN was again employed (appendix A6). The resulting filled polymerised capillaries appeared to contain very few air bubbles. This is likely to be due to care when filling and a slower polymerisation rate.

4.3.4   Altering Charge Concentration

Comparing the compositions in appendix A7 and A8 the amount of charged species present in the resulting monolithic stationary phase was altered in order to assess the effect of increased DEAEMA on the ability of the new composition to form a microemulsion, assuming the resulting capillaries were porous. A flow could not be established through these capillaries as the resulting monoliths polymerised in-situ did not show a porous structure.

4.3.5   Initiator system

The microemulsion described in appendix A6 was prepared. In order to enable filling of the capillaries required for use in CEC the initiator is either required to decompose at a slow enough rate at room temperature to enable filling prior to the gel stage or must decompose at a temperature above room temperature.

The system employed in the present work is a redox couple consisting of ammonium persulfate and N, N'-tetramethylethylene diamine (TMEDA). On transfer of an electron from the TMEDA to the ammonium persulfate, a radical species is produced as shown in Figure 4.6. As this reaction takes place at room temperature, polymerisation of the acrylates occurs rapidly after addition of the TMEDA. Due to the fast rate of this reaction the gel stage is reached quickly and the microemulsion becomes too viscous prior to injection into the capillaries.
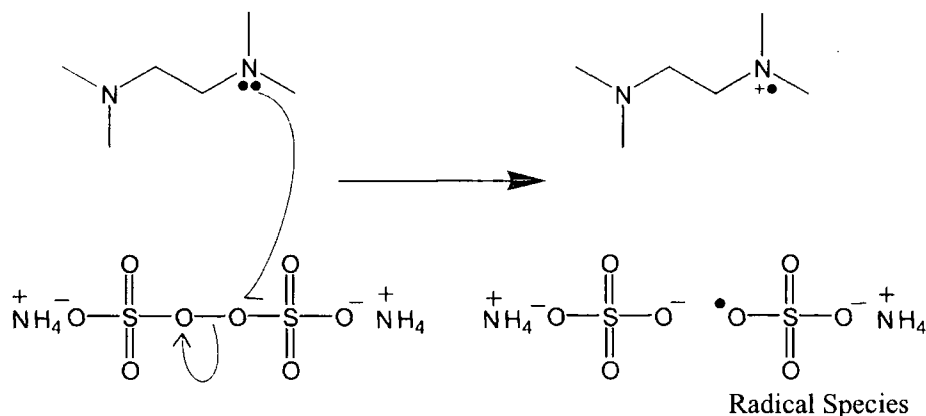
Figure 4.6 Decomposition of ammonium persulfate by the addition of TMEDA.

In addition to this, a thermally initiated system, α,α'-azobis isobutyronitrile (AIBN), was investigated.
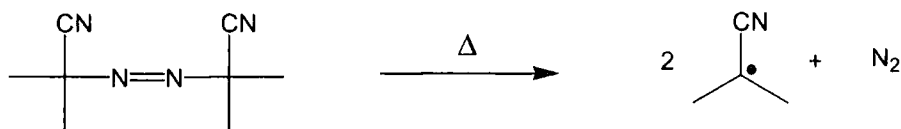
Figure 4.7 Thermal decomposition of AIBN

4.3.6 Surfactants

Early experiments assessed the need for a co-surfactant by employing a non-ionic surfactant which has been shown to produce a microemulsion without the addition of a co-surfactant. The addition of DDAB, which is a two tailed ionic surfactant, enables a sufficient reduction in surface tension to produce a microemulsion.

However, relatively large amounts are required. SEM images (Figure 4.3) showed a porous structure when observing the fractured surface of the foam, however the monolith inside the capillary essentially showed a non-porous structure. As the bulk monolith has been cleaned by Soxhlet extraction all of the residual monomer, surfactant and water have been removed to reveal a porous structure. Attaching the capillary to an HPLC pump, however, proved to be unable to clean the monolith inside as a flow of solvent could not be established. This was thought possibly to be due to the high surfactant content (ca 65 wt%) blocking the pores.

$$CH_3(CH_2)_8CH_2 - \overset{\overset{\displaystyle CH_3}{|}}{\underset{\underset{\displaystyle CH_3}{|}}{N^+}} - CH_2(CH_2)_8CH_3 \qquad Br^-$$
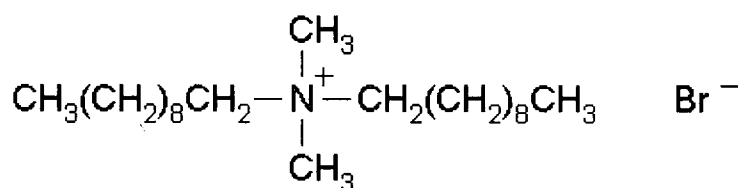
Figure 4.8 The structure of didecyldimethylammonium bromide

The pore sizes of the monoliths prepared using DDAB are smaller than those prepared using SDS. This may be related to the two-tailed nature of the DDAB having a greater solubility in the oil phase compared to SDS. A larger head group will give rise to a positive curvature due to the surfactant-packing parameter. If the DDAB produces a more stable interface than the SDS system the narrow oil and water domains of the microemulsion will be more effectively retained upon polymerisation.

4.3.7 Effect of Polymerisation Temperature and Rate

It was postulated that the temperature of polymerisation could have an effect on the structure of the microemulsion, producing a different structure of the resulting monolith. If phase separation occurs during polymerisation inside the capillaries then the resulting packing of those prepared at a higher temperature would show a less

homogeneous packing. Polymerisation of the same microemulsion at three different temperatures (room temperature, 40°C and 70°C; appendix A4) gave no conclusive evidence of this. SEM images in Figure 4.9 show an increase in aggregate size with temperature of polymerisation. Different polymerisation temperatures did not alter the porosity of the monolith inside the capillaries. Rapid polymerisation should yield channel and aggregate sizes comparable to those found in the microemulsion if the polymerisation the gel stage is reached rapidly leaving little time for coalescence. As the aggregates are larger when polymerisation is carried out at higher temperature this suggests a change in microemulsion structure prior to the gel stage induced by the temperature change prior to the onset of polymerisation. As the temperature increases the hydration of the lyophilic group decreases and the surfactant becomes less hydrophilic. As the HLB value of SDS drops to below 40 it may not be as effective preventing coalescence of the water and oil domains.

At lower temperatures polymerisation is slower and any effect of coalescence on polymerisation would be seen here. However, the microemulsion remains stable, preserving the narrow channel size of the microemulsion. Comparing SEM images of monoliths prepared at room temperature with a redox initiator (Figure 4.2), which is efficient at low temperatures and a thermally initiated system which will slowly decompose in solution at room temperature (Figure 4.9(i)) shows that polymerisation rate or type of initiator has a greater effect on aggregate size than temperature.

4.3.8 Initiator Efficiency

Primary recombination can occur if the diffusion of the radical fragments in solution is impeded and a cage effect leads to reaction of two the initiator radical species. The solvent usually plays an important part in the extent of the decomposition.
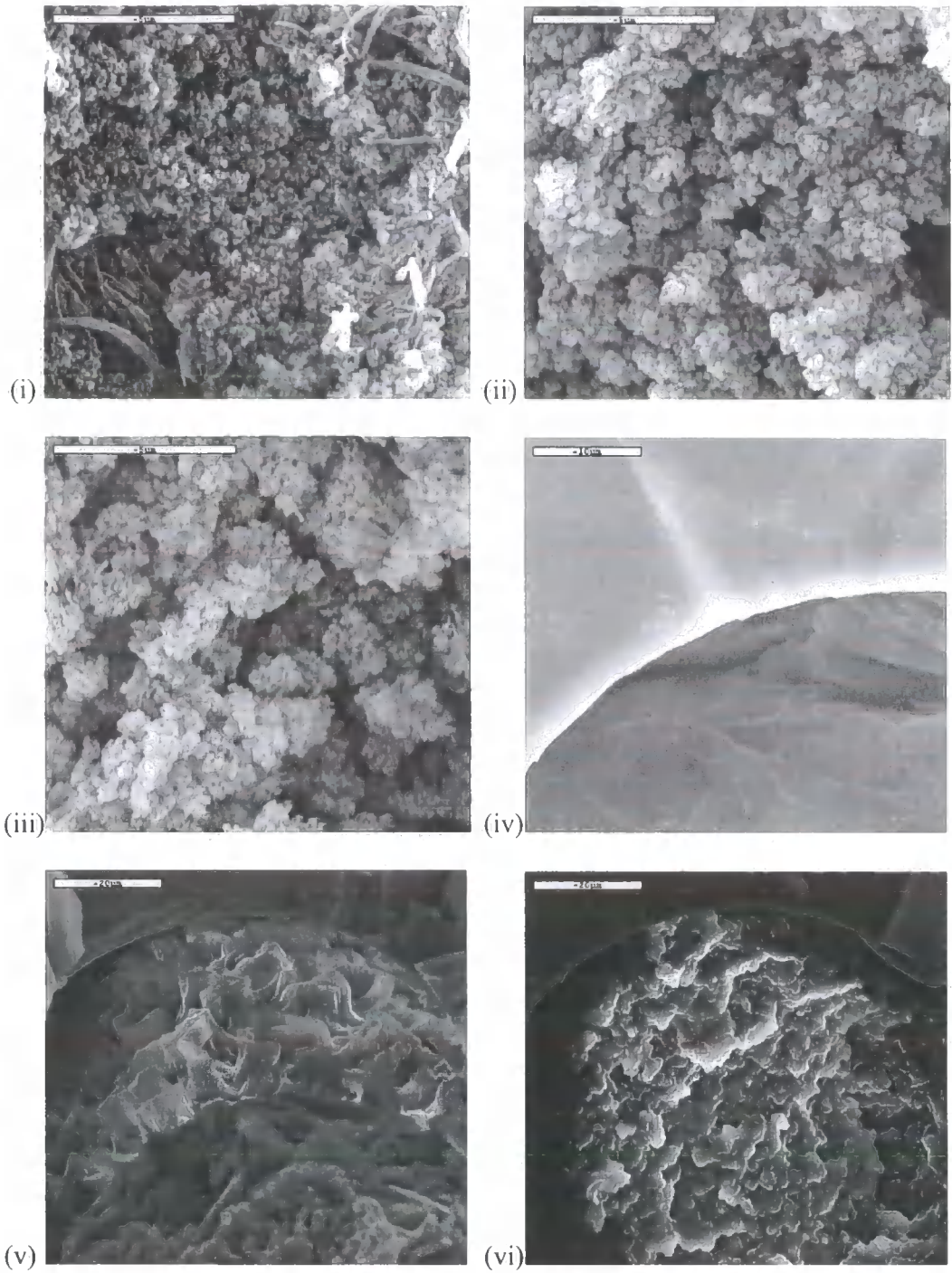
Figure 4.9   SEM images of monoliths prepared at (i) room temperature for 10 days; (ii) 40°C for 65 hours; (iii) 70°C for 2 hours and their corresponding capillaries (iv) room temperature for 10 days; (v) 40°C for 65 hours; (vi) 70°C for 2 hours

Induced decomposition can also occur when the radical species attacks an active centre. This is typical in peroxide initiators. In the case of microemulsion polymerisation the initiator needs to be efficient enough to enable gelling to take place prior to phase separation to retain the bicontinuous channel structure.

4.3.9 Effect of Water and Surfactant Content.

The compositions assessed in appendix A9 – 13 all formed optically transparent system. Upon polymerisation where the oil to water ratio was low the resulting monolith was very soft with a fine, brittle structure. Where the oil content was high the resulting monolith was very hard and difficult to fracture. Altering the pore size of monolith produced by the polymerisation of a microemulsion can be achieved by altering the surfactant to water ratio as shown in Figure 4.10. At a lower surfactant concentration the interfacial tension at the water-oil interface will be higher and the interface more prone to coalescence. As the polymer chains grow and the composition of the oil phase changes, the lower surfactant concentrations will not be able to stabilise the interface as well and coalescence of the oil channels will occur producing larger aggregates.

Increasing the water content will reduce the overall surfactant concentration in the aqueous phase altering the surfactants equilibrium with the interface. The ratio of micelles to surfactant monomer will change and the possibly the surface pressure. (see Figure 2.4) cause the interface to expand, spreading the monolayer of surfactant and increasing the rigidity of the interface. At higher water (and lower surfactant) contents the channels within the microemulsion will be wider, the size of the resulting aggregates will be larger and the pore size will increase. This effect can be seen in Figure 4.11.

For a constant water concentration increasing the oil to SDS ratio increases the modal pore size. With less surfactant, the interface will be less stable and the oil domains will be more prone to coalescence, resulting in larger aggregates which will pack less efficiently leaving larger voids. As the surfactant level is increased the interface will be more stable and coalescence will be reduced. Where there is a bimodal distribution or a 'shoulder' to the distribution this will represent the larger channels resulting from the water domains and the smaller pores in between the aggregates where the oil domains have undergone coalescence.
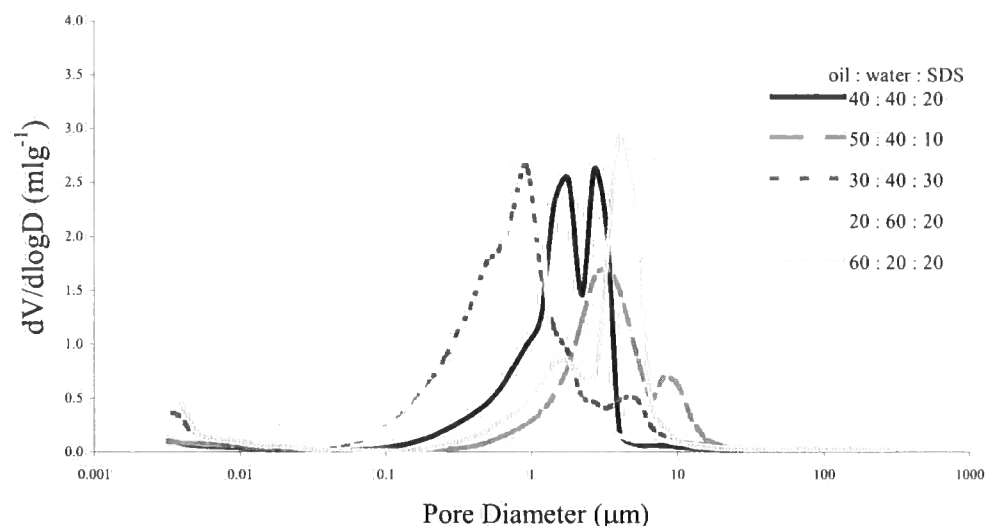
Figure 4.10 Pore size distribution of methyl methacrylate monoliths from microemulsions containing various ratios of oil, water and SDS.

Surfactant molecules pack at the oil-water interface causing a lowering of the surface tension. Different concentrations of different surfactants are required to achieve the same surface tension due to the size and shape of the surfactant molecule. Surfactants with a large head group will pack less effectively than those with a smaller head group.

For example SDS yields a larger bicontinuous region than DTAB due to the less effective packing of the larger head group in the latter [7]. At higher water

concentrations DTAB has a larger bicontinuous region due to the less rigid (less packed) monolayer having a higher flexibility.
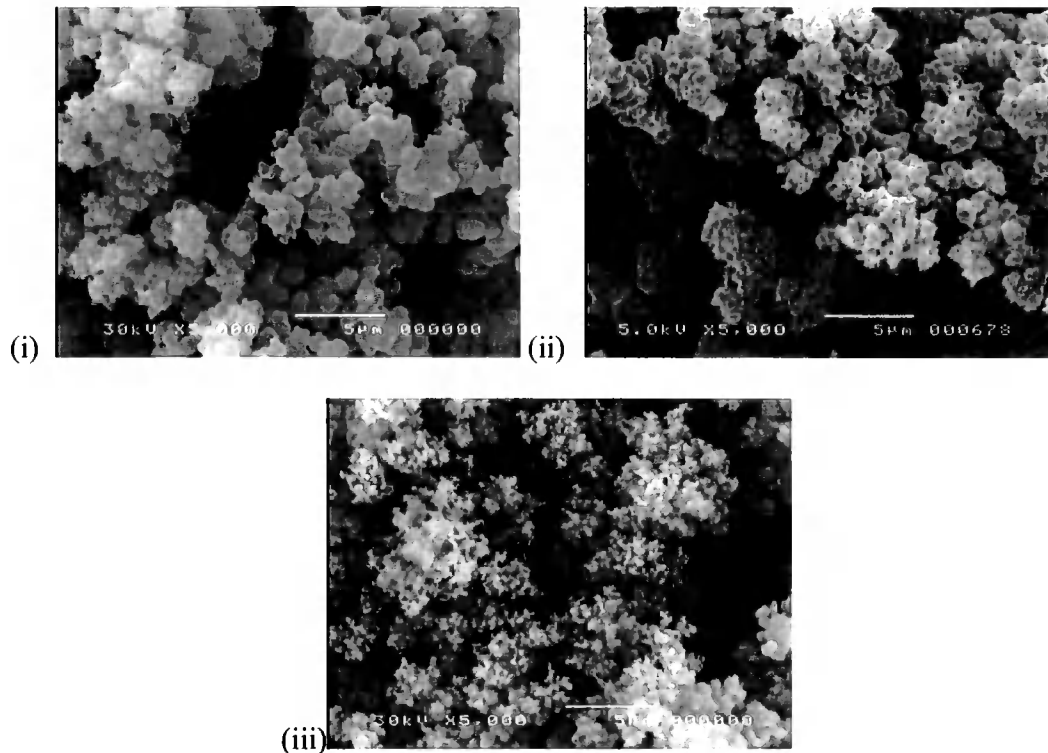
Figure 4.11 SEM images of monoliths prepared from microemulsions containing (i) 50.8 wt% oil, 39.5 wt% water, 9.7 wt% SDS (appendix A10); (ii) 41.0 wt% oil, 39.4 wt% water, 19.6 wt% SDS (appendix A9); (iii) 31.0 wt% oil, 39.4 wt% water, 29.6 wt% SDS (appendix A11).

Increasing the surfactant concentration will decrease the aggregate size as the microemulsion will be more stable. At lower surfactant concentrations the globules become bigger due to extensive coalescence of growing polymer particles of lower stability. At higher concentrations a more rigid interfacial film is obtained and more polymer particles are generated [7].

4.3.10 Effect of Co-surfactant Species

Altering the co-surfactant species from HEMA to 1-pentanol still allows the formation of a microemulsion. Direct replacement of HEMA with 1-pentanol (appendix A9 versus A14) results in the formation of a single phase microemulsion. Upon polymerisation the resulting monolith is more fragile due to the reduction of the polymerisable species. The inclusion of 1-pentanol still allows the solublisation of close to 70 wt% water with only a 10 wt% level of surfactant. The ability to replace the polymerisable co-surfactant with a non polymerisable one while still keeping the surfactant level low should allow the production of large pore size materials. Polymerisation of the corresponding microemulsions in capillaries however still did not result in pores that allowed flow through of solvent.
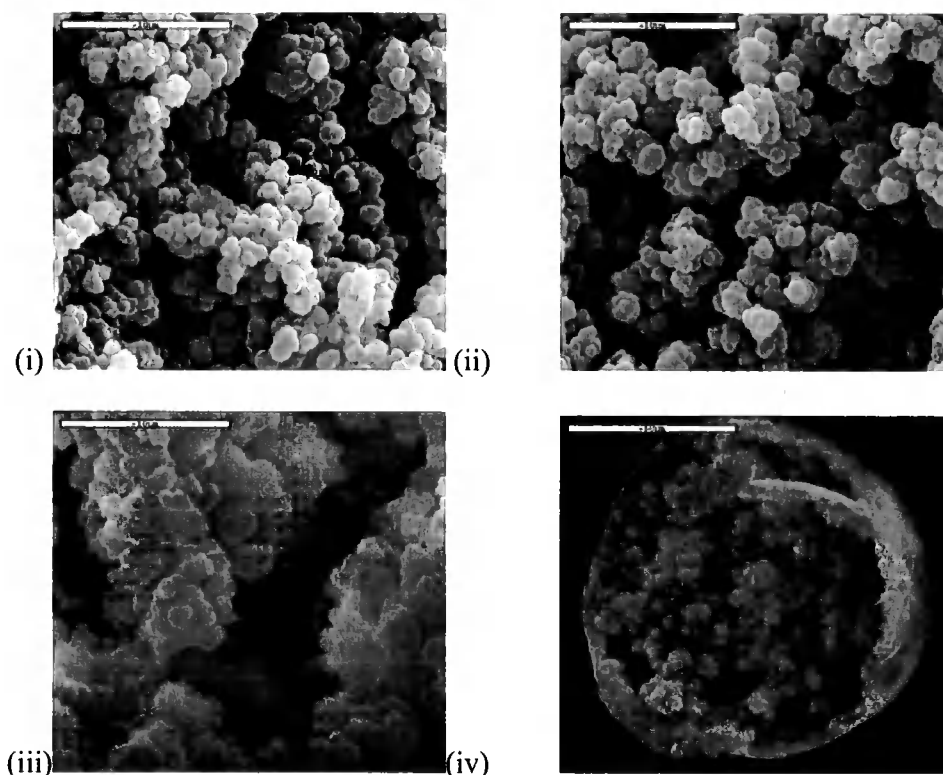
Figure 4.12 SEM images of monoliths prepared in glass vials and a capillary. (i) with AMPS (ii) without AMPS (iii) uncleaned capillary packing (iv) packed capillary.

It can be seen from the SEM images in Figure 4.12 of monoliths prepared from 40 wt% oil (50:50 MMA:HEMA, 4 wt% EGDMA) that there is little difference between the aggregate and channel size either with (i) or without (ii) the presence of AMPS. It can also be seen that upon polymerisation inside a capillary the porous structure is retained (iv) and (iii) the aggregates appear to be of similar size but coated in what is most likely to be surfactant.

4.3.11 Capillary Cleaning

All of the capillaries prepared in this section could not be cleaned by attaching to an HPLC pump. As a flow of solvent could not be established and the SEM images showed mainly a non-porous structure on the fractured surfaces of the unclean monoliths, pore blockage by surfactant is thought to be the main problem. In order to remove all of the impurities from the monoliths prepared in capillaries a suitable solvent needs to be identified if the blockage is to be removed to produce a porous structure. It can be seen from Figure 4.13 that methanol will be the most successful solvent for cleaning monoliths prepared using SDS. The use of ethanol or THF appears to cause the monolith to shrink.

4.3.12 The Effect of a Liquid Interface

It can be seen that from the SEM images in Figure 4.14 that different species in contact with the microemulsion interface produce different monolith surface topographies upon polymerisation suggesting a change in interfacial tension.

The addition of heptane to the surface will slowly mix with any excess oil on the surface of the microemulsion should phase separation begin to occur during polymerisation. As polymerisation occurs and the growing chains precipitate they will be dispersed in the heptane rather than forming a flat non-porous surface. Where the microemulsion is polymerised in contact air, a less porous surface is obtained.

This suggests that phase separation prior to polymerisation is occurring, resulting in a layer of monomer which produces a non-porous surface on polymerisation. However, addition of a non-polymerisable solvent is not a viable solution to the problem of a film at the interface. It is difficult to add the solvent to the top of the microemulsion within the capillary without the solvent mixing with the bulk microemulsion.
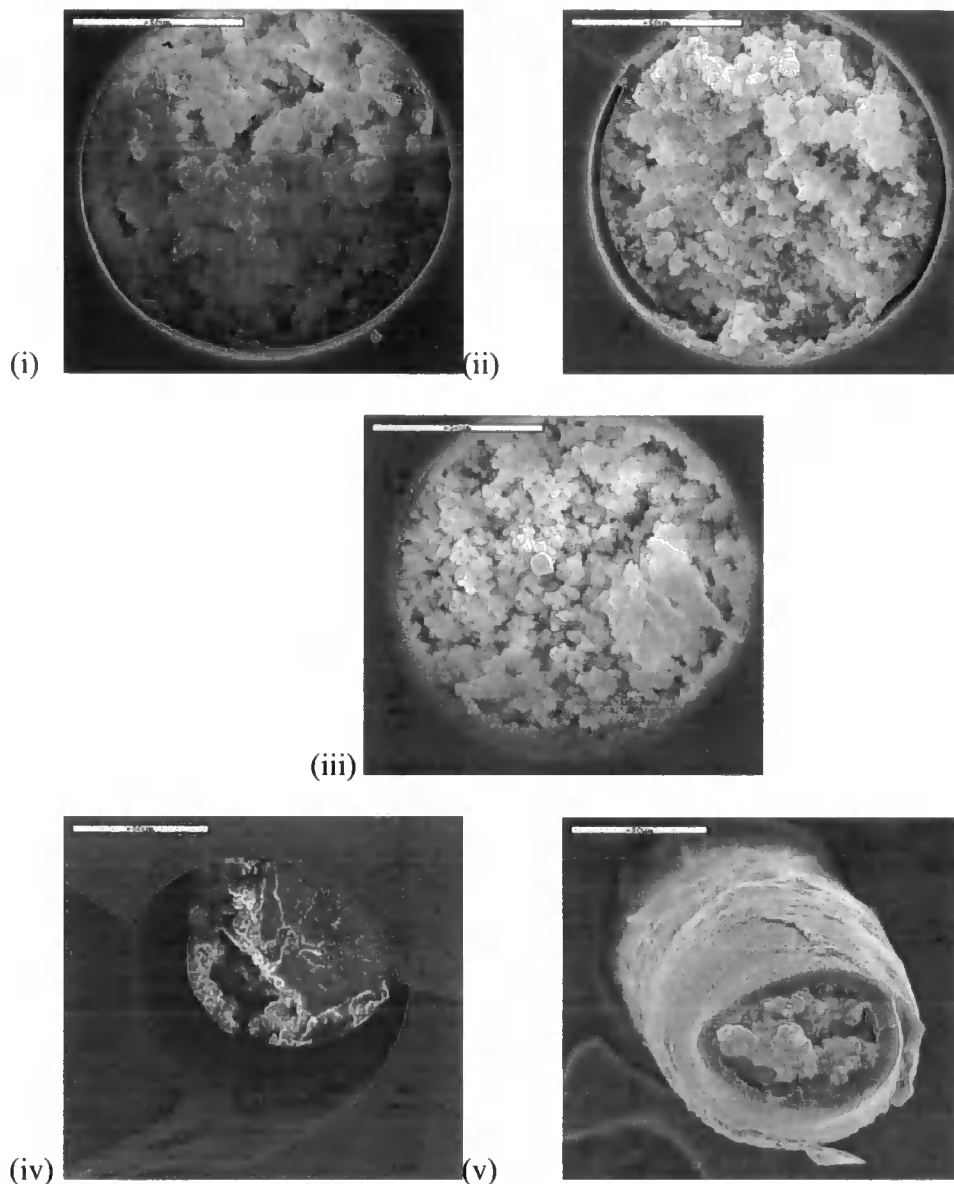
Figure 4.13 SEM images of in situ prepared monoliths (i) unwashed or washed in (ii) water; (iii) methanol; (iv) ethanol; (v) THF.
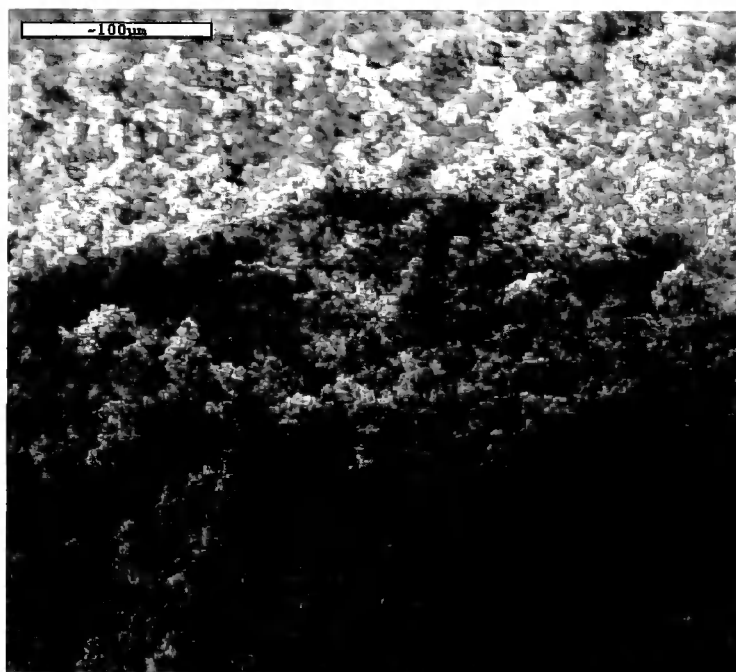
(i)
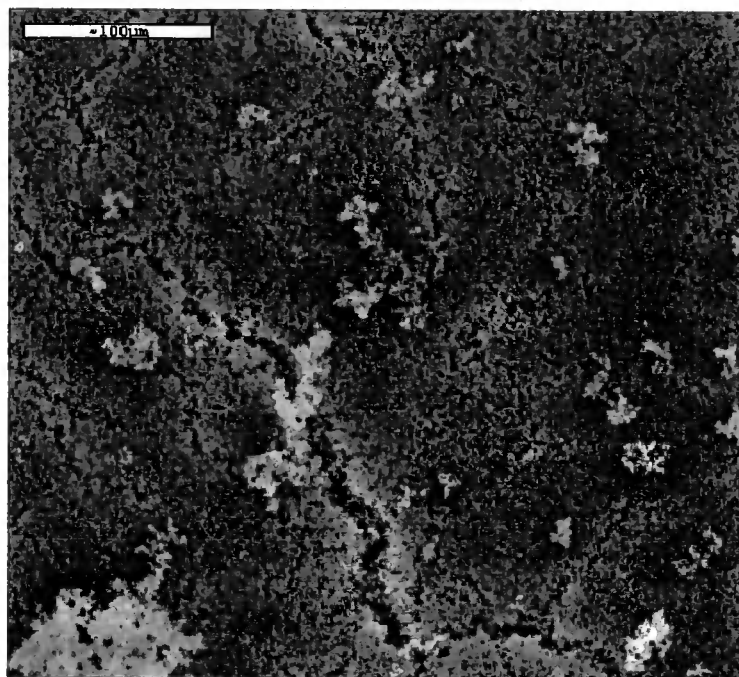
(ii)

Figure 4.14 SEM images of monolith prepared with (i) a layer of heptane on the surface; (ii) an air, microemulsion interface.

4.3.13 *Application to HPLC*

When formed in an HPLC column, the resulting monolith prepared from the microemulsion in appendix A9 was flushed successfully with methanol with a negligible build up of back pressure. No gaps could be observed between the wall and the monolith. This suggests that during polymerisation in a capillary, the resulting monolith, where it appears to be homogeneous, either does not have pores that are interconnected along its length or there is a loss of bicontinuity of the microemulsion upon filling or polymerisation. This result requires further investigation.

4.4 Conclusions

Monoliths prepared from microemulsions containing methyl methacrylate are not suitable for use as stationary phases for capillary electrochromatography. The use of DDAB prevents the cleaning of the monolith when packed into a capillary due to the high levels involved. Upon polymerisation, this blocks the resulting pores to the extent that it cannot be removed by a through flow of solvent.

At a low concentration of SDS in the presence of a co-surfactant blockage should not occur, however the resulting monoliths inside the capillary did not show a porous structure. This is possibly due to a partial collapse of the bicontinuous structure upon filling into capillaries or upon polymerisation. The method of filling of the capillaries has also been determined to be an important factor in the preparation. Care and a constant pressure are vital. There is potential for these MMA monoliths to be used as stationary phases for HPLC, however further investigation would be required.

4.5 References

1.   Chieng, T. H.; Gan, L. M.; Chew, C. H.; Ng, S. C.; Pey, K. L. *Polymer* **1996**, *37*, 2801-2809.

2.   Li, T. D.; Gan, L. M.; Chew, C. H.; Teo, W. K.; Gan, L. H. *Langmuir* **1996**, *12*, 5863-5868.

3.   Gan, L. M.; Liu, J.; Poon, L. P.; Chew, C. H.; Gan, L. H. *Polymer* **1997**, *38*, 5339-5345.

4.   Gan, L.-M.; Chew, C.-H. *Colloid Surf. A Physicochem. Eng. Asp.* **1997**, *123-124*, 681-693.

5.   Chew, C. H.; Li, T. D.; Gan, L. H.; Quek, C. H.; Gan, L. M. *Langmuir* **1998**, *14*, 6068-6076.

6.   Shindoa, K.; Hironobu, K. In *Microemulsions; Theory and Practice*; Price, L. M., Ed.; Academic Press, Inc.: New York, 1977, p 57-89.

7.   Chieng, T. H.; Gan, L. M.; Chew, C. H.; Lee, L.; Ng, S. C.; Pey, K. L.; Grant, D. *Langmuir* **1995**, *11*, 3321-3326.

Butyl Methacrylate Systems

5 Butyl Methacrylate Systems

5.1 Introduction

Monoliths prepared from butyl methacrylate have been successfully used as stationary phases for CEC [1,2]. Microemulsions prepared containing BMA in the oil phase will potentially yield monoliths with a porous structure. Alteration of the composition has been shown in previous experiments to affect the porosity of the resulting monolith. In this chapter we assess the conductivity of the microemulsions in order to determine whether the system is in a bicontinuous state and use NMR diffusion studies to give an insight into the phase structure. Porosity measurements and imaging using SEM show relationships between parent microemulsion composition and pore size of the resulting monolith.

5.2 NMR Diffusion Studies.

5.2.1 Introduction

Molecules in solution or in the liquid state have translational motion often referred to as diffusion or self diffusion. In the absence of interactions, i.e. at infinite dilution, the self diffusion of a spherical colloidal particle is given by the Stokes-Einstein relation:

$$D_0 = \frac{k_B T}{6\pi\eta R_H}$$

Equation 5.1

where k_B is the Boltzmann constant, T is the absolute temperature, η is the solvent viscosity and R_H is the hydrodynamic radius. Interactions become important at higher concentrations and the self diffusion coefficient decreases with increasing concentration. Another issue is that in the case of surfactants the mere act of altering

their concentration can have a dramatic effect on their self assembled structure (Equation 5.2, where k_D is a function of inter-aggregate potential). An increase in the molecular weight and hydrodynamic radius with concentration may not just imply a growth of micelles but the effect of interactions. The relative importance of these effects will depend on the composition and temperature of the solution.

$$D = D_0\left(1 + k_D c\right)$$

Equation 5.2

Work by Jönsson et al. [3] shows that the presence of spherical and rod shaped aggregates gives rise to minor obstruction effects in the continuous medium while oblate or disk shaped particles have a greater effect. Solvation also reduces the observed diffusion coefficient.

A system composed of a mixture of a hydrophile, a lipophile and an amphiphile (e.g. a surfactant) will be segregated into 'oil' and 'water' domains separated by a layer of surfactant molecules. Depending on the composition of the mixture, the size and shape of the domains differ, from finite aggregates, for example, or a structure where there is interconnection over macroscopic distances in one, two or three dimensions. NMR can be used to shed light on these issues providing information on the distribution of surfactant molecules and oil and water domains, enabling conclusions to be drawn as to whether the microemulsion is of an oil-in-water, water-in-oil or bicontinuous type. A component in the system can diffuse through the continuous phase as an individual molecule at a rate dependent on its concentration or can be transported with droplets subjected to Brownian motion. Diffusion of the droplets will be subjected to obstruction effects from other droplets. In the case of a bicontinuous system there will be an absence of a dispersed phase and the two

individual continuous phases will exhibit a diffusion similar to that of the 'pure' solvent.

In NMR, diffusion measurements are usually made using a magnetic-field gradient pulse to label molecules spatially. After a certain time (Δ) a second gradient is used to decode their new position. If the spins remain stationary during the time between pulses, the intensity and phase of the NMR signal after the second pulse will be independent of the strength and length of the gradient pulse. However, molecular motion due to diffusion will result in an attenuated signal as the spins will move between the phase labelling. The intensity attenuation is dependant on the gradient parameters (g, δ) and the diffusion time (Δ). The intensity change is described by Equation 5.3

$$I(\Delta,\delta,g) = I_0 \exp\left[-\gamma^2 g^2 \delta^2 (\Delta - \frac{\delta}{3})D\right]$$

Equation 5.3

where I is the observed intensity and I_0 is the unattenuated signal intensity. D is the diffusion coefficient, γ the gyromagnetic ratio of the observed nucleus, g the gradient strength, δ the length of the gradient and Δ the diffusion time.

In this experiment a conventional DOSY (diffusion-ordered spectroscopy) experiment was employed where the diffusion coefficient was measured by acquiring a series of one-dimensional spectra with different amounts of diffusion weighting. The diffusion coefficients are then calculated by fitting the variations in the intensities of the peaks between the spectra. The resulting coefficients are then plotted against chemical shift. Recent work by Morris et al. [4] has shown that one-dimensional DOSY measurements can yield the same results as conventional DOSY

using a nonuniform magnetic field gradient to encode the diffusion information into the line shapes of the peaks in the chemical shift dimension.

Söderman and Nyden investigated the microstructure of microemulsions using the NMR pulsed field gradient (PFG) method by which self-diffusion coefficients can be determined [5]. In fact, self-diffusion studies gave the first direct evidence for a bicontinuous structure [6,7].

By varying the magnitude (g) and the length (δ) of the spin or altering the distance between the leading edges of the gradient pulses (Δ) while keeping the distance between the rf pulses (beam of radiofrequency energy used to irradiate the precessing nucleus) constant, D can be determined by fitting Equation 5.3 to the observed echo intensities.

.In this case where a bipolar gradient for dephasing and rephasing is used a correction for the time τ between bipolar gradients is applied (Equation 5.4). This reduces the errors associated with the experiment including reducing the effects of radiation damping [8].

$$I(\Delta,\delta,g) = I_0 \exp\left[-\gamma^2 g^2 \delta^2 (\Delta - \frac{\delta}{3} - \frac{\tau}{2})D\right]$$

Equation 5.4

Generally, the equation holds true for microemulsion systems. The value of T_2 (spin-spin relaxation time) often limits the lowest value of D that can be measured. Slow diffusion is found in systems that show rapid transverse relaxation. As a consequence the echo intensity gets severely damped by T_2 relaxation. This problem is virtually non existent for microemulsion systems, while the accuracy for the surfactant molecules is often reduced because of T_2 effects. A basic pulse sequence is outlined in Figure 5.1.

Self diffusion of the solvent molecules (both oil and water) can give a direct insight into the connectivity of the domains and NMR relaxation of the surfactant molecules at different magnetic fields allows determination of the surfactant film curvature and thus aggregate shape and size.
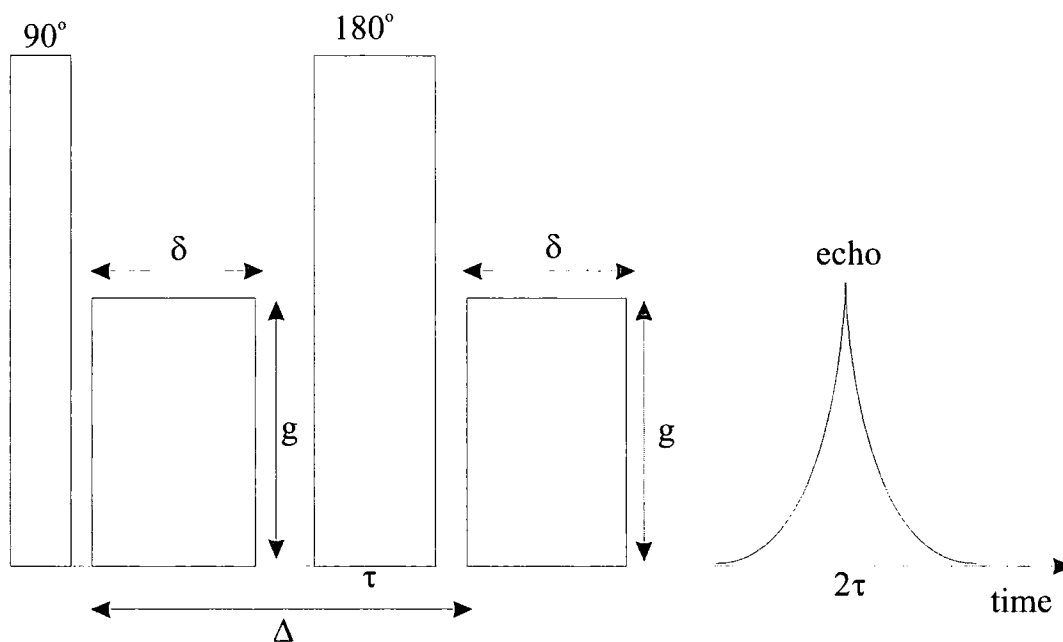
Figure 5.1 **Pulse sequence for a bipolar pulsed field-gradient spin echo (BPPGSE) experiment.**

In a simplified system consisting of one phase dispersed in another, if the droplets of the dispersed phase are considerably larger than that over which diffusion is measured the self diffusion of both components will be unrestricted and D values will be similar to those observed for the neat solvents. For microemulsions this case is invalid due to the reduced size of the structures observed. Where a surfactant system is in equilibrium, as in microemulsions, the aggregates or droplets extend over much smaller distances than the distances monitored in a diffusion experiment. This means that the experiment is sensitive to the translation of the droplet rather than the molecular displacement within the structure. The diffusion of the whole structure is going to be much slower than that of the displacement within it or a

solvent component of the microemulsion. Where we find a microemulsion of droplet type with one phase dispersed in the other the diffusion of the dispersed phase will differ greatly from that of the continuous phase.

The diffusion coefficients that can be measured using a PGSE experiment range from very fast diffusing small molecules in solution with D values of around $10^{-9} m^2 s^{-1}$ to very slow diffusion of polymers in more concentrated solutions where D values can be measured down to $10^{-16} m^2 s^{-1}$ [9].

5.2.2 Radiation Damping

Radiation damping affects intense signals in high field NMR. When the rotating transverse magnetisation of the sample induces a strong rf current in the detection coil (which produces the observed resonance) the current then induces its own rf field which is fed back to the sample. The damping of the signal produces a reduced apparent T_2. In the case of a DOSY experiment where diffusion is calculated from the exponential decay of the signal intensities, the initial peak intensity (I_0) will be attenuated by radiation damping to a greater extent than a less intense decayed signal detected at time Δ. A non linear attenuation effect by radiation damping will therefore reduce the gradient of the exponential and in turn decrease the calculated diffusion.

In the experiment discussed earlier these effects are not taken into account as the concern is not that of the actual diffusion but that of the relative diffusion. Further investigation will be required to ensure this is the case.

5.3   Experimental

5.3.1   Standard solutions

5.3.1.1   Aqueous amphiphile solutions.

Aqueous solutions of SDS and co-surfactant were made up as in Table 5.1 and subsequently. The ratio of SDS:co-surfactant was kept constant at 1:2 (by weight). Mixing of each solution was achieved by sonication.

Table 5.1 Aqueous phase stock solutions.

SDS/CS:water ratio (w/w)	SDS/g	Co-surfactant/g	Water/g
75:25	25.00	50.00	25.00
60:40	20.00	40.00	40.00
50:50	16.67	33.33	50.00
49:51	16.33	32.67	51.00
40:60	13.33	26.67	60.00
*30:70	10.00	20.00	70.00
20:80	6.67	13.33	80.00

*Composition forms a viscous gel type phase.

The following solutions were prepared and used in the 2nd part of this chapter.

5.3.1.2   SDS solution

40.00g SDS was dissolved in deionised water and made up accurately to 200ml.

5.3.1.3   AMPS solution

0.7500g AMPS was made up to 25g with 20% SDS solution.

5.3.1.4   Oil Phase

1.00g AIBN was dissolved in 60.00g BMA and 40.00g EGDMA.

5.3.2 General Procedures

5.3.2.1 Microemulsion Formation

Each microemulsion composition detailed in the appendices was prepared by adding the components in a glass vial and shaking. Where the determination of the phase boundary is required one phase is added to the other dropwise with stirring. To ensure stability each composition was allowed to equilibrate at room temperature for a minimum of 15 minutes. Where the phase region is determined using different co-surfactants phases were added to each other along the lines in Figure 5.2.
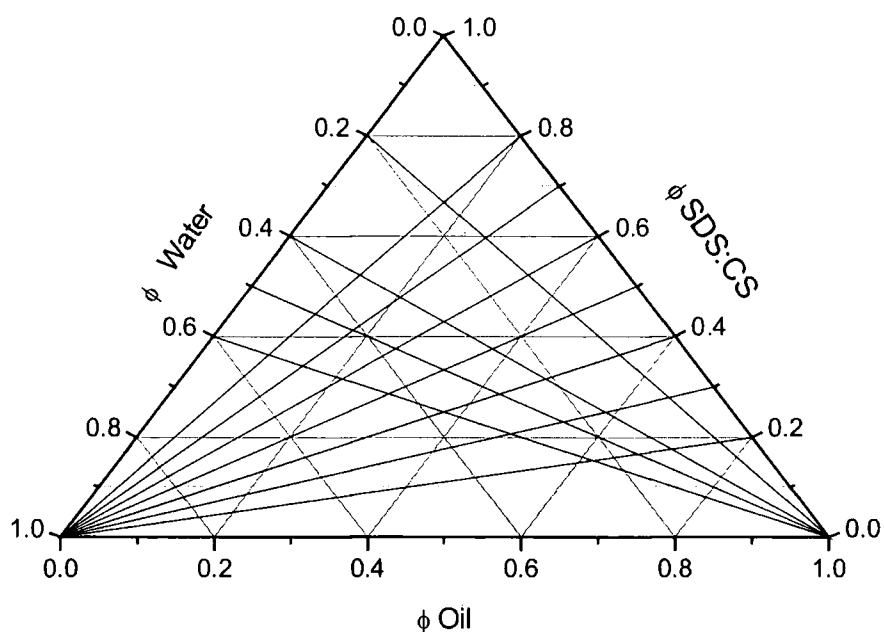
Figure 5.2   **Ternary diagram showing the lines along which phase regions were determined.**

5.3.2.2   Microemulsion Polymerisation.

Each composition was prepared in a glass vial as in 4.2.1.1 and purged with nitrogen for 10 minutes. The vials were then sealed and polymerisation took place in an oven at 60°C for 20 hours. After polymerisation the vials were fractured from around the resulting monoliths, which were then washed by Soxhlet extraction with methanol and dried in a vacuum oven at 50°C until a constant weight was achieved.

5.3.2.3   Capillary Preparation and Cleaning

Capillaries were filled with microemulsion using the glass filling apparatus found on page 63 of chapter 4.

75% of a 50cm length of capillary (100μm i.d.) was filled in each case and each end sealed with rubber. Each capillary was placed in the oven so that the outlet (unfilled) section of the capillary was raised above the inlet (filled) section. Polymerisation took place in an oven at 60°C for 20 hours.

After polymerisation the capillaries were inspected using a light microscope for inhomogeneous sections along the packed length.

Cleaning was carried out by fracturing a 5mm section from the inlet end of the capillary before attaching it to an HPLC pump. A mixture of acetonitrile and water (50:50 v/v) was applied at a flow rate of up to 2.5 ml/min. The maximum pressure was limited to 60 bar. 2 hours after a flow was obtained the water/acetonitrile was replaced with 5mM phosphate buffer in acetonitrile (20% v/v) at pH 7 and flushed for a further 4 hours.

5.3.3   Conductivity Measurements

Conductivity was measured using an in-house prepared platinum conductivity electrode. The platinum plates were 1cm^2 and 1cm apart attached to platinum wire

encased in a glass tube. The 100% oil composition was used to zero the conductivity

meter.
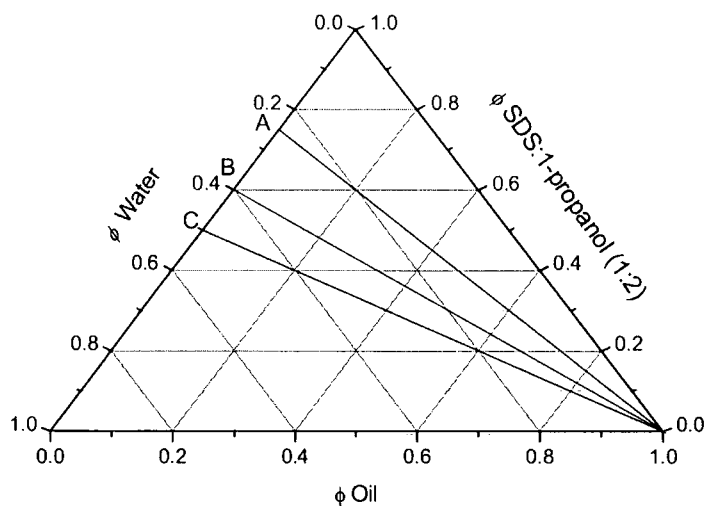
Figure 5.3 **Ternary phase diagram for conductivity measurements taken at**

5wt% increments of oil along lines A, B and C.

Aqueous phases were prepared as in Table 5.1 and 1-propanol was used as the co-

surfactant. Compositions were prepared using the procedures in 4.2.1.1 at 5 wt%

increments of the oil phase (60:40 BMA:EGDMA, w/w) along lines A, B and C in

Figure 5.3. All were well mixed and allowed to equilibrate at room temperature for

30 minutes. AMPS was added at 0.3 wt% of the oil phase.

Measurements were also taken using the 20 wt% SDS solution detailed in 5.3.1.2.

Measurements were taken at 40:60 (w/w) SDS$_{(aq)}$:1-propanol at 5 wt% increments of

oil phase.

5.3.4 Self diffusion measurements

All proton self-diffusion measurements were performed on a 500MHz Varian Unity

Ionova spectrometer. The relaxation delay was 20s with an acquisition time of 4s.

Gradient pulses were 2 ms with a delay of 50ms. The temperature was controlled at 21.0 +/- 0.1 °C. Diffusion was calculated from 25 points.

All experiments were carried out using an internal capillary containing deuterium oxide.

The protons of the EGDMA methacrylate group at 6.1 ppm were used in the evaluation of the oil diffusion coefficient. The protons of the dodecyl chain adjacent to the sulfate head were used to determine the surfactant diffusion coefficient.

5.3.4.1   *Sample preparation*

Samples were prepared on lines A and B of the ternary diagram in Figure 5.4.
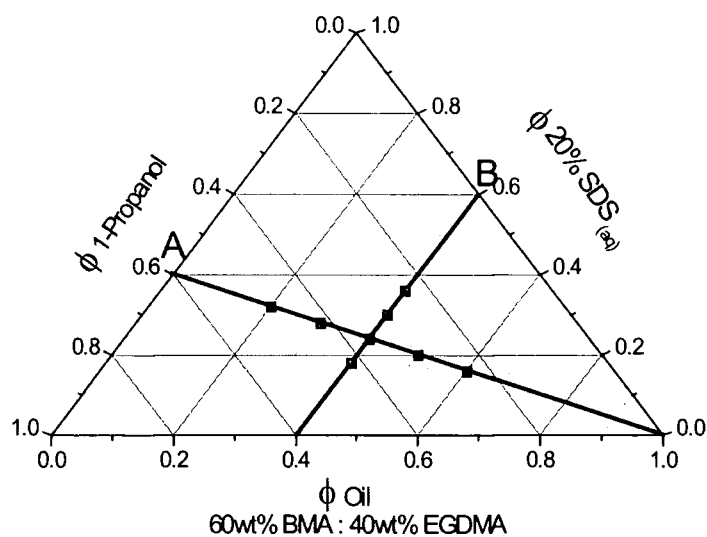
Figure 5.4   Ternary phase diagram of 60:40 BMA:EGDMA system. Points represent compositions used for self diffusion measurements.

Table 5.2 Compositions of the points on the ternary diagram in Figure 5.4

SDS$_{(aq)}$/1-propanol ratio	Oil (%)	SDS$_{(aq)}$ (%)	1-Propanol (%)	AMPS (% wrt oil)
40:60	0	40	60	0
40:60	10	36	54	0.3
40:60	20	32	48	0.3
40:60	30	28	42	0.3
40:60	40	24	36	0.3
40:60	50	20	30	0.3
40:60	60	16	24	0.3
40:60	100	0	0	0
30:70	40	18	42	0.3
50:50	40	30	30	0.3
60:40	40	36	24	0.3

5.4 Results and Discussion.

5.4.1 *Butyl methacrylate systems – 1.*

5.4.2 *Determination of the Phase Boundary where the Oil Phase is BMA*

Figure 5.5 indicates the compositions where a single phase is observed for microemulsions containing 100% BMA in the oil phase. Upon heating phase separation occurs prior to polymerisation and a block of poly(butyl methacrylate) results. An absence of cross linker prevents any gelling prior to phase separation and hence a loss of microemulsion structure. The compositions in appendix B1 –3 represent the compositions at the phase boundary.
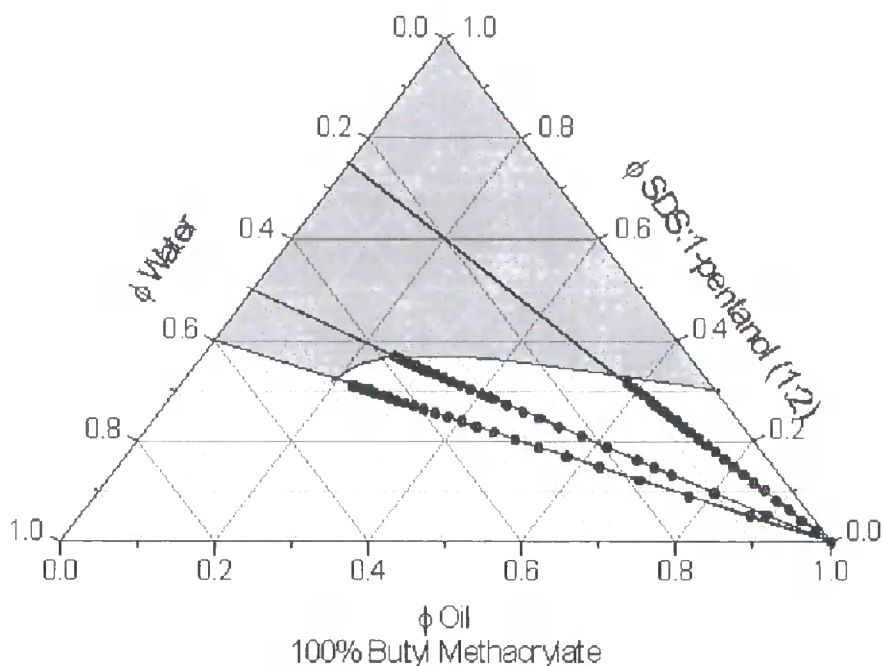
Figure 5.5   Ternary Diagram for 100% Butyl Methacrylate. Dots represent determined two-phase compositions and the shaded region represents the determined single phase region

5.4.3   The Effect of EGDMA on the Microemulsion Single Phase Boundary

With an increasing EGDMA level less oil can be stabilised at a constant amphiphile – water level. At 20 wt% EGDMA a transparent single phase was not formed with a mixture containing 60 wt% water. The compositions at the phase boundary can be found in appendix B4 – 7. Higher water levels are added here at the expense of surfactant and co-surfactant therefore there is less surfactant available to stabilise the microemulsion.

As the BMA is replaced by EGDMA the reduction in single phase area suggests an increase in the interfacial tension. This increase will require more surfactant to form a microemulsion. If EGDMA has a higher surface tension than BMA therefore γ_0 will be increased with increasing EGDMA level.

5.4.4   Microemulsions prepared from 95 wt% BMA and 5 wt% EGDMA

5.4.4.1   Microemulsion Phase Boundary

Figure 5.6 shows points at which a single phase is not formed when the oil phase contains 5 wt% EGDMA. The continuing line represents compositions into the single-phase region. The compositions represented in appendix B8 – 11 are the compositions at the phase boundary and were polymerised in capillaries.

The filled polymerised capillaries contained gaps in the packing to varying degrees along each length. This is possibly due to phase separation during the polymerisation process. As the compositions are on the single phase boundary there will be little change required to revert the microemulsion back to two phases. Where the amphiphile : water ratio is 40:60 (w/w) in this set of experiments more oil is able to be solublised than in the previous set of experiments. This is due to the presence of AMPS in the composition. When it is present may will increase the surface tension of the interface as it introduces charged species. The negative sulfate groups will be

repelled by the negative sulfate of the surfactant causing less efficient packing. As the area per surfactant is increased the interface free energy will increase resulting in an increase in interfacial tension.

SEM pictures in Figure 5.7 show monoliths prepared from the microemulsions at the phase boundary. Shown is both the fractured surface and the surface on the top of the monolith where it has not been in contact with the glass walls of the vial. From the fractured surface a porous structure made up of aggregates can be seen. It would appear that from these resulting structures the parent microemulsions were of an oil-in-water type and coalescence of the droplets upon polymerisation has resulted in a solid monolith.
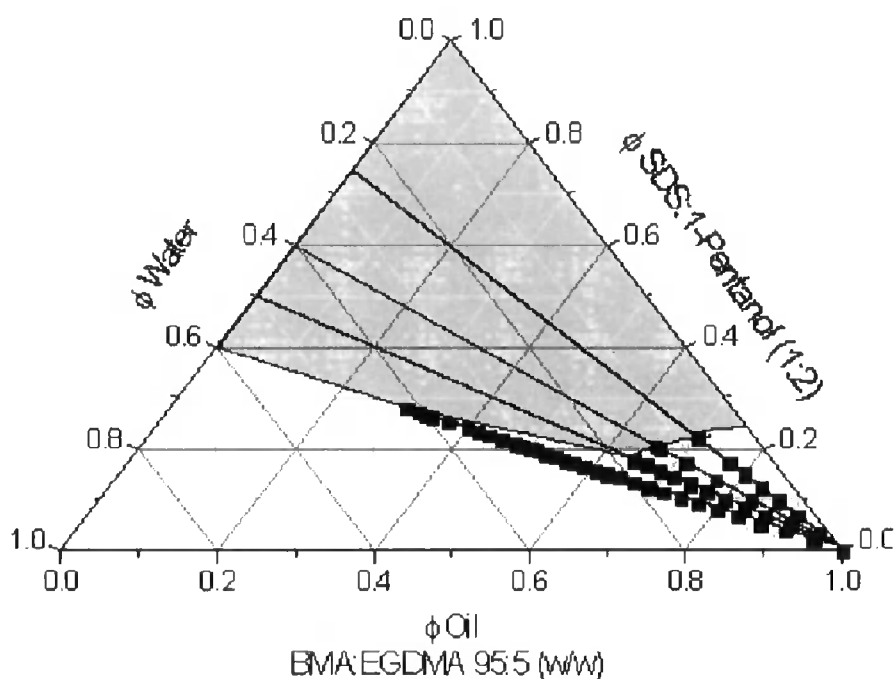
Figure 5.6   Ternary phase diagram for 95:5 BMA:EGDMA microemulsion. See text for details.

The air surface shows a non porous topography suggesting a microemulsion existing with an excess oil phase typical of a Winsor I type microemulsion prior to gelation. A layer of 'pure' oil phase would result in a non porous polymer film at the surface.

At higher oil levels the surface of the polymerised microemulsion becomes less porous resulting in a totally non-porous topography.

A less porous structure was also observed by Gan et al when preparing MMA microemulsions with polymerisable surfactants [10]

5.4.4.2 The Effect of Surfactant and Co-surfactant to Water Ratio

All of the capillaries produced were non-homogeneously packed. The foams are also quite firm indicating denser, stronger polymer aggregates.

Figure 5.8 shows that for the compositions in appendix B13 and 13 at a constant oil level (50wt%) there is no significant difference of varying the surfactant and co-surfactant content on the surface structure.

5.4.4.3 Effect of Oil Fraction on Topography of the Resulting Monolith.

As the water : SC ratio at a constant oil ratio is increased from 1/3 to 1 (appendix B14 –18), the surface topology of the polymerised microemulsion can be seen to change (Figure 5.9). There is only a slight change in the aggregates at the fractured surface as the water : SC ratio is increased. With an increase in water content wider channels can be observed above 40 wt% total water content. There also appears to be a greater coalescence of the aggregates resulting from a decrease in stabilising surfactant. At higher surfactant/co-surfactant levels there will be a greater stabilisation of the interface, less coalescence of the oil droplets and possible retention of the microemulsion structure. A great difference can be observed between the air and the fractured surface. At 50 times magnification the fractured surface shows a textured, potentially porous structure confirmed at higher magnification

whereas the air surface appears flat and non porous. At a high magnification a slight porosity is observed on the surface but not to the extent of the porosity of the fractured surface. Again this is possibly due to phase separation during polymerisation resulting in excess oil at the microemulsion surface.
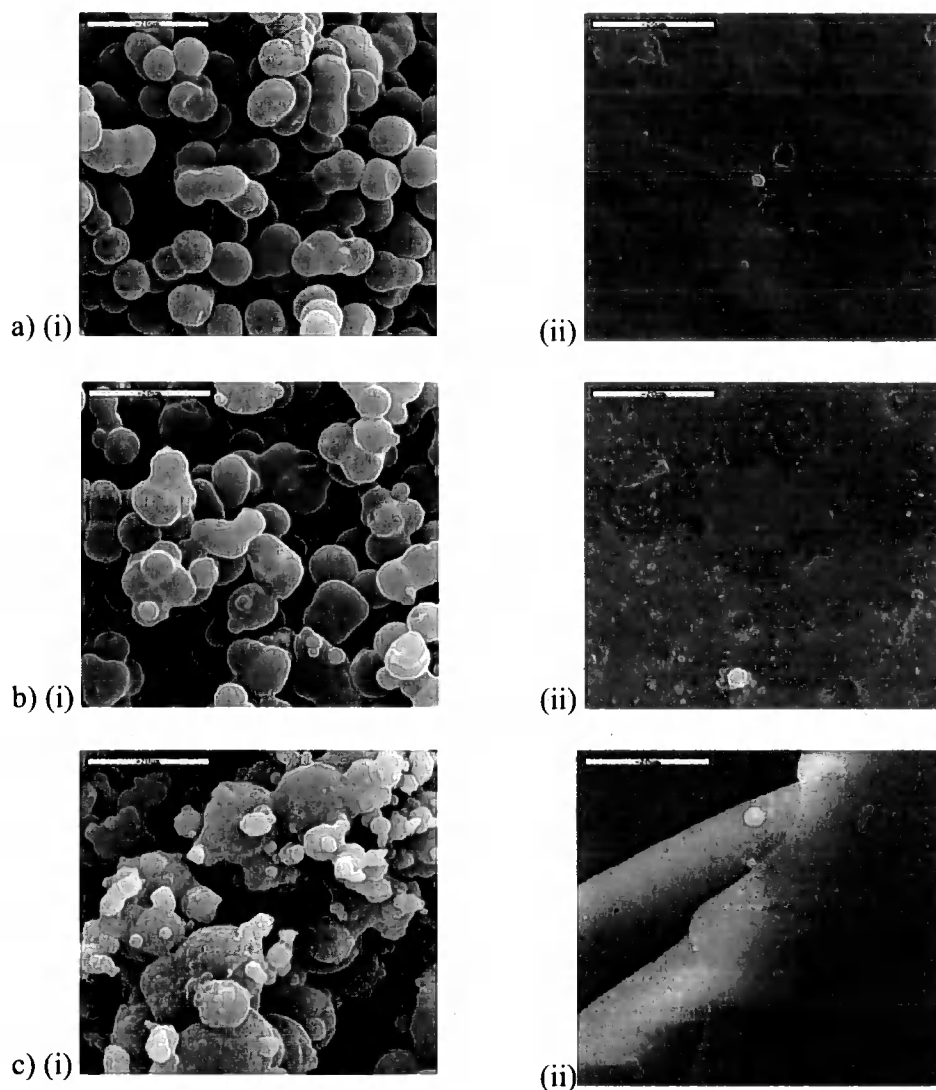
Figure 5.7 SEM images at 2000X magnification of monoliths prepared from the microemulsions at the phase boundary; (i) the fractured surface and (ii) the surface on the top of the monolith where it has not been in contact with the glass walls of the vial. a) 70.6 wt% oil, 7.3 wt% SDS, 14.7 wt% 1-pentanol, 7.3 wt% water; b) 66.1 wt% oil, 6.8 wt% SDS, 13.6 wt% 1-pentanol, 13.6 wt% water; c) 48.7 wt% oil, 8.6 wt% SDS, 17.1 wt% 1-pentanol, 25.7 wt% water.
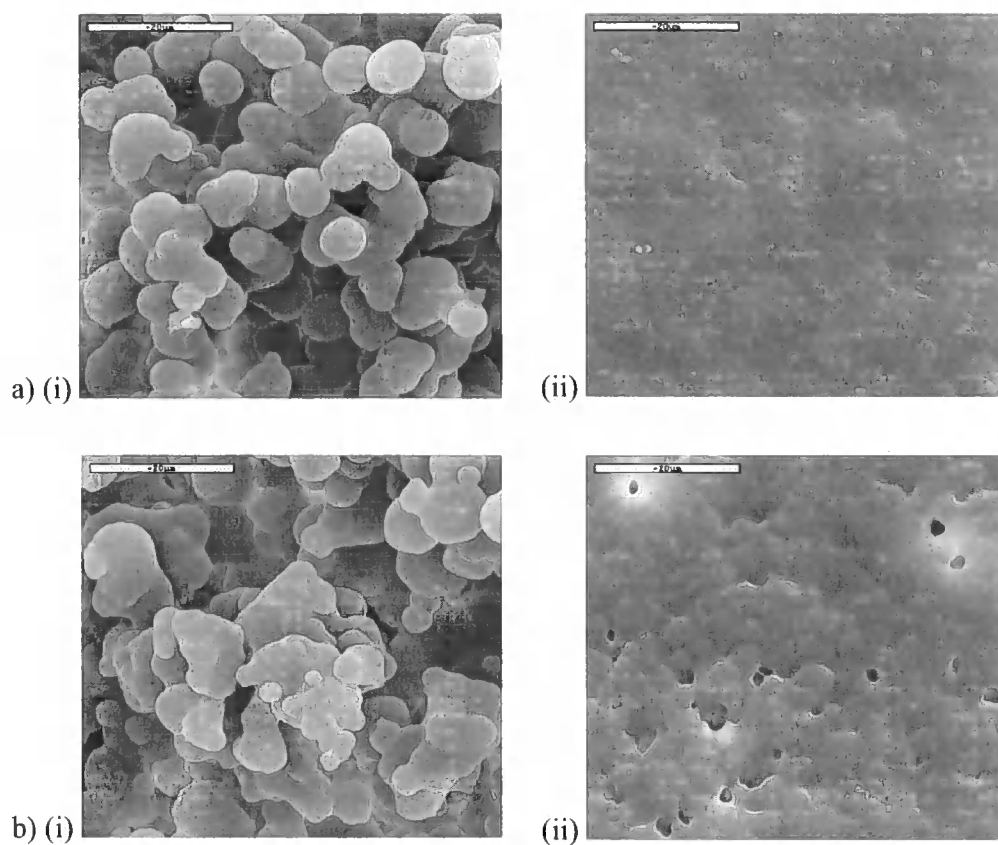
Figure 5.8 SEM images at 2000X magnification of (i) the fractured and (ii) nonfractured surface of monoliths prepared from microemulsions containing 50.0 wt% oil. a) 12.5 wt% SDS, 25.0 wt% 1-pentanol, 12.5 wt% water; . b) 10.0 wt% SDS, 20.0 wt% 1-pentanol, 20.0 wt% water.
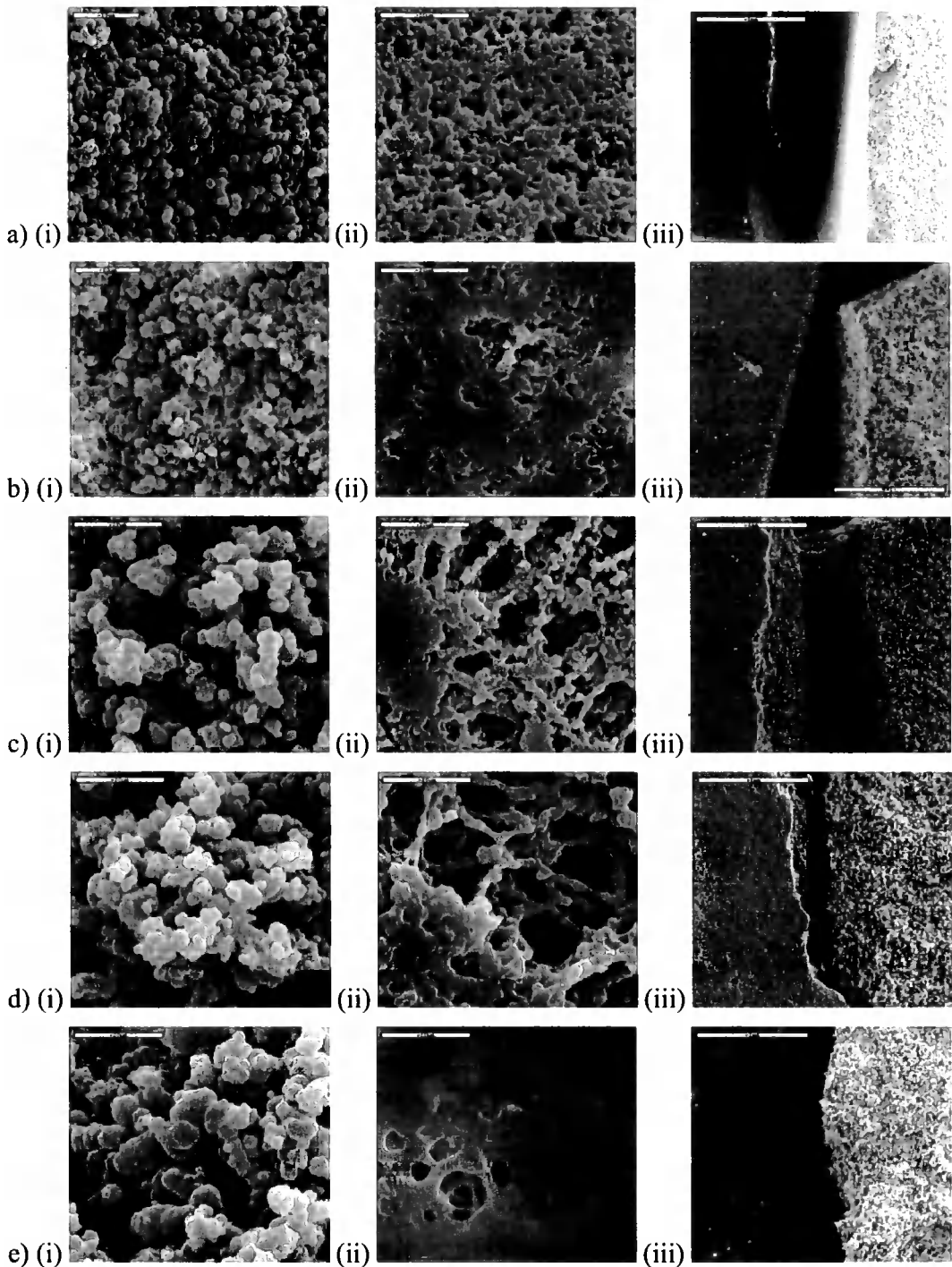
Figure 5.9 SEM images showing the effect of various SDS:1-pentanol:water ratios Images a – e represent parent compositions in appendix B14 – 18 respectively; i) the fractured surface at 600X magnification, ii) unfractured surface, iii) compares the air surface (left) and the fractured surface (right), c) shows the unfractured surface (left) and the fractured surface (right) at 50X magnification.

5.4.5 *Microemulsions prepared from 80 wt% BMA, 20 wt% EGDMA*

5.4.5.1   Determination of Single Phase Microemulsion Compositions and Composition Effect on Monolith Structure

Figure 5.10 shows points in the single phase region (filled) and those in the two phase region (unfilled). The percentage compositions of each can be found in appendix B19 – 35.
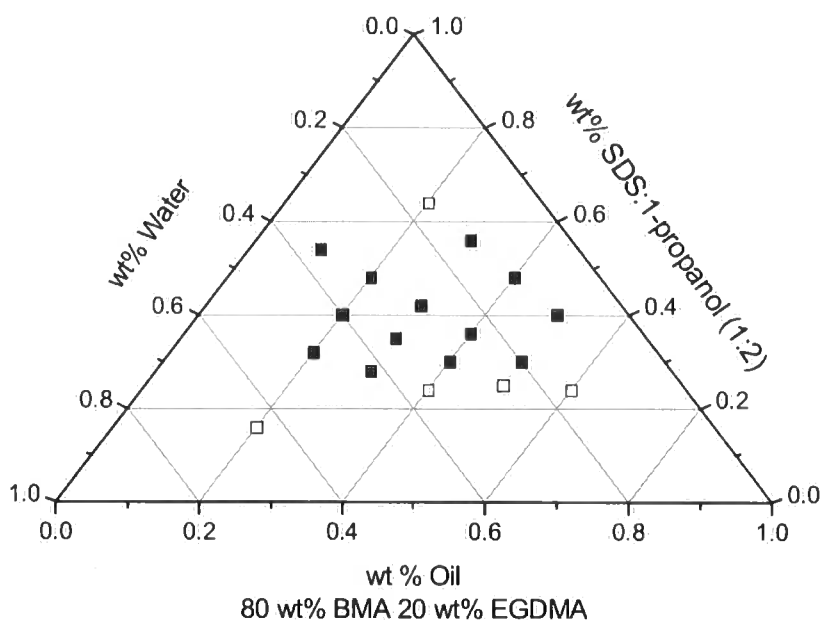
Figure 5.10 Ternary phase diagram for 80:20 BMA:EGDMA microemulsions (□) two phase, (■) single phase.

Figure 5.11 shows that there is little change in the void size left by the water channels upon polymerisation with variation of surfactant/co-surfactant : water ratio. SEM images in Figure 5.12 show that at high oil fractions the monoliths exhibit a non porous film at the air interface. This film is connected to the porous section and extends about 250 μm into the monolith (Figure 5.13) indicating the bicontinuous section of the microemulsion is in equilibrium with excess oil prior to gelling. At 60

101

wt% oil, 16 wt% water the parent microemulsion has two visible phases which appear to consist of a microemulsion region below a thin layer of oil. Upon polymerisation the non porous layer on the surface on the monolith is about a millimetre thick.

(a)

(b)

(c)
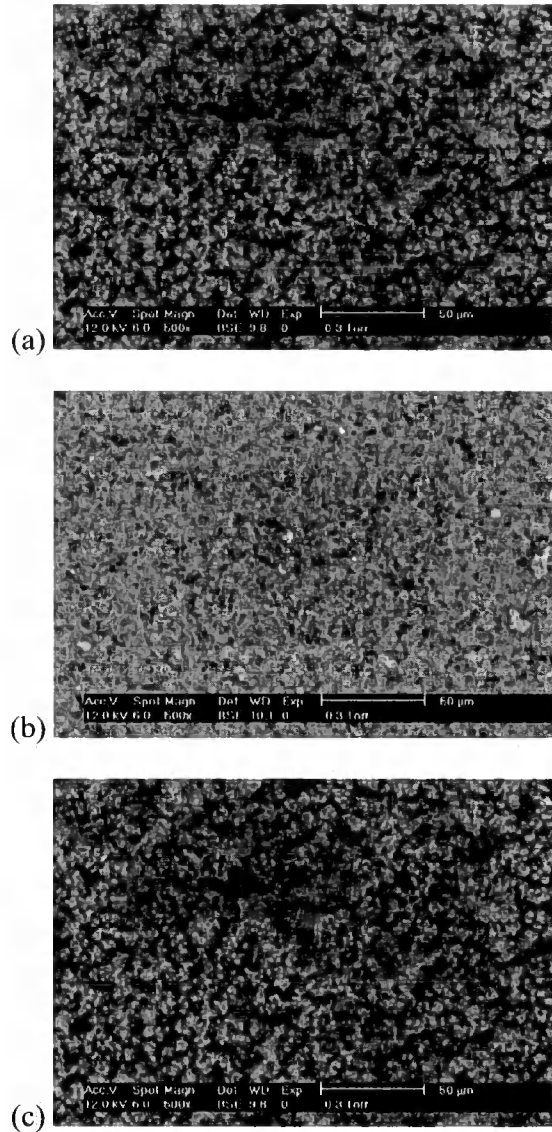
Figure 5.11 SEM images (500X magnification) of the fractured surface of monoliths prepared from microemulsions containing 30.0 wt% oil. (a) 35.0 wt% water, 11.7 wt% SDS, 23.3 wt% 1-propanol; (b) 28.0 wt% water, 14.0 wt% SDS, 28.0 wt% 1-propanol; (c) 14.0 wt% water, 18.7 wt% SDS, 37.3 wt% 1-propanol
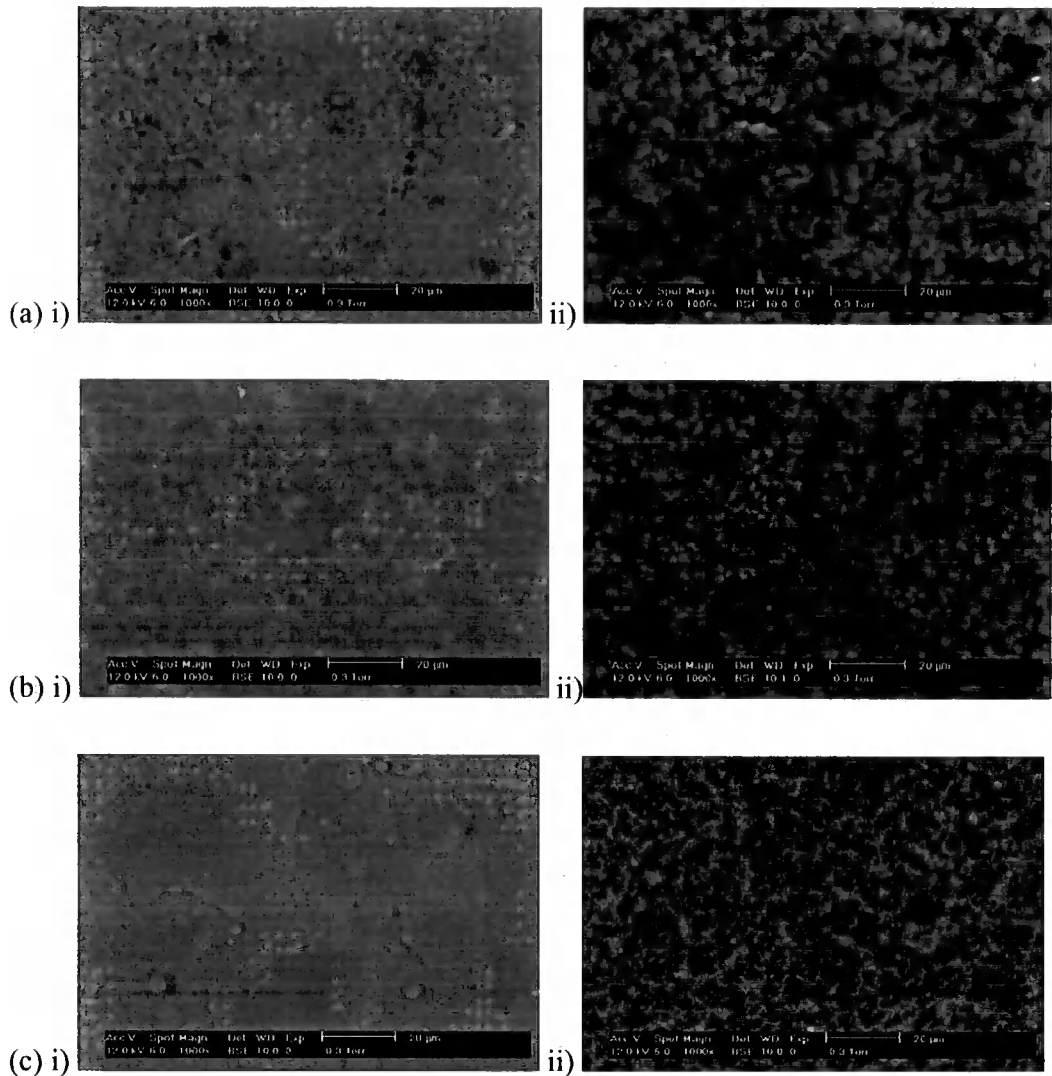
Figure 5.12 SEM images (1000X magnification) of the monolith surface polymerised in contact with air (i) and the fractured section (ii) of monoliths prepared from (a) 50.0 wt% oil, 20.0 wt% water, 10.0 wt% SDS, 20.0 wt% 1-propanol; (b) 60.0 wt% oil, 16.0 wt% water, 8.0 wt% SDS, 16.0 wt% 1-propanol; (c) 50.0 wt% oil, 10.0 wt% water, 13.3 wt% SDS, 26.7 wt% 1-propanol

From the fractured surface shown in Figure 5.13 the interconnecting water and oil domains can clearly be seen.

Figure 5.14 shows a linear increase in modal pore diameter with increasing oil level from 20 wt% to 50 wt%. This increase is not observed above 50 wt% oil possibly due to the conversion from a bicontinuous structure extending all the way to the surface of the microemulsion to a microemulsion where the bicontinuous region coexists in equilibrium with an excess oil phase.
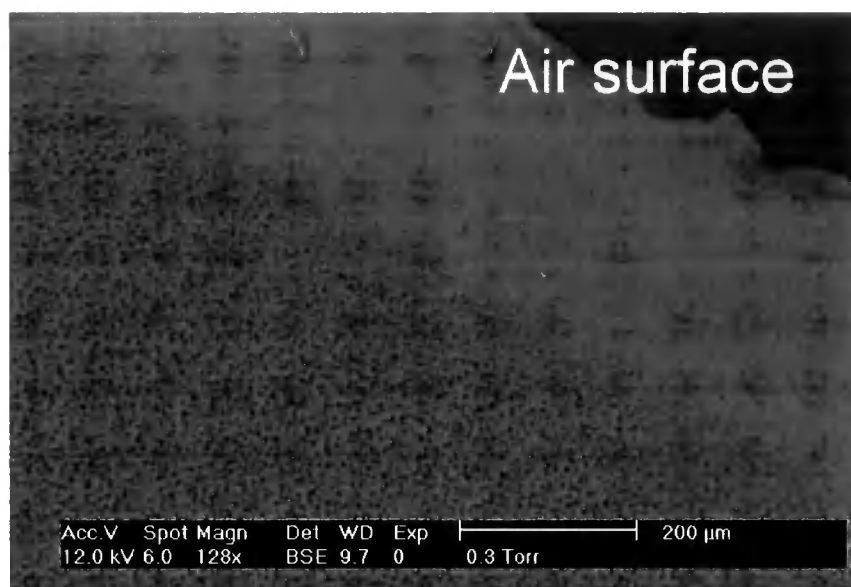
Figure 5.13 SEM image of the longitudinal cross section of a monolith prepared from 50 wt% oil (20 wt% EGDMA 80 wt% BMA), 20 wt% water, 10 wt% SDS, 20 wt% 1-propanol.

Figure 5.15 shows SEM images of the monoliths prepared with constant SDS and 1-propanol to water ratio. The channels and aggregates of the monolith prepared containing 10 wt% oil are narrow and small. The resulting monolith did not hold its structure and collapsed on drying.

The surface area can be seen from Figure 5.14 to be inversely proportional to the weight fraction of oil. As the size of the pores increases the surface area decreases. The increasing oil level is coupled with a decrease in water and surfactant. This will result in a decrease in channel width. With less stabilising species available the oil

channels will be more susceptible to coalescence and the aggregates will grow. Larger aggregates do not pack as efficiently as the smaller ones, resulting in more free space between them. The surface area increases with increasing amounts of surfactant and water as there are more smaller aggregates giving overall a larger surface area.

Figure 5.16 shows the region which has been determined to produce two phase systems. The compositions at the phase boundary can be found in appendix B36 – 38. The unmapped region is potentially single phase. This region contains high amounts of surfactant and low levels of oil. The high level of surfactant could result in difficult cleaning of the monoliths inside the capillaries.

Table 5.3   Pore diameter and surface area data for a range of compositions of 60:40 BMA:EGDMA microemulsions. (n = 2-6.)

SDS/1-pentanol: water ratio		Pore Diameter (μm)		Surface Area (m^2/g)	
	Oil wt%	Average	stdev	Average	stdev
40:60	20	2.253	0.0122	5.760	0.0049
50:50	30	3.242	0.0054	3.820	0.0530
60:40	20	1.946	0.0031	7.220	0.0219
60:40	30	2.643	0.0146	4.516	0.1301
60:40	40	3.187	0.0066	2.785	0.0460
60:40	50	3.902	0.0110	1.772	0.0177
60:40	60	3.718	0.0006	1.164	0.0339
80:20	30	5.719	0.2978	1.605	0.0064
80:20	40	5.758	0.0238	1.267	0.0438
80:20	50	0.607	0.0001	11.476	0.0580

The capillaries filled with monolith prepared from parent microemulsions containing 13 wt% SDS, 26 wt% 1-pentanol, 38.8 wt% water and 22.2 wt% oil were homogeneously filled containing no gaps along the length of the packing. After cleaning and flushing with buffer solution a current of 1.6 to 1.8 μA was achieved when a 20cm packed length was attached to the CE and a voltage of 25kV was applied. This current was only steady for approximately 5 minutes. In this case the vials containing the buffer solutions were held at atmospheric pressure. It has previously be shown [11] that a constant pressure needs to be applied to the inlet and outlet vials in order to prevent degassing of the buffer solution at heterogeneous sections of the packing where there may be differences in electroosmotic flow.
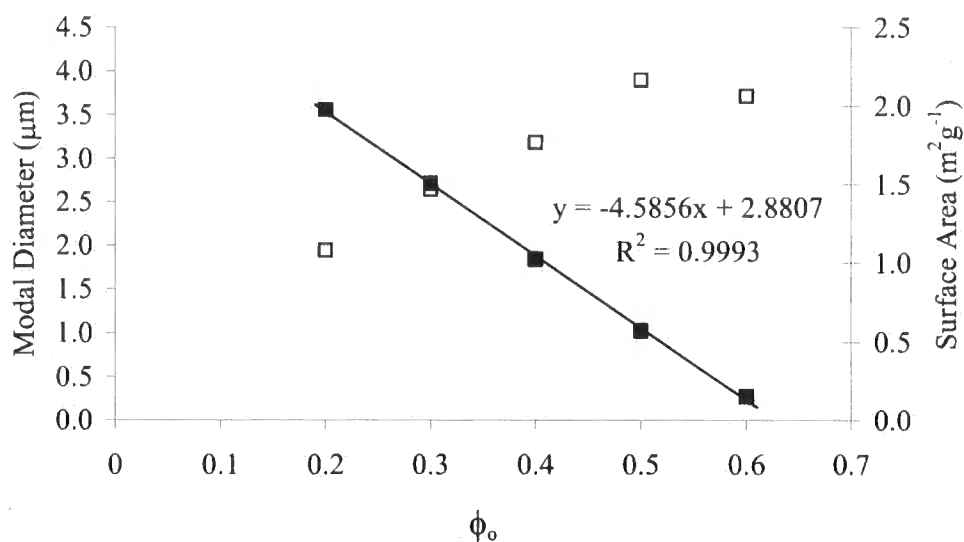
Figure 5.14 Modal pore diameter (□) and surface area (■) against oil fraction, ϕ_o. The remaining fraction consists of SDS, 1-propanol and water in a 20:40:40 ratio. The error bars are smaller than the data points.
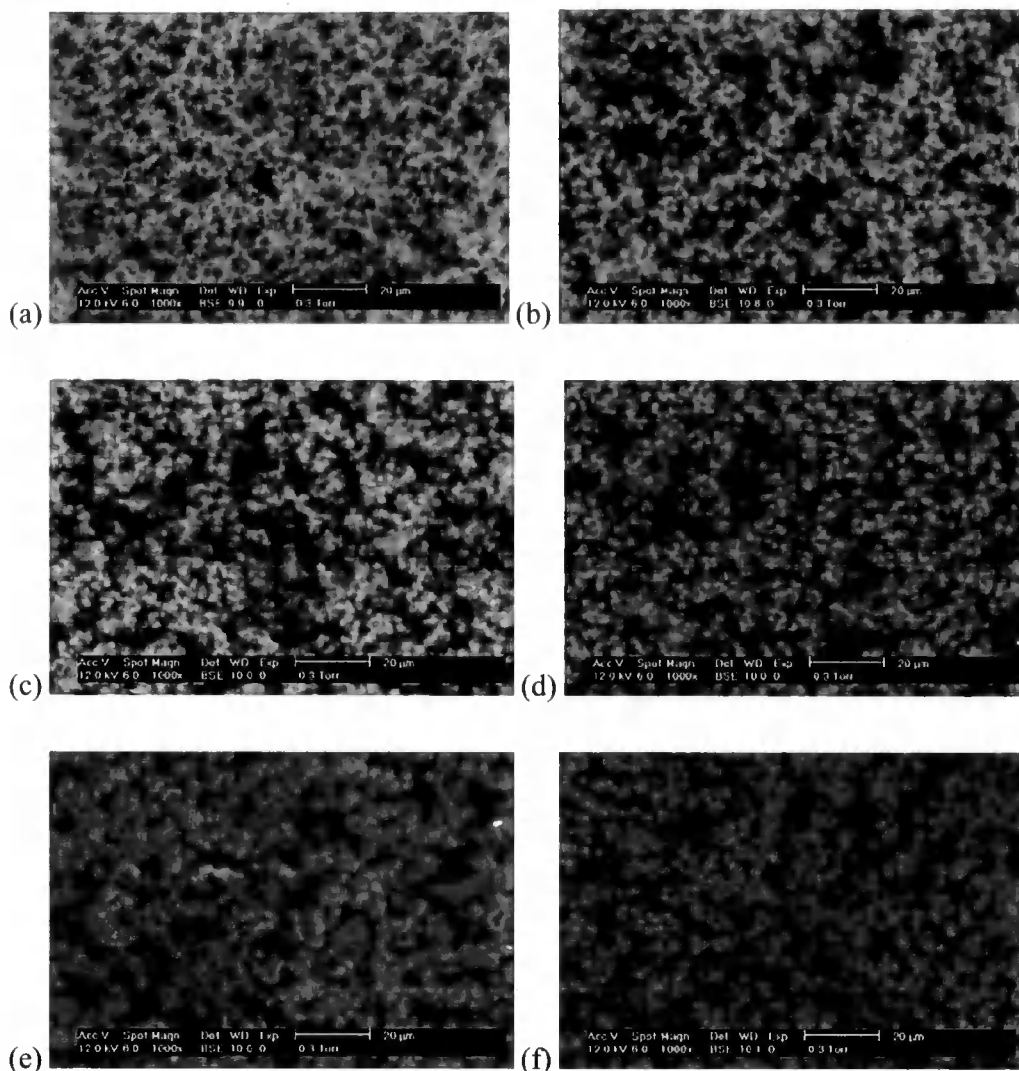
Figure 5.15 Parent microemulsions contain a) 10 wt%, b) 20 wt%, c) 30 wt%, d) 40 wt%, e) 50 wt%, f) 60 wt% oil. The surfactant, 1-propanol and water are in 20:40:40 wt% ratio making up the remainder of the microemulsion.
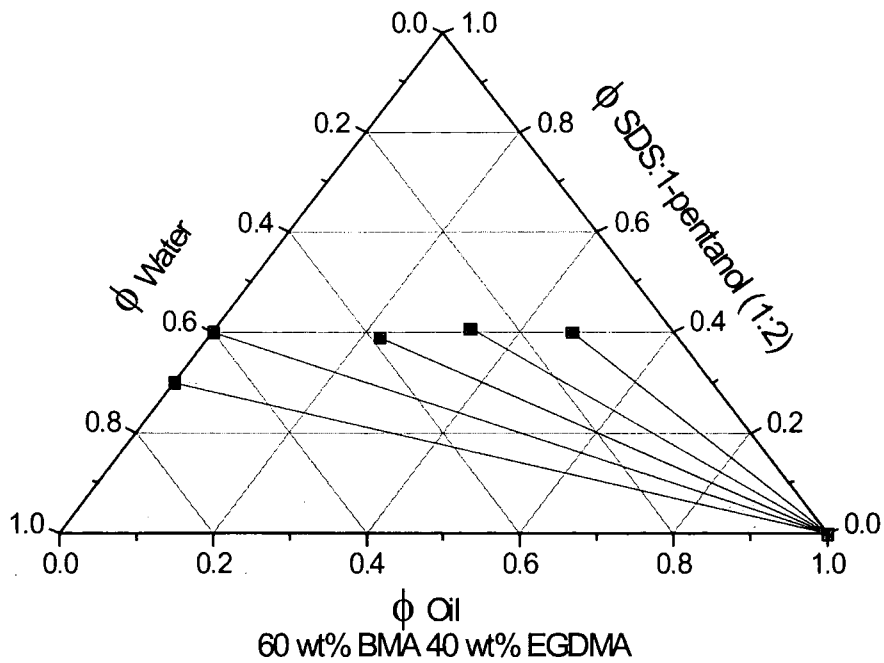
Figure 5.16. Ternary phase diagram for the system containing SDS, 1-pentanol, water and oil where the oil consists of 60 wt% BMA and 40 wt% EGDMA. The lines show the non optically homogeneous region.

5.4.6 The Effect of Co-surfactant Species

5.4.6.1 Effect on Microemulsion Boundary Determination

The most important quantities, which control all structuring processes in microemulsions are free energy and entropic factors as well as the curvature free energy. This energy can be described by the Helfrich equation, Equation 5.5.

$$F = \frac{1}{2}\kappa(C_1 + C_2 - 2C_0)^2 + \overline{\kappa}C_1C_2$$

Equation 5.5

Here, κ and $\overline{\kappa}$ are the mean and the Gaussian bending elastic constants. C_1 and C_2 are the curvatures of the formed structure and C_0 the spontaneous curvature. The first term in Equation 5.5 characterises the rigidity, the energy required to bend a unit area of interface by a unit amount of curvature. The role of the second term is a change in

membrane topography and subsequently phase transition. The elasticity parameters, κ, $\bar{\kappa}$ and C_0 depend strongly on the type and concentration of surfactant and co-surfactant, salt concentration, and also temperature. A calculation of the dependence of the curvature elasticity on chain length when mixing a surfactant and co-surfactant has been published [12] where the replacement of long chain molecules by short ones is shown to be efficient in lowering the bending constant κ of the surfactant film. Reducing the alcohol chain length this the interfacial membrane and in turn causes a reduction of the rigidity modulus k_c [13].

Figure 5.17 shows a change in the position of the single phase boundary dependent on the co-surfactant. Compositions on the phase boundary can be found in appendix B39 – 78. The smaller the alcohol chain length the less it will penetrate the interface. The addition of an alcohol as a co-surfactant will reduce the interfacial rigidity by causing a thinning of the mixed membrane and a larger single phase region will be obtained. The observed effect of the co-surfactant may also be due to its partitioning between the oil and water phases and the interface.

5.4.6.2   Effect of Co-surfactant on the Porosity of the Resulting Monolith

Polymerisation of microemulsions represented by the points in Figure 5.18 and detailed in appendix B79 – 90, gives monoliths with pore diameters and surface areas outlined in Figure 5.19. The composition containing 33 wt% oil and 1-pentanol falls outside the single phase range and therefore would not form a monolith upon polymerisation. As discussed earlier a decrease in pore size is coupled with an increase in surface area. The results show that an alteration of the co-surfactant can also be used in tailoring the pore size of the resulting monoliths. Changing the co-surfactant chain length from C_5 to C_3 has a greater effect at lower oil levels. At 18 wt% oil the modal pore size decreases by 42% from 1.64 to 0.95 μm possibly due to

the effect of destabilisation and coalescence overwhelming the effect of the co-surfactant. This is coupled with an increase in surface area from 7.13 to 11.34 m^{2}g^{-1},

(i)

(ii)

(iii)
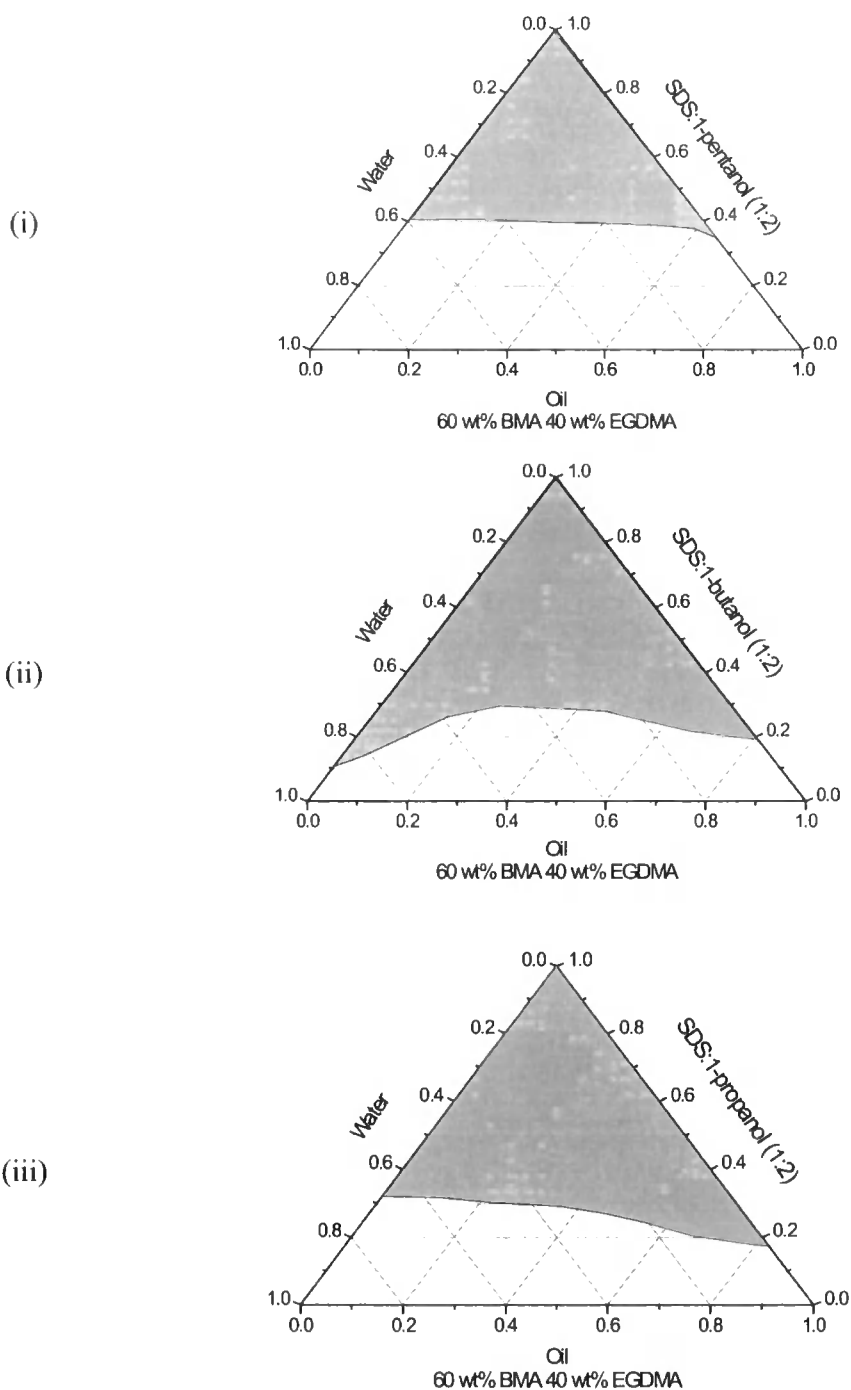
Figure 5.17 Pseudo ternary phase diagrams for systems containing SDS, water, oil (60:40 BMA:EGDMA) and (i) 1-pentanol; (ii) 1-butanol and (iii) 1-propanol. The shaded area represents the single phase region.

an increase of 59%. This is compared to a decrease in surface area of 0.6 % and an increase in modal pore diameter of 19 % for the monolith prepared where the parent microemulsion contains 41 wt% oil. At a low level of oil, (18 wt%) the resulting monolith shows the highest surface area and the lowest pore diameter. Increasing the oil level increases the pore size and subsequently reduces the surface area. This is due to smaller aggregates having a larger overall surface area than the aggregates resulting from monoliths prepared using higher fractions of oil. The SEM images in Figure 5.20 show there is no significant difference in the pore structure to support the corresponding changes in pore size and surface area. For the monoliths prepared using 1-propanol there is a greater range of pore size and surface area available for investigation therefore further systems are prepared using this as the co-surfactant.

Using Figure 5.18 as a reference, the pore size increases along lines A and B as the oil level is increased at a constant surfactant/co-surfactant: water ratio and coalescence of the oil domains is more probable in a less stable system. The pore size decreases along lines D and E where the water level is reduced at a constant oil : surfactant/co-surfactant ratio. This will be due to a constant surfactant/co-surfactant film and an increasing water domain. Rather than produce an expanded interface the intertwining water domains will widen resulting in an increased modal pore size. The reverse is true regarding surface area due to packing mechanics. Along line C there is little change in surface area at constant water to oil ratio with a surfactant/co-surfactant. There is however, an increase in pore size possibly due to the introduction of more co-surfactant. The exception is the surface area along line C for the composition prepared using 1-propanol. The pore size decreases slightly.
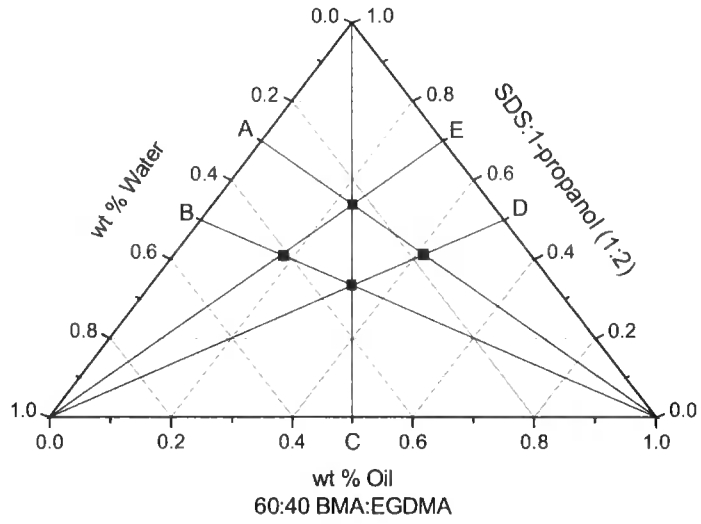
Figure 5.18 Ternary diagram showing the compositions from which monoliths were produced using either 1-pentanol, 1-butanol or 1-propanol.
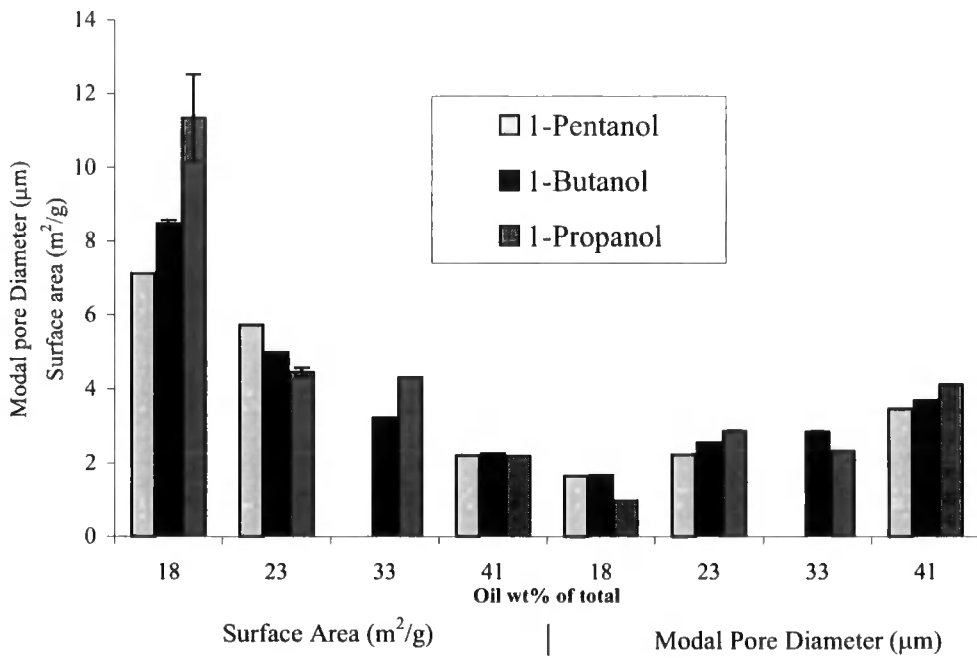
Figure 5.19 The effect of co-surfactant type and concentration on surface area and pore size.
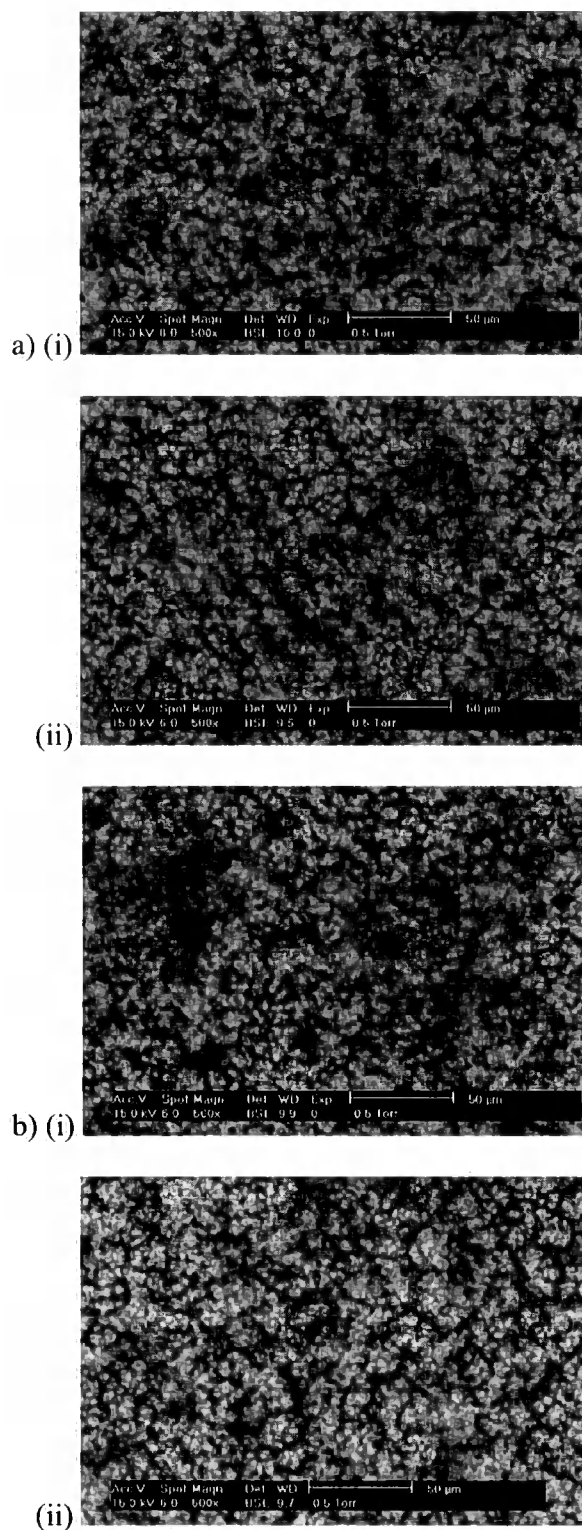
Figure 5.20 Monoliths prepared from microemulsions along line C of Figure 5.18 containing approximately equal proportions of oil and water. a) 1-propanol; b) 1-butanol (i) 23 wt% oil; (ii) 33 wt% oil.

5.4.7 Effect of Surfactant to Water Ratio on Conductivity

From the three lines in the ternary diagram of the 2:3 EGDMA:BMA system, the single phase microemulsions were formed between 30 and 40 wt% SCW. Where the SDS and 1-propanol is in a 50% ratio to the water the single phase at 40 wt% exhibits a bluish tint due to increased light scattering suggesting it is composed of a dispersed and continuous phase rather than a bicontinuous phase.

Where the microemulsion is in a two-phase or oil continuous state, containing mainly oil, the conductivity approaches that of the pure oil. As the oil level is decreased a water continuous state is reached enabling a flow of ions. Phase inversion to a water continuous phase would result in a sharp change in conductivity over a narrow oil fraction range to that of the 'aqueous' phase. In Figure 5.21 a gradual increase in conductivity with decreasing oil concentration from a critical composition referred to as the percolation threshold can be seen [14]. This gradual phase inversion suggests there is an intermediate structure(s) present as well as an observed increase due to the increase in surfactant content of the microemulsion.

The conductivity slope of the higher SDS composition is shallower due to larger micelles in solution, which will have a slower mobility than the more dilute composition.

A higher concentration of surfactant should yield a higher conductivity due to the increased ion concentration. However, this is not observed here. As the surfactant levels increase the molecules will arrange into organised structures. Equation 5.6 expresses the electrical conductivity, K of a microemulsion as a function of the electrostatic migration of individual ions and microemulsion globules in the continuous water phase. Counter-ions bind to micelles [15] and it is assumed that they will bind to the droplets in a microemulsion. The net valence of a droplet

depends on the total number of ionic surfactant molecules at the interface and the number of counter-ions, which move with the droplet when an electric field is applied. Assuming ions flow only in water continuous states, the electrical conductivity of a microemulsion has been expressed by Lam and Schechter [16].

$$K = \omega_{wc} \frac{e^2}{kT} \left\{ \Sigma Z_i^2 C_i^{(wc)} \overline{D}_i^{wc} (1 - \phi_o)^2 + Z_m^2 D_m^{(wc)} N_o^* \right\}$$

Equation 5.6

Where ω_{wc} is the volume fraction which is water continuous, e is the fundamental unit of charge, Z_i is the valence of ion i, C_i is the concentration of i, $\overline{D}_i^{wc}$ is the molecular diffusivity of i in the water continuous phase, φ is the oil phase volume fraction, Z_m is the net valence of the droplet, N_o^* is the number of oil drops per unit volume and D_m is the Brownian diffusion coefficient of a droplet given by the Stokes-Einstein equation

With more surfactant in solution there is a limited packing density at the interface. Once the interface is saturated with surfactant molecules and counter ions the remaining molecules in the water continuous phase will self assemble into organised structures. As the conductivity is related to the motion of ions in the aqueous phase, which at a higher surfactant level will contain a greater number of larger aggregate structures subject to more obstruction effects there will be a hindrance of their diffusion with a resulting drop in conductivity.
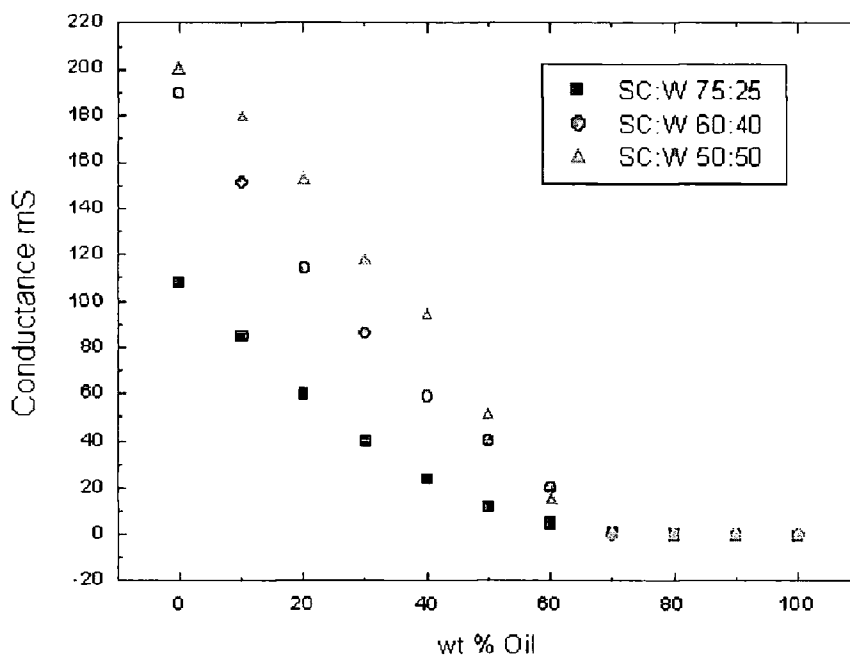
Figure 5.21 The effect of surfactant concentration on conductivity

5.4.8   Butyl methacrylate systems – 2.

5.4.9   Microemulsion boundary where the oil phase is BMA and EGDMA

The bold lines shown in Figure 5.22 indicate a large single phase microemulsion region. This provides many potential compositions available for analysis. The corresponding percentage compositions of the phase boundary can be found in appendix C1-3.

5.4.10   Effect of composition on pore size

Determining the pore size of the monoliths prepared from the microemulsions in appendix C4 - 7 enables us to assess the degree to which we can alter the pore size by only altering the weight fraction of surfactant solution, co-surfactant and oil. The resulting pore sizes of the monoliths and the corresponding compositions of the parent microemulsions can be found in Table 5.4. It is shown that at equal weight fractions of SDS solution and 1-propanol, increasing the oil fraction increases the pore size. As the oil level is increased the amount of surfactant available to stabilise

116
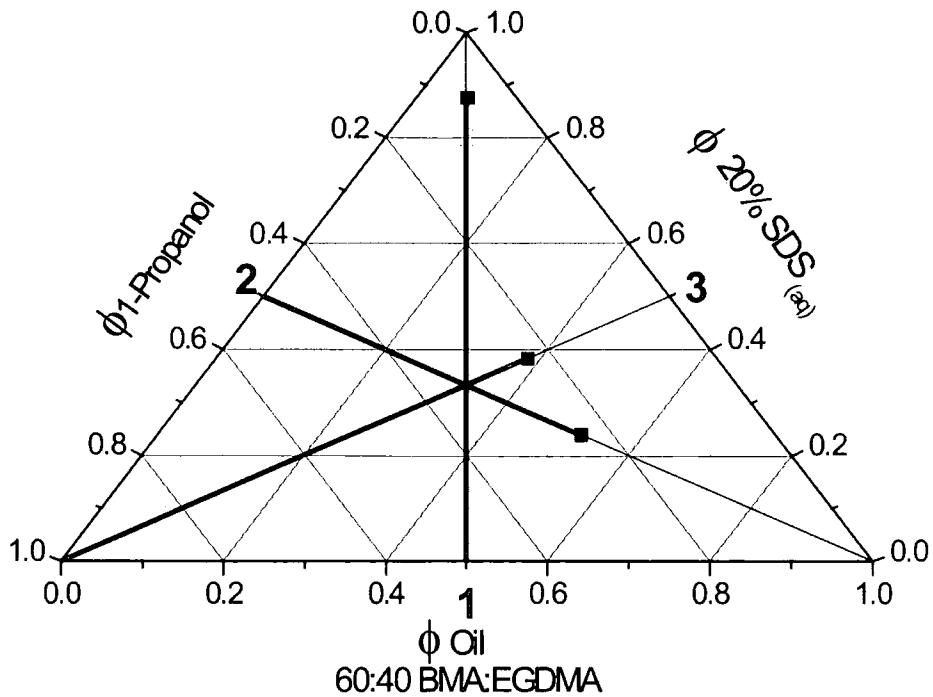
Figure 5.22 **Ternary phase diagram showing a large single phase microemulsion region (weighted lines). Squares represent points on the single – two phase boundary**

the interface is decreased. The oil domains are more prone to coalescence and as this happens the width of the aqueous domains will widen resulting in a larger modal pore size. From Figure 5.23 a marked decrease in surface area can be seen as the oil level is increased from 18 wt% to 33 wt% at equal levels of SDS solution and 1-propanol. The SEM images in Figure 5.24 (a and c) show that the monolith prepared from 18 wt% oil has smaller aggregates with slightly narrower channels through them. A small aggregate size will increase the overall surface area of the monolith. At constant oil to surfactant solution weight fractions, increasing the 1-propanol fraction by 20 wt% increases the modal pore size from 3.8μm to 10.7μm. The surface area also increases from $0.26m^2g^{-1}$ to $1.60 \ m^2g^{-1}$. An increase in surface area with pore size suggests additional structural features on the surface of the aggregates. From the SEM images in Figure 5.24 (b and c) the monoliths prepared with 23 wt%

oil appears to have wider channels than the monolith prepared with 33 wt% oil in agreement with the porosimetry results. The resolution of the ESEM at high magnifications is not high enough to determine clearly any substructure of the material. Upon polymerisation of microemulsion 4 containing 41 wt% oil there was some structural collapse and the resulting monolith was structurally tough and very difficult to fracture suitably for porosity analysis. In Figure 5.24 the smaller aggregates and close packed structure of the monolith containing 41 wt% oil can be seen This correlates with indications of microemulsion collapse.

All of the microemulsions formed an optically homogeneous phase. Upon polymerisation, all formed solid monoliths. The filled capillaries all appeared visually to be homogeneously filled. Upon attachment to the HPLC pump, compositions 1 - 3 flushed easily with methanol. Capillary 4 did not enable a flow. The monolith prepared from composition 4 is also very difficult to fracture and appears to have reduced in volume compared to the initial volume of the microemulsion.

Table 5.4 The pore size of the resulting monoliths is altered by altering the fraction of components in the microemulsion.

	Oil (%)	SDS$_{(aq)}$ (%)	1-Propanol (%)	Pore size/μm	Surface area/m^{2}g^{-1}
1	18.0	41.0	41.0	2.09	7.169
2	23.0	23.1	53.9	10.65	1.596
3	33.0	33.5	33.5	3.81	0.258
4	41.0	17.7	41.3	-	-
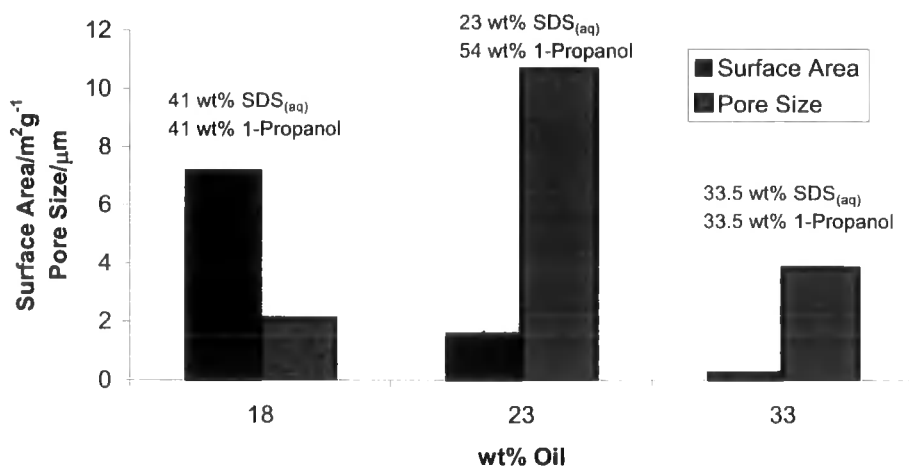
Figure 5.23 **The pore size and surface area of monoliths prepared from microemulsions in appendix C 4 – 7.Error bars are obscured by the data bar borders.**

5.4.11 Correlation between parent microemulsion composition and porosity.

In order to be suitable as a stationary phase the monolithic packing must be able to sustain an electroosmotic flow on the application of an electric field when filled with a buffer solution. This is achieved by the introduction of a potentially charged species along the polymer backbone. The species used is AMPS where the acrylamide group will polymerise into the developing matrix and the sulfonate head group will support the flow of ions along the length of the packed bed. The introduction of this species may increase the surface tension of the interface hence influencing the formation and structure of the microemulsion. From Figure 5.25 a large single phase region can still be seen. The two phase region is at compositions where the surfactant and co-surfactant levels are insufficient to stabilise the oil in the system.
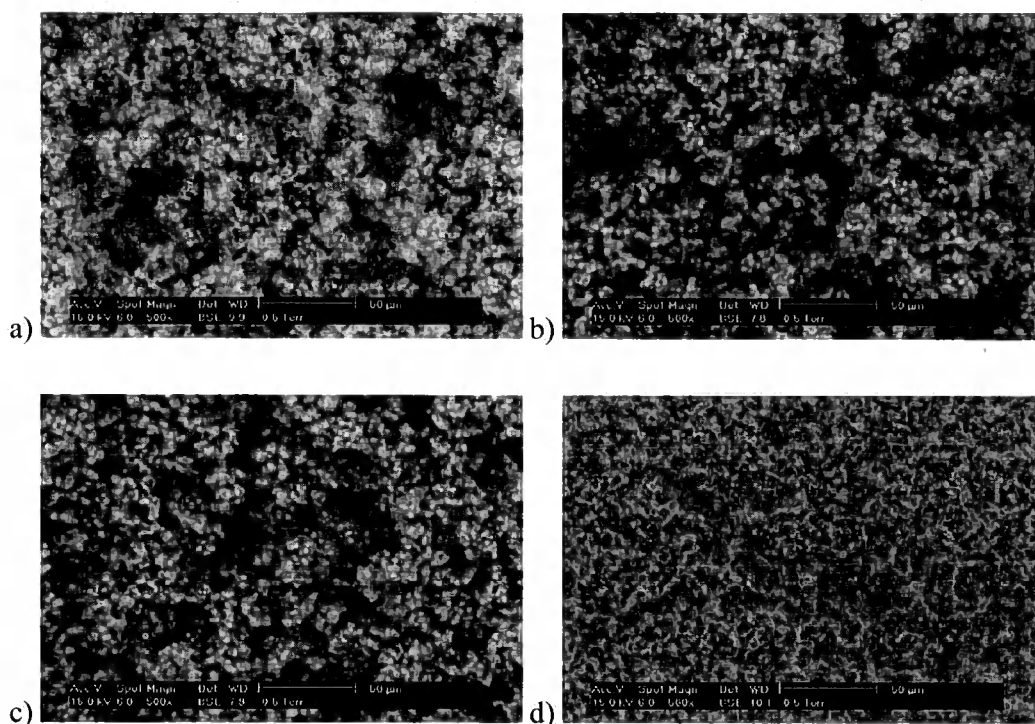
Figure 5.24 Altering the oil, SDS$_{(aq)}$ and 1-propanol fractions can control the porosity of the resulting monoliths. a) 18.0 wt% oil, 41.0 wt% SDS$_{(aq)}$, 41.0 wt % 1-propanol; b) 23.0 wt% oil, 23.1 wt % SDS$_{(aq)}$, 53.9 wt % 1-propanol; c) 33.0 wt% oil, 33.5 wt% SDS$_{(aq)}$, 33.5 wt% 1-propanol; d) 41.0 wt% oil, 17.7 wt% SDS$_{(aq)}$, 41.3 wt% 1-propanol.

As the volume fraction of the oil phase is increased, the fraction of surfactant is decreased. This results in a lowering of the microemulsion stability as there are less surfactant molecules available to stabilise the interface. As polymerisation proceeds and the temperature of the microemulsion is increased there will be an alteration in microemulsion structure from bicontinuous tending towards oil-in-water. This will result in the coalescence of the oil phase producing growing aggregates. The higher the oil level the more coalescence will occur prior to the gel phase resulting in larger aggregates. This can be seen from the SEM pictures in Figure 5.26. As the oil level is

increased from 30 wt% oil to 50 wt% the aggregate size increases. The graph in Figure 5.27 shows a linear trend of increasing pore diameter with increasing oil content. At 60 wt% oil the aggregates appear to be smaller as do the channels throughout the monolith. This also results in a considerable decrease in pore size. Visually, the resulting monolith has undergone noticeable shrinkage compared to the initial volume occupied by the parent microemulsion, possibly due to destabilisation of the microemulsion resulting in a loss of or alteration of microemulsion structure.
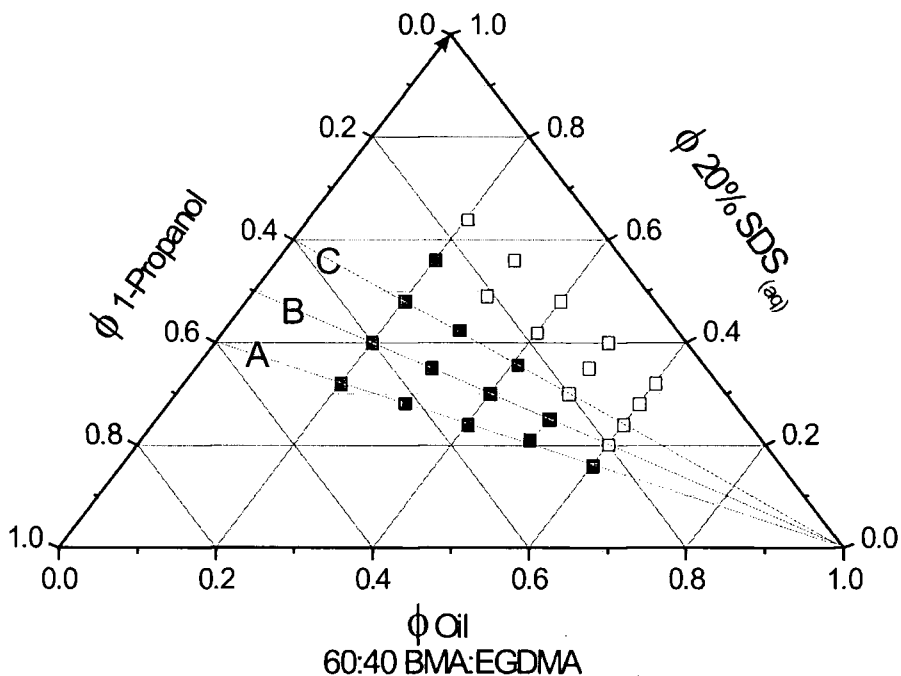
Figure 5.25   **Ternary phase diagram for 60:40 BMA:EGDMA system (appendix C 8 – 32). Filled squares indicate optically homogeneous microemulsions and unfilled squares represent two phase compositions.**

From Figure 5.27 it can also be seen that as the surfactant:1-propanol ratio is decreased at a constant fraction of oil the modal pore diameter increases. Again, if there is less surfactant at the oil-water interface, the microemulsion formed with a ratio of SDS$_{(aq)}$ to 1-propanol of 40 wt% to 60 wt% will have a less stable interface

than that for the microemulsion formed with a ratio of $SDS_{(aq)}$ to 1-propanol of 60

wt% to 40 wt%. The addition of a higher level of 1-propanol serves to reduce the

mean curvature of the surfactant film stabilising the microemulsion, however an

increase in temperature during polymerisation is promoting a greater shift towards an

oil-in-water phase.

From the plots in Figure 5.28 it can be seen that the pore size distribution of the

monoliths decreases with increasing oil. A gradual increase in intrusion volume

shows large pores filling followed by a sharp increase in intrusion at the modal pore

volume. This suggests a structure with channels larger than the void space between

the aggregates. As the aggregates increase in size the space between them becomes

similar to the channel width left by the water domains and a narrow pore size

distribution is observed as intrusion is only observed over a narrow pressure increase.

Figure 5.27 also shows that at a constant oil level, as the surfactant:co-surfactant

ratio is increased, the pore size of the resulting monolith decreases. At a lower

surfactant concentration the tension of the interfacial film will be higher and so it

will be less stable. Larger globules will form due to coalescence of the growing

polymer particles which will not be stabilised as well. Disregarding the channel size,

larger aggregates will pack less effectively and have a larger void volume than

smaller aggregates. As the SDS level is increased the interface will be more stable

and the channels within the microemulsion are more likely to be retained upon

polymerisation. The aggregates produced as the oil phase polymerises will be less

prone to coalescence and therefore the resulting monoliths will have smaller

aggregates packed more efficiently with less void space between them resulting in a

smaller modal pore diameter. In Figure 5.29 the cumulative intrusion for the

monoliths shown in Figure 5.30, prepared from a microemulsion containing different

levels of SDS solution, shows intrusion at lower pressures for lower SDS levels suggesting the presence of channels as well as the space between the aggregates. The more uniform the channels the sharper the intrusion gradient.
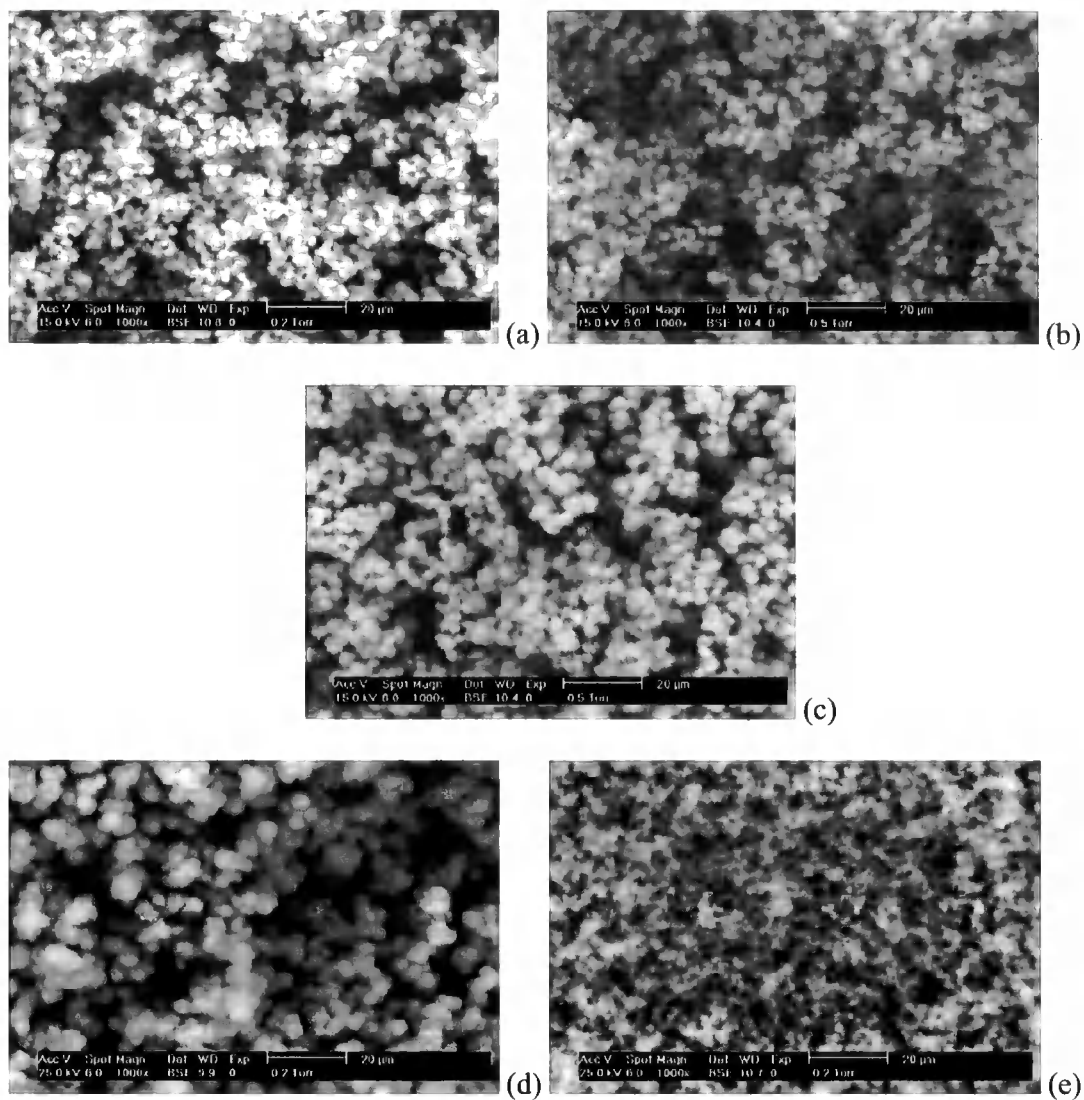
Figure 5.26 SEM images (1000X magnification) of monoliths prepared with a constant surfactant solution : co-surfactant ratio (40:60 SDS$_{(aq)}$:1-propanol) and an increasing oil content: (a) 20wt%, (b) 30wt%, (c) 40wt% oil, (d) 50wt%, (e) 60wt%.
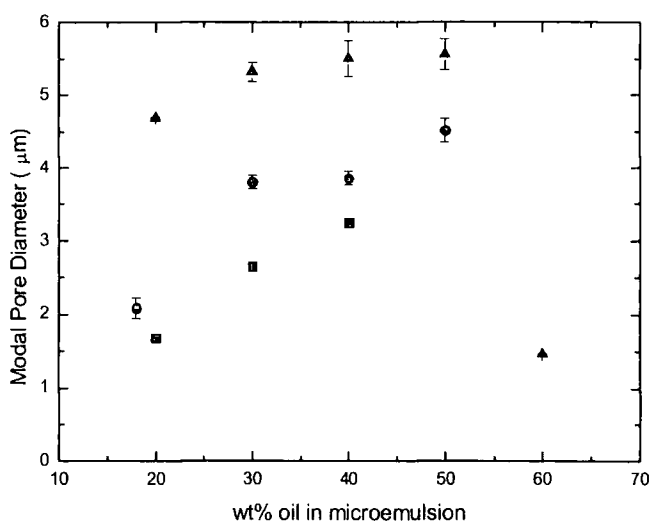
Figure 5.27 Increasing the oil concentration increases the pore size of the resulting monolith (SDS$_{(aq)}$:1-propanol ratios ▲ – 40:60 ● - 50:50, ■ - 60:40)
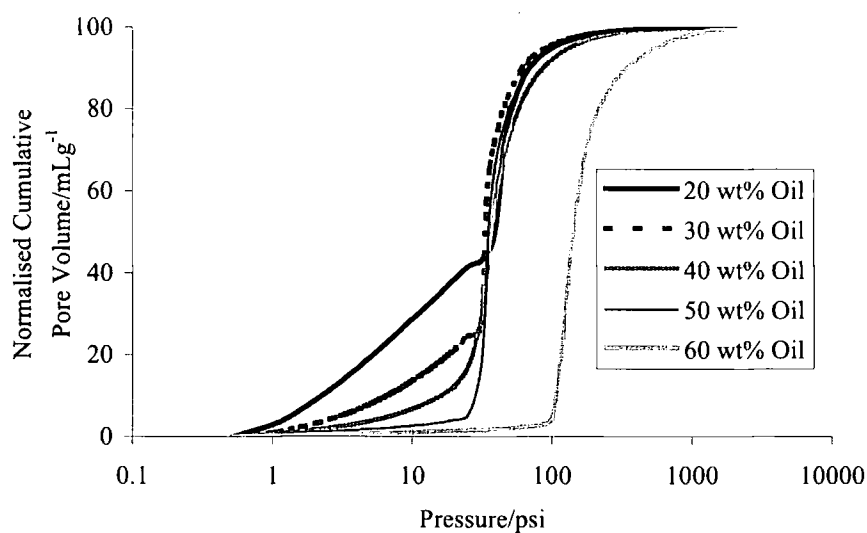
Figure 5.28 Normalised intrusion volume over a range of pressures for monoliths prepared from microemulsions containing SDS solution and 1-propanol in a 40 to 60 wt% ratio with varying proportions of oil.
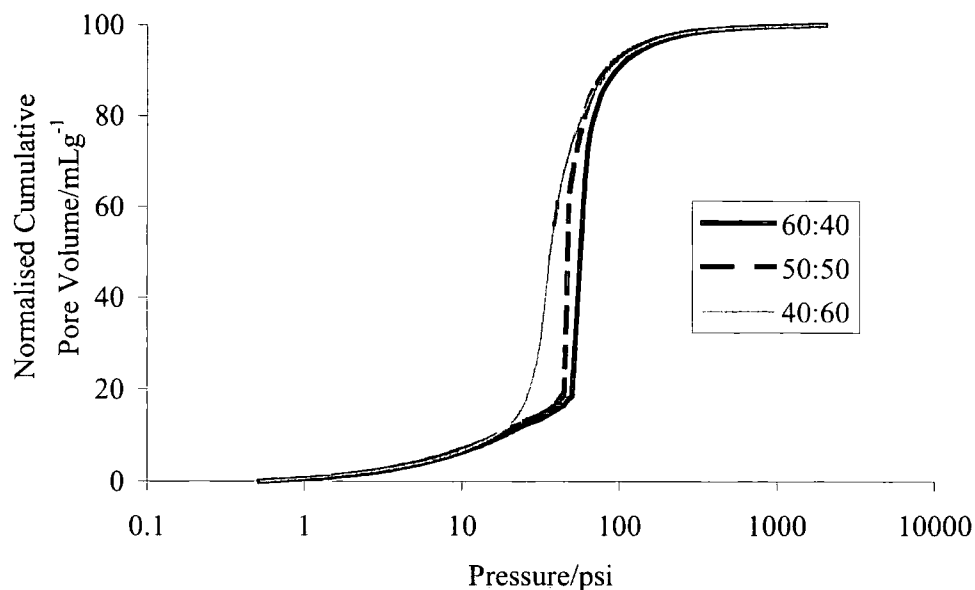
Figure 5.29 Normalised intrusion volume over a range of pressures for monoliths prepared from microemulsions containing 40 wt% oil with the remaining SDS solution and 1-propanol in various ratios.

Now that it has been established that the pore size of the resulting monoliths for this system can successfully be controlled by altering the basic composition of the microemulsion, their suitability for CEC needs to be established.

Figure 5.31 shows that the topography of the monoliths at the air-microemulsion interface is porous. It does however have different characteristics compared to the bulk. At the air interface, the surface that is in contact with vapour, there is a negligible force attracting the molecules away from the liquid, therefore there is a net inward attraction and the molecules at the surface have an excess Gibbs energy relative to the interior of the liquid. A greater number of surfactant molecules at the air interface will have a greater stabilising effect on the channels towards the surface. The result of this is similar to that observed in systems with a higher surfactant concentration (Figure 5.32); the aggregates are much smaller.
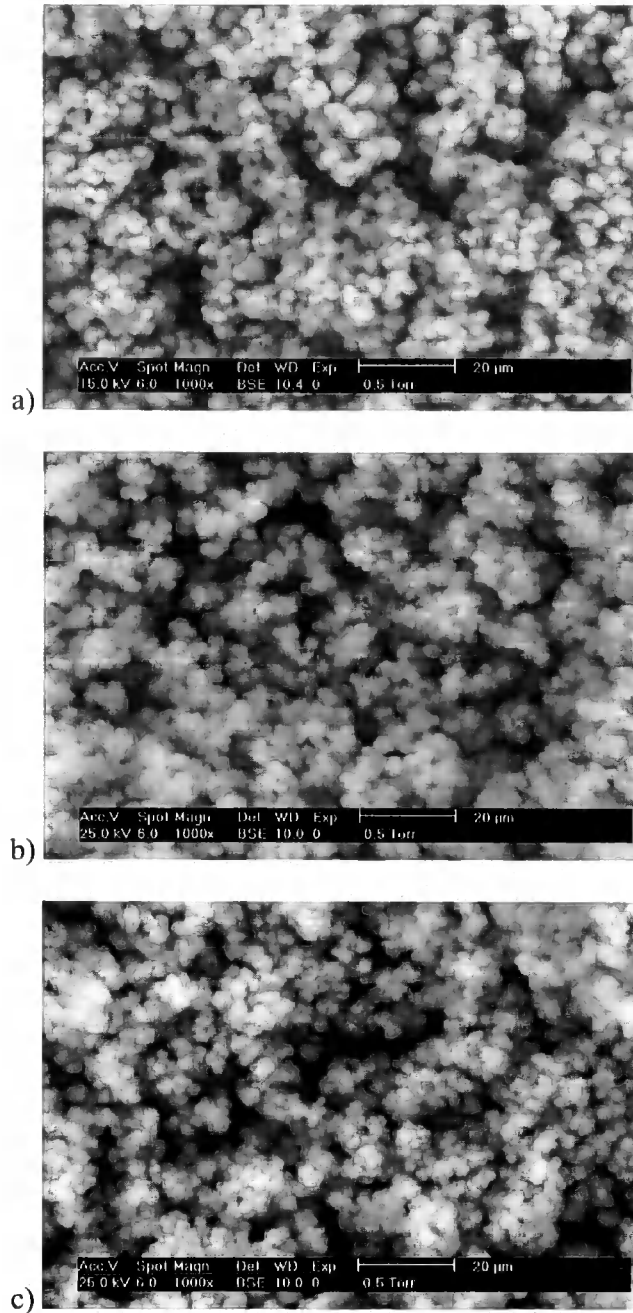
Figure 5.30 SEM images (1000X magnification) of monoliths prepared with a constant 40 wt% oil (60:40 w/w BMA:EGDMA) and varying the SDS solution to 1-propanol ratio. a) 40:60; b) 50:50; c) 60:40.
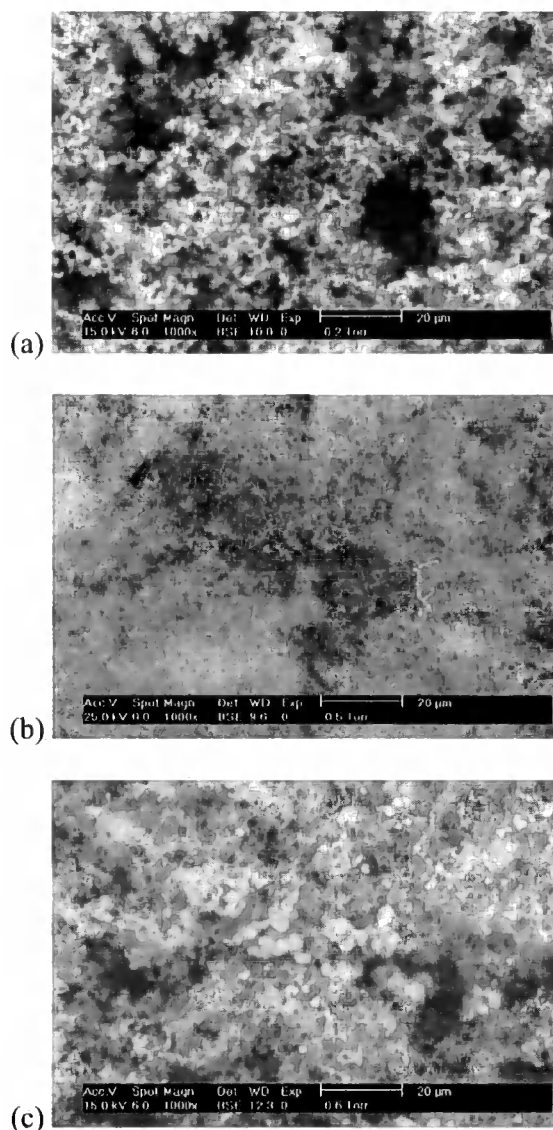
Figure 5.31 SEM images (1000X magnification) of the air-microemulsion interface of monoliths prepared with a constant surfactant solution: co-surfactant ratio (40:60 $SDS_{(aq)}$:1-propanol) and an increasing oil content (a) 20 wt%, (b) 30 wt%, (c) 40 wt%,

(a)　　　　　　　　　　　　(b)
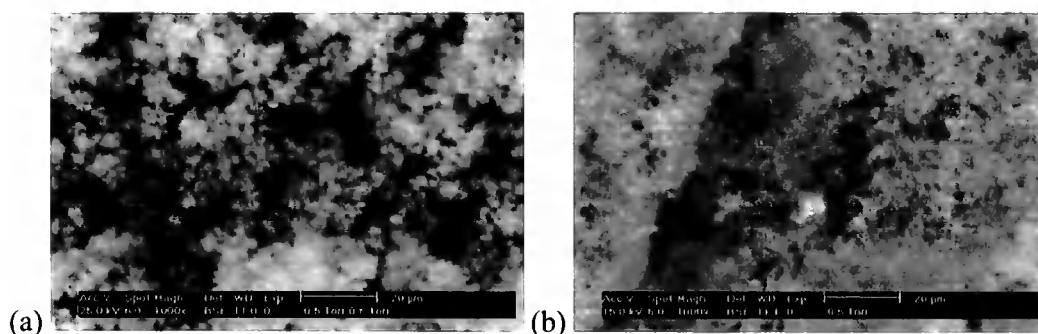
Figure 5.32 SEM images (1000X magnification) of a monolith prepared with an SDS$_{(aq)}$;1-propanol ratio of 60:40 wt/wt containing 20 wt% oil. (a) fractured surface and (b) air-microemulsion surface.

(i)　　　　　　　　　　　　(ii)

(iii)
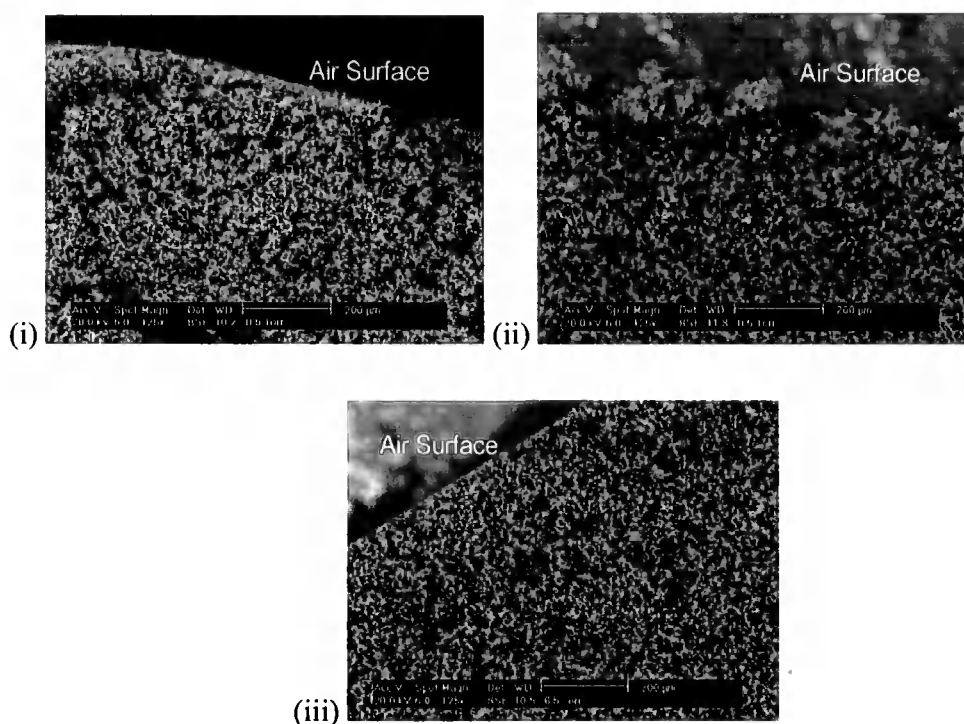
Figure 5.33 SEM image of the longitudinal cross section of monoliths prepared from (i) 50 wt% oil, 20 wt% SDS solution (20% SDSw/v), 30 wt% 1-propanol; (ii) 20 wt% oil, 32 wt% SDS solution (20% SDSw/v), 48 wt% 1-propanol; (iii) 30 wt% oil, 35 wt% SDS solution (20% SDSw/v), 35 wt% 1-propanol where the oil phase consists of EGDMA:BMA (40:60, w/w).

In the previous section, the microemulsion type prior to polymerisation was shown to have an effect on the topography of the monolith at the air surface. In the case of the monoliths discussed here the topography is porous and it can be seen from Figure 5.33 that the bicontinuous structure of the microemulsion continues all the way to the surface without the presence of an excess oil layer.

5.4.12 Conductivity Measurements

Mixtures were prepared with a constant SDS solution:1-propanol ratio of 40:60 w/w along line C in Figure 5.25. The conductivity meter was set to zero using the 100% oil phase in order to measure a normalised conductivity.
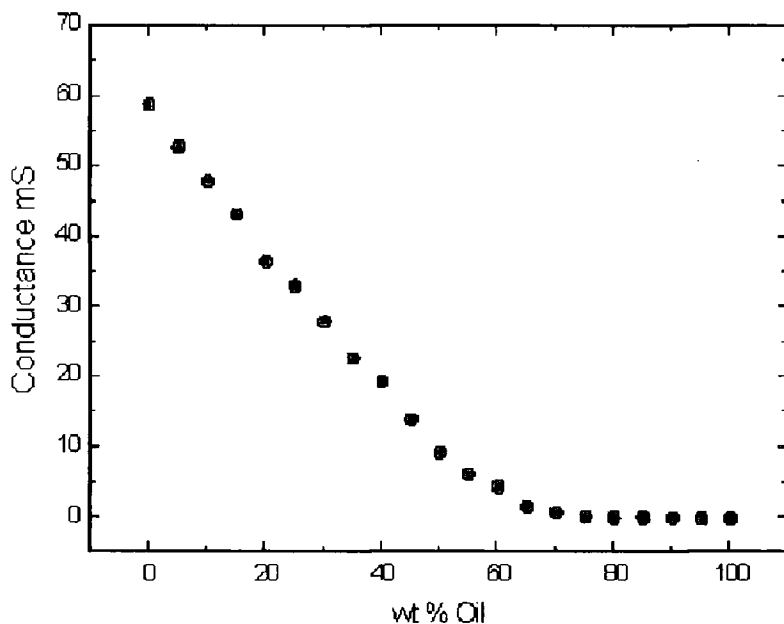
Figure 5.34 Conductivity measured along line C in Figure 5.25 at a constant SDS solution:1-propanol ratio of 40:60. Altering the oil content shows a conductivity gradient through the single phase region.

As discussed earlier in this chapter ions only flow in the water continuous states and when the microemulsion is in a two-phase or oil continuous state, containing mainly oil, the conductivity approaches that of the pure oil. As the oil level is decreased a

water continuous state is reached enabling a flow of ions. Phase inversion to a water continuous phase would result in a sharp change in conductivity over a narrow oil fraction range to that of the 'aqueous' phase. In this case we see a gradual increase in conductivity from a critical composition referred to as the percolation threshold [14]. This gradual phase inversion suggests there is an intermediate structure(s) present as well as an observed increase due to the increase in surfactant content of the microemulsion.

5.5 NMR Diffusion Studies.

The diffusion of the 20 %w/v SDS solution is slow at 0.192×10^{-10} m^{2}s^{-1} due to the solution concentration being above the CMC of the surfactant. If the system consists of a droplet structure dispersed in a continuous medium the diffusion of the dispersed phase will match that of the surfactant.

In this system a divergence of diffusion coefficients is observed, indicating that the diffusion mechanisms can not be due to swollen droplets (Figure 5.35). The divergence suggests that channels of the oil and water domains exist stabilised by a less mobile surfactant film. A value of D_s is less than D_o indicates bicontinuity. D_o increases with oil concentration indicating that the diffusion of the oil molecules is less constrained and tends towards that of the pure oil phase. This situation would arise if the oil channels of the microemulsion increased or organised into a less hindered structure such as a layered system. As the channels increase in size and the surfactant content of the microemulsion is reduced the lateral diffusion of the surfactant molecules along the hydrophobic/hydrophilic interface decreases, indicating either less mobile channel domains at higher oil concentrations or the formation of discrete droplets dispersed in an oil continuous phase. The latter

scenario would be coupled with a significant decrease in the diffusion of the water domains which is not observed here.
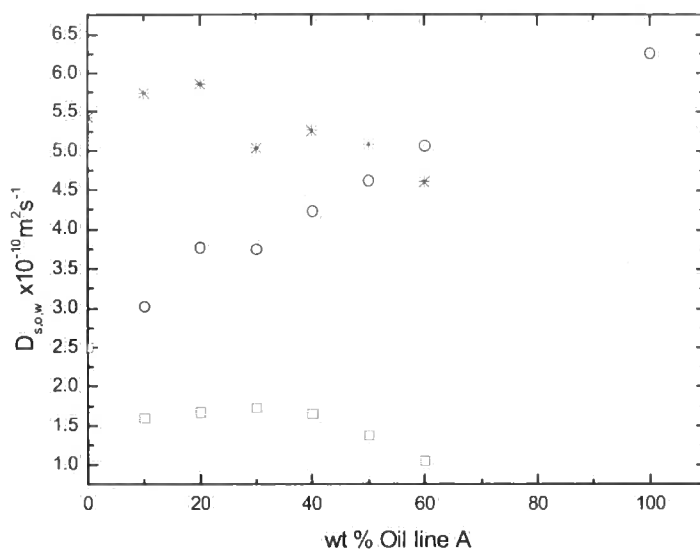
Figure 5.35 Self-diffusion coefficients of surfactant (□), water (✱) and oil (○) represented by points along line A in Figure 5.4.

Anderson and Wennerström [17] calculated the geometrical obstruction factors for the effective self-diffusion rate of components forming cubic phases, bicontinuous microemulsions and L_3 (lamellar) phases. These calculations serve as good approximations in order to investigate the bicontinuity of the structures; the normalised diffusion coefficient, or obstruction factor, D/D_0 was used, where D is the measured diffusion coefficient in the structured system and D_0 is the diffusion coefficient in 'pure' solvent. From Figure 5.36, in which the normalised self-diffusion coefficients for microemulsions represented by line A in Figure 5.4 are plotted, a branched tubular system can be deduced using the approximations outlined by Anderson and Wennerström [17] and applying them to a disordered bicontinuous structure. It was observed that in the case of a lamellar phase the obstruction factor

will be 2/3 and 1/3 when the diffusion is confined to a cylindrical region of negligible diameter. The obstruction from the cylinders is small resulting in the normalised diffusion of the water phase being close to 1. D/D_0 for the oil phase is approximately 0.5 at low oil concentrations suggesting a tubular structure where the distance between branching points is greater than the tube diameter and diffusion is allowed along the axes of the tubes. Increasing the oil level gives an increase in D/D_0, diffusion is becoming less hindered suggesting a tendency towards a layered structure where diffusion is only hindered in one direction and free in the other two.

Table 5.5   Diffusion coefficients of the oil phase (D_o) and surfactant (D_s) along line A in Figure 5.4. D_o at 100% oil is the self-diffusion coefficient of the 'pure oil' and D_s at 0% oil is the self-diffusion of the surfactant at 20 %w/$v_{(aq)}$, 60wt% 1-propanol.

% Oil line A	$D_o \times 10^{-10}$ m^{2}s^{-1}	$D_s \times 10^{-10}$ m^{2}s^{-1}
100	6.255	-
60	5.078	1.057
50	4.63	1.38
40	4.244	1.655
30	3.751	1.73
20	3.776	1.672
10	3.029	1.599
0	-	2.502

Another possibility is a widening of the tubules. In this case there will be less of a hindrance to diffusion within the tubes from effects at the tube walls, as the solvent

molecules will have a lower mobility in the vicinity of the surfactant film due to possible solvation effects.
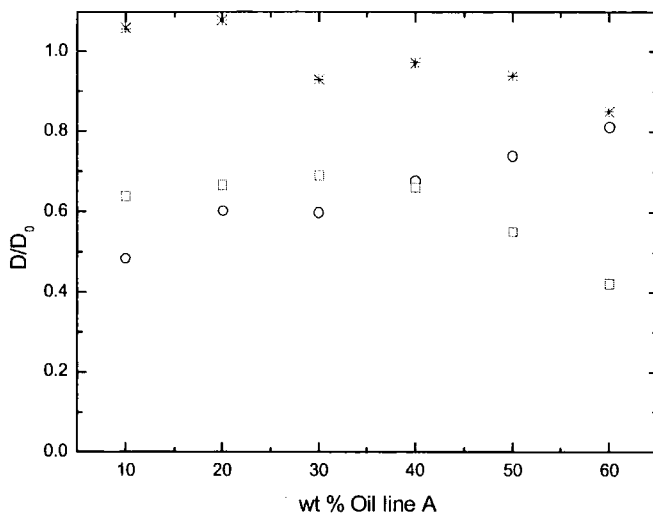
Figure 5.36 Normalised diffusion of surfactant (□), water (✱) and oil (○)

represented by points along line A in Figure 5.4.

From Figure 5.37, it can be seen that altering the aqueous surfactant solution to 1-propanol ratio while keeping the fraction of oil in the system constant has little effect on the structure of the microemulsion. D/D_0 for the oil phase remains approximately 2/3 whereas it is close to 1 for the water domains suggesting hindered diffusion of the oil domains and a layer of surfactant whereas the water domains are less hindered and are similar to the molecules in free solution. With an increase in surfactant level a normalised diffusion of surfactant close to the oil phase diffusion can be seen and a divergence at 36 wt%. As the surfactant will exist in three different forms at any given time, at the interface, as micelles or as single molecules, the observed diffusion will be an average of the diffusion coefficients in the different states. As there is an increase in surfactant the ratio of these states may change. As the oil level decreases and the surfactant level increases the interface will become saturated with surfactant

and the remaining molecules will be free in solution or exist as aggregates. An increase in the diffusion coefficient and hence the normalised diffusion suggests there is a higher proportion of faster diffusing species in the mixture. Again the diffusion coefficient of the surfactant is lower than that of the oil indicating all four compositions are still within the bicontinuous region.
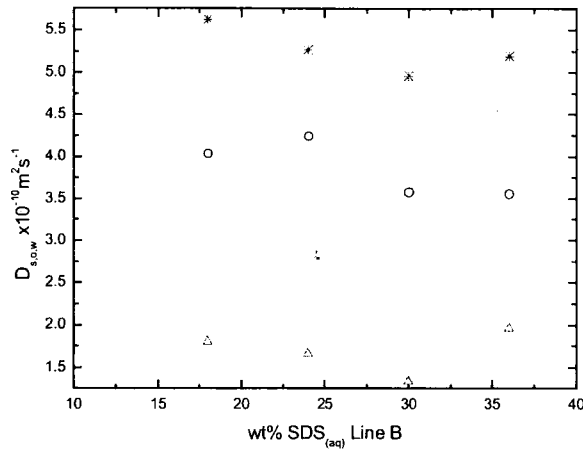
a)
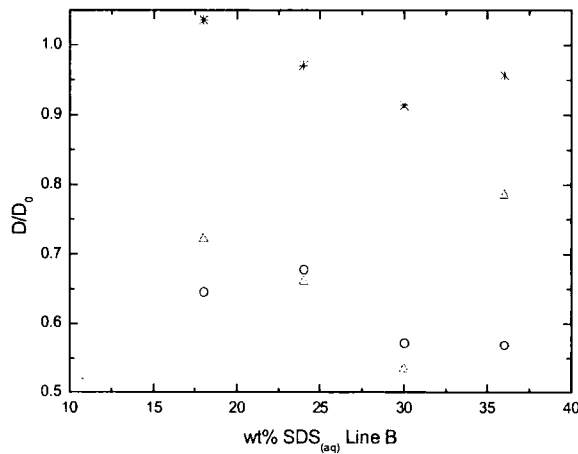
b)

Figure 5.37 (a) Self-diffusion coefficients and (b) normalised diffusion of surfactant (Δ), water (∗) and oil (O) represented by points along line B in Figure 5.4.

5.6 Conclusions and Further Work

In the earlier part of this chapter it was shown that the polymerisation of microemulsion systems containing a high proportion of surfactant were unsuitable for use as stationary phases due to the apparent production of an excess phase upon polymerisation. It was shown that with a high surfactant to co-surfactant ratio the resulting monoliths exhibited a porous structure, which could be controlled by altering the volume fractions of each phase. However, a non porous topography was observed where the polymerising microemulsion was in contact with the air in the sealed glass vial. As this film on the top of the monolith represents the section of stationary phase packing at the outlet end of the capillary prior to the detection window and cannot be altered prior to use, a non porous structure renders systems of this type unsuitable. Increasing the water content of the microemulsion increases the porosity of the resulting monolith but in doing so for a constant fraction of oil we reduce the fraction of stabilising species (surfactant and co-surfactant). A high porosity material that enables a flow through the pores is required. The bicontinuous structure (and hence a porous topography) at the surface needs to be retained during polymerisation. This is achieved by reducing the surfactant level and achieving stabilisation by increasing the volume fraction of co-surfactant. This then creates a more fluid interface or a different microemulsion structure while retaining bicontinuity and reduces the portion of excess oil on the surface of the microemulsion.

5.7 References

1. Svec, F.; Peters, E. C.; Sykora, D.; Yu, C.; Frechet, J. M. J. *HRC-J. High Resolut. Chromatogr.* **2000**, *23*, 3-18.

2. Svec, F.; Peters, E. C.; Sykora, D.; Frechet, J. M. J. *J. Chromarog. A* **2000**, *887*, 3-29.

3. Jonsson, B.; Wennerstrom, H.; Nilsson, P. G.; Linse, P. *Colloid Polym. Sci.* **1986**, *264*, 77-88.

4. Loening, N. M.; Keeler, J.; Morris, G. A. *J. Magn. Reson.* **2001**, *153*, 103-112.

5. Soderman, O.; Nyden, M. *Colloid Surf. A-Physicochem. Eng. Asp.* **1999**, *158*, 273-280.

6. Lindman, B.; Stilbs, P.; Moseley, M. E. *J. Magn. Reson.* **1980**, *40*, 401-4.

7. Lindman, B.; Kamenka, N.; Kathopoulis, T. M.; Brun, B.; Nilsson, P. G. *J. Phys. Chem.* **1980**, *84*, 2485-90.

8. Parella, T. *Magnetic Resonance in Chemistry* **1998**, *36*, 467-495.

9. Callaghan, P. T.; Coy, A. *Phys. Rev. Lett.* **1992**, *68*, 3176-3179.

10. Li, T. D.; Chew, C. H.; Ng, S. C.; Gan, L. M.; Teo, W. K.; Gu, J. Y.; Zhang, G. Y. *J. Macromol. Sci.-Pure Appl. Chem.* **1995**, *A32*, 969-980.

11. Dittmann, M. M.; Wienand, K.; Bek, F.; Rozing, G. P. *Lc-Gc* **1995**, *13*, 800-814.

12. Szleifer, I.; Kramer, D.; Ben-Shaul, A.; Gelbart, W. M.; Safran, S. A. *J. Chem. Phys.* **1990**, *92*, 6800-17.

13. Safinya, C. R.; Sirota, E. B.; Roux, D.; Smith, G. S. *Phys. Rev. Lett.* **1989**, *62*, 1134-7.

14. Lagues, M.; Sauterey, C. *J. Phys. Chem.* **1980**, *84*, 3503-8.

15. Scriven, L. E.; Kaler, E. W.; Bennett, K. E.; Davis, H. T. *J. Chem. Phys.* **1983**, *79*, 5673-84.

16. Lam, A. C.; Schechter, R. S. *J. Colloid Interface Sci.* **1987**, *120*, 56-63.

17. Anderson, D.; Wennerstrom, H. *J. Phys. Chem.* **1990**, *94*, 8686-8694.

6   Capillary Electrochromatography

6.1   Introduction

Capillary electrochromatography has been in development for several years with stationary phase materials being developed from a wide range of analytes for a diverse range of applications. The limitations of capillaries packed with beads has lead to the development of stationary phases prepared in-situ in the form of hydrogels or solid porous monoliths. There is also a wide range of proven preparation methods. This section assesses the suitability of polymerising bicontinuous microemulsions in-situ to form a solid monolith and its application to capillary electrochromatography as a stationary phase. The effect of pore size and operating conditions are assessed.

6.2   Experimental

6.2.1   Chemicals

Acetonitrile was of HPLC grade and supplied by BDH.

6.2.2   Columns
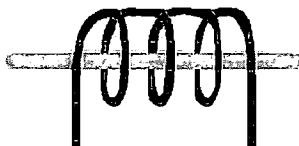
Figure 6.1 Electrical coil through which the fuses silica capillary is placed to remove the polyamide coating.

Packed CEC capillaries were supplied by ThermoHypersil™ (Runcorn, Cheshire). Fused silica capillaries were supplied by Composite Metals (Worcs., UK). Table 6.1 details the properties and composition of the capillaries prepared using the standard

procedures in the previous chapter. The polyamide coating was removed from the capillary close to the packing by electrical heating as shown in Figure 6.1 to produce a detection window required for on-line detection. It was determined that a low setting for a longer period prevented damage to the capillary packing enabling the dead volume between the stationary phase and the window to be reduced.

6.2.2.1   Column reference, x:y:z

x:y is the 20% $SDS_{(aq)}$:1-propanol (w/w) ratio; z is the oil concentration (BMA:EGDMA, 60:40,w/w) of the parent microemulsion.

Table 6.1 Columns prepared for analysis.

Sample No.	Column	$[SDS]_{(aq)}$ (%)	AMPS (wt%)	Length to detector/ cm	Pore Diameter/ μm	Surface Area/ m^2g^{-1}
1	40:60:30	20	0.3	20	5.3	2.25
2	40:60:20	20	0.3	20	4.9	3.50
3	40:60:40	20	0.3	20	5.8	0.98
4	40:60:40	20	0.6	20	5.8	1.08
5	60:40:40	20	0.3	20	3.3	2.27
6	60:40:20	20	0.3	20	1.7	7.88
7	60:40:40	20	0.3	30	3.3	2.27
8	50:50:50	20	0.3	30	4.5	1.24
9	50:50:50	20	0.3	40	4.5	1.24
10	54:46:34	10	0.6	20	3.3	2.37
11	37:63:29	10	0.6	20	6.6	1.78

6.2.3 Instrumentation

CEC experiments were carried out using a Beckman Coultier P/ACE™ MDQ Methods Development System discussed in chapter 3. Detection was by online UV detection at 214nm. The column temperature was thermostatically controlled to 25°C with the exception of temperature studies.

6.2.4 Stock solutions

6.2.4.1 Buffer solutions

50mM phosphate buffer was prepared using phosphoric acid, using 2M sodium hydroxide to adjust the pH to pH 8.

The buffer solutions in Table 6.2 were prepared daily as required.

6.2.4.2 Sample solutions

The structures of the substituted phthalates are shown in Figure 6.2. All analytes were dissolved in acetonitrile:buffer (80:20, v/v; Table 6.2, solution 1) to give a concentration of 4 mg ml^{-1}. Thiourea was added as a EOF marker to give a concentration of 1mg ml^{-1}.

6.2.5 CEC Analysis

Columns were conditioned by initial flushing with 80:20 MeCN: 1mM buffer at a pressure of 60 p.s.i for at least 5 minutes or until a flow through the capillary was observed. A voltage of 25 kV was then applied across the capillary until a steady current and a flat baseline were observed. During analysis both vials were pressurised to 60 p.s.i. Sample injection was electrokinetic for 3 seconds at 5 kV.

Table 6.2 Buffers prepared for CEC analysis.

	Phosphate Buffer		Water	Acetonitrile	
	μl	mM	ml	ml	% (v/v)
1	100	5	1.90	8.0	80
2	100	5	2.90	7.0	70
3	100	5	3.90	6.0	60
4	100	5	4.90	5.0	50
5	100	5	5.90	4.0	40
6	50	0.5	4.95	5.0	50
7	200	2	4.80	5.0	50
8	300	3	4.70	5.0	50
9	400	4	4.60	5.0	50
10	500	5	4.50	5.0	50
11	600	6	4.40	5.0	50
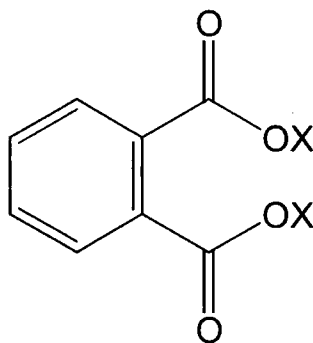
Figure 6.2   The general structure of phthalate compounds where X is a propyl or phenyl group.

6.3 Results and Discussion

6.3.1 Capillary conditioning

6.3.1.1 Monolithic columns

After flushing with buffer under pressure a steady current was achieved within 10 minutes of the application of an electric field. This current remained steady and constant throughout experiments with a single buffer solution. Upon changing the operating conditions, namely the buffer system, column equilibrium was achieved again within 5 minutes.

6.3.1.2 Commercial ODS columns

In contrast to the monolithic columns the bead packed capillaries were unreliable. Initial conditioning was difficult and time consuming. Due to the tight packing of the capillaries containing 3μm beads, filling the capillary with the required buffer under pressure was difficult due to the build up of back pressure. Conditioning with different buffer systems by electroosmosis frequently required up to and beyond an hour to achieve a steady and stable current. This meant that method development with these columns was time consuming in comparison to the monolithic columns.

6.3.2 Effect of Acetonitrile Concentration

By altering the composition of the mobile phase to increase or decrease the analyte's affinity for that phase, its retention time on the column can subsequently be decreased or increased respectively. In this case the acetonitrile content of the mobile phase was decreased from 80 % (v/v) to 50 % (v/v) at a constant overall ionic strength. In all cases the retention of the phthalates increased with decreasing acetonitrile concentration and ln k (capacity factor) remains linearly related to percentage acetonitrile content of the mobile phase in line with well established

HPLC theory (Figure 6.4). The retention time of the thiourea added as a flow marker remained constant as expected as it has negligible interactions with the stationary phase packing. The effect of acetonitrile concentration on separation can be seen from Figure 6.3.

The analytes investigated here have a higher affinity for the ODS packing. The analyte peaks are resolved at a higher acetonitrile content and have much greater retention times (Figure 6.6). This is due to the ten-fold increase in surface area of the ODS packing in comparison to the porous monolithic material. A higher surface area results in an increased number of binding sites and is evident from the increased gradient in Figure 6.5. At 50 % v/v acetonitrile on the ODS columns the capacity factors for dipropyl- and diphenylphthalate are 3.25 and 6.03 respectively compared to between 0.3 and 0.8 for dipropylphthalate and between 0.8 and 1.7 for the monolithic columns investigated.

i)

ii)

iii)

iv)
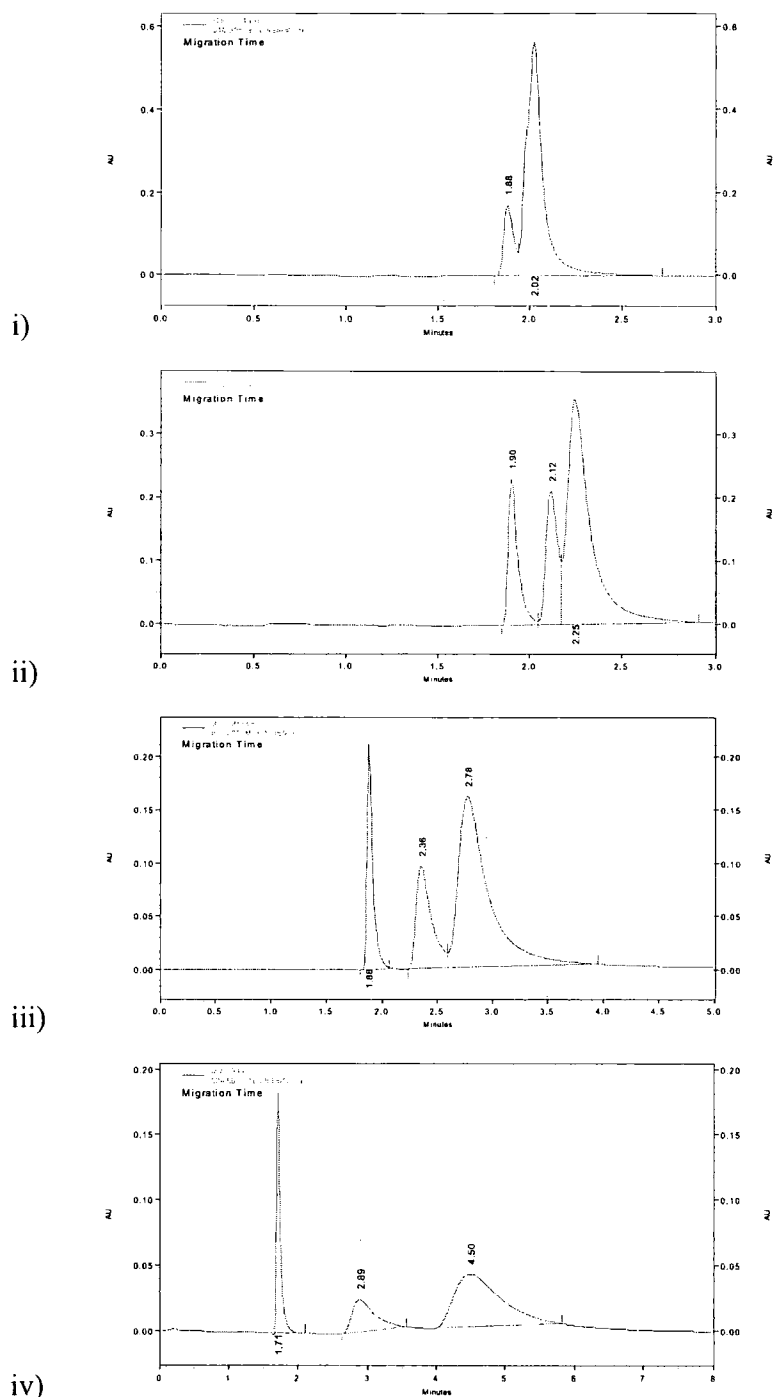
Figure 6.3 Electrochromatograms of (in order of elution) thiourea, dipropylphthalate and diphenylphthalate in 1mM total phosphate buffer at pH 8 and (i) 80 %; (ii) 70 %; (iii) 60 %; (iv) 50 % (v/v) acetonitrile. Column – 20cm 3.3μm monolithic packing (Table 6.1.5).
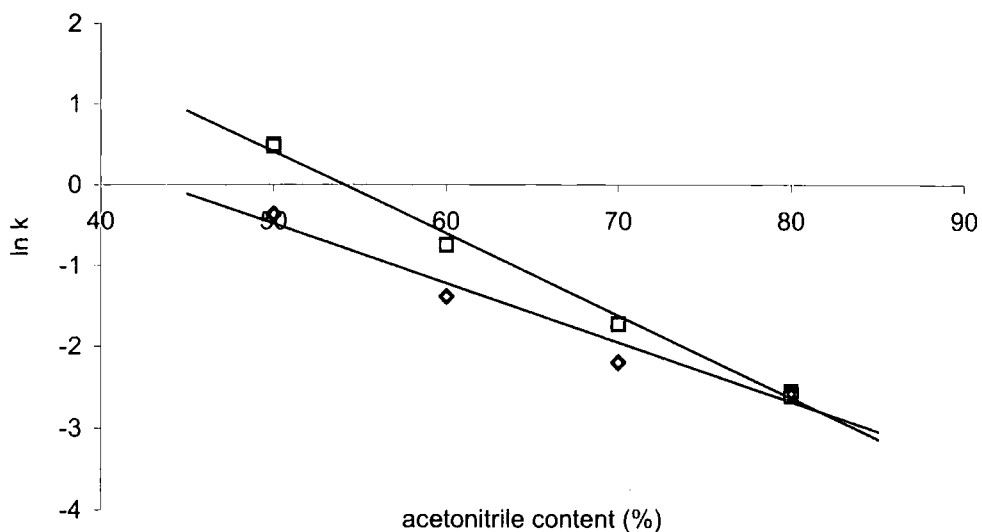
Figure 6.4 **Effect of acetonitrile content of the mobile phase on the logarithm of the capacity factor, k, of dipropylphthalate (◊) and diphenlphthalate (□) on a 3.3µm monolithic stationary phase (Table 6.1.5).**
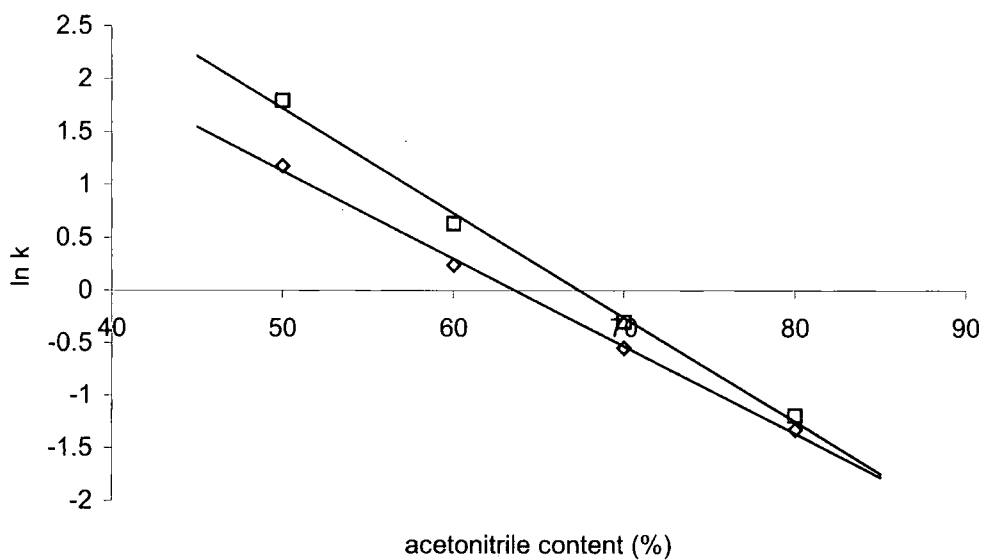
Figure 6.5 **Effect of acetonitrile content of the mobile phase on the logarithm of the capacity factor, k, of dipropylphthalate (◊) and diphenlphthalate (□) on 3µm ODS packing.**

i)

ii)

iii)
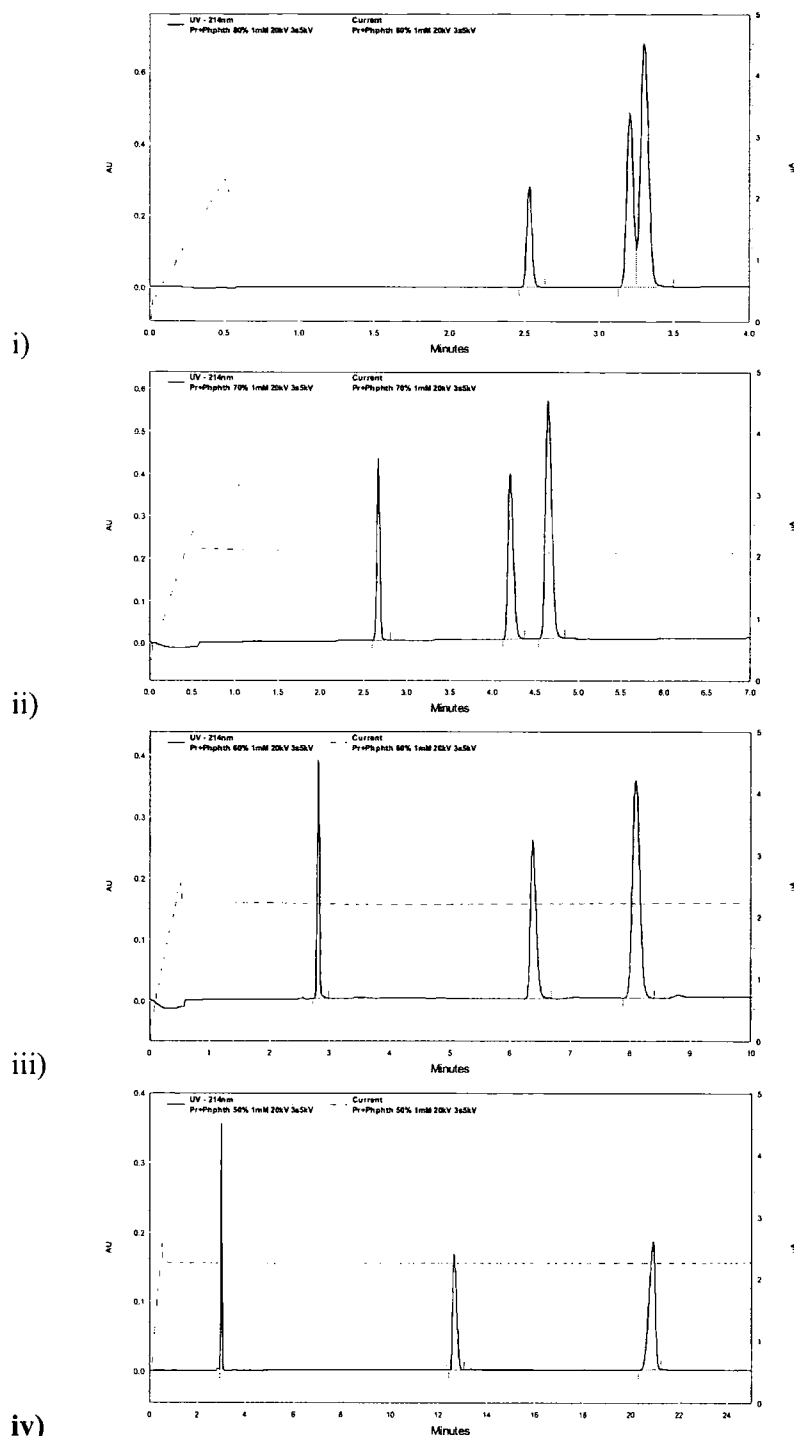
iv)

Figure 6.6 Electrochromatograms of (in order of elution) thiourea, dipropylphthalate and diphenylphthalate in 1mM total phosphate buffer at pH 8 and (i) 80 %; (ii) 70 %; (iii) 60 %; (iv) 50 % (v/v) acetonitrile. Column – 20cm 3μm ODS beads.

6.3.3   Linear Velocity

6.3.3.1   Effect of acetonitrile

Acetonitrile was chosen as the organic modifier as it supports a high EOF.

The concentration of acetonitrile in the buffer system should have no effect on the linear velocity of the mobile phase through the capillary at a constant ionic strength. As the linear velocity is mainly dependant on the ionic strength of the buffer, if the organic modifier present does not contribute towards the generated electrical double layer there should be no change in linear velocity over a range of concentrations. Figure 6.7 shows that the acetonitrile level has some effect on the linear velocity. An increase in linear velocity could be attributed to a decrease in mobile phase viscosity, (acetonitrile is 40% less viscous than water) however, a higher linear velocity at lower concentrations is observed for columns with pore sizes of 5.3μm and 4.9μm.
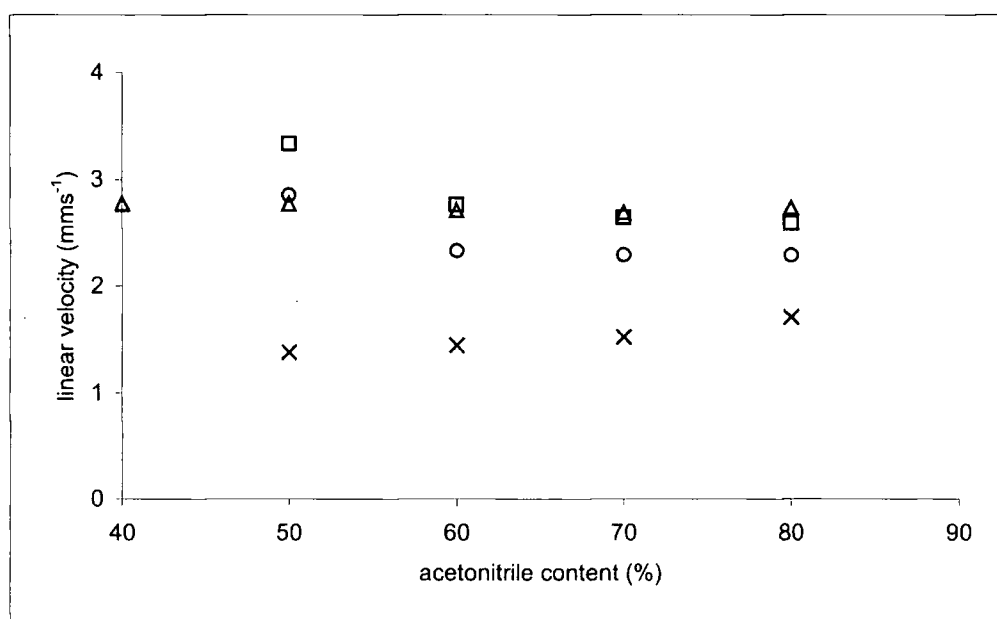
Figure 6.7   Effect of acetonitrile content on linear velocity. ($\triangle$, 5.8μm; $\square$, 5.3μm; O, 4.9μm; ✕, 1.7μm)

6.3.3.2   Effect of Pore Size

At a standard buffer concentration and field strength it can be seen from Figure 6.8 that the linear velocity u_{eo} is proportional to the pore size of the monolithic stationary phase packing. The Smoluchowski equation (Equation 6.1) shows how the EOF is governed by the zeta potential ζ, the permittivity, ε_r and the viscosity, η of the mobile phase as well as the electric field strength, E. ε_0 is the permittivity of a vacuum:

$$u_{eo} = \frac{\varepsilon_o \varepsilon_r \zeta E}{\eta}$$

Equation 6.1

All the terms in Equation 6.1 remain constant leaving a variability in zeta potential responsible for the change in linear velocity. The zeta potential is related to the surface charge, σ and the double layer thickness, δ by

$$\zeta = \frac{\sigma \delta}{\varepsilon_0 \varepsilon_r}$$

Equation 6.2

As the pore size is increased the surface area of the stationary phase decreases. It has been shown theoretically by Rice and Whitehead [1] that the flow velocity will be independent of diameter, d when d is greater than δ. As d approaches δ double layer overlap will occur coupled with a decrease in flow velocity. In this case the added charged species, AMPS, is added at a constant level (0.3 wt% of the monomers) therefore it is assumed that the surface coverage is at the same density across all the columns. Figure 6.9 shows that the correlation between surface area and linear velocity is not perfect but there is a general downward trend of linear velocity as surface area is increased. This corresponds to a decrease in surface area with increasing pore size and hence permittivity.
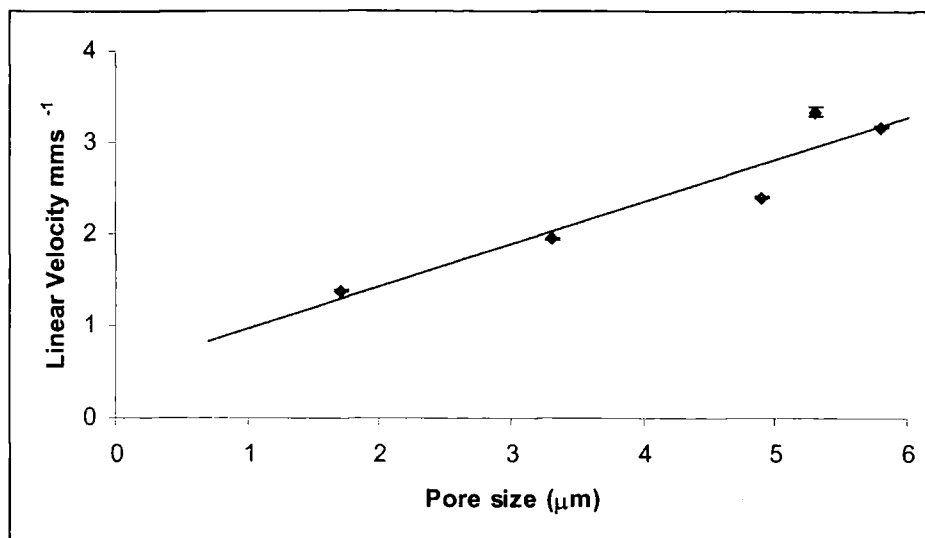
Figure 6.8 Effect of pore size on EOF for monolithic stationary phases prepared using BMA and EGDMA (60:40 w/w).
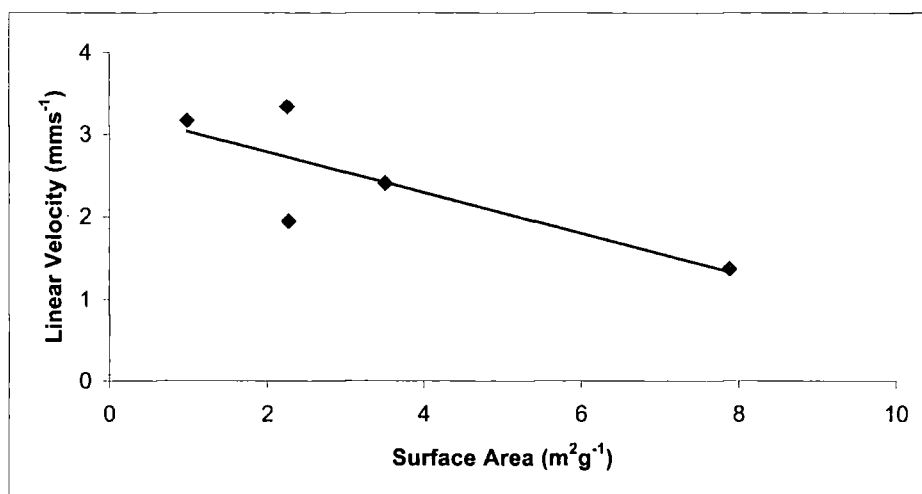
Figure 6.9 Effect of surface area on EOF for monolithic stationary phases prepared using BMA and EGDMA (60:40 w/w).

6.3.3.3   Effect of Ionic Strength

The linear flow velocity through a capillary is related to the ionic strength, I of the buffer by the following relationship:

$$u_{eo} = \sigma \left(\frac{\varepsilon_o \varepsilon_r RT}{2F^2 I \eta} \right)^{\frac{1}{2}} E$$

Equation 6.3

Linear velocity is directly proportional to the zeta potential and the electric field applied to the column. The zeta potential is in turn directly proportional to the double layer thickness at a given ionic strength as defined by the Poisson-Boltzman distribution and Debye-Hückel approximation.

$$\zeta = \frac{\sigma \delta}{\varepsilon_o \varepsilon_r}$$

Equation 6.4

$$\delta = \left(\frac{\varepsilon_o \varepsilon_r RT}{2F^2 I} \right)^{\frac{1}{2}}$$

Equation 6.5

An increase in the ionic strength will cause a decrease in the linear flow velocity. At lower ionic strengths a larger double layer is observed. If the double layer distance is greater than the size of the pores in the stationary phase, double layer overlap will occur. This may result in the inability to maintain a steady current flow across the column. Figure 6.10 shows the effect of ionic strength on flow velocity for the Hypersil ODS column and two of the monolithic columns. The linear velocity through the monolithic column is greater than through the commercial column. This is mainly attributed to the porosity of the columns, the monolithic column being more porous than the commercial column.

a)

b)
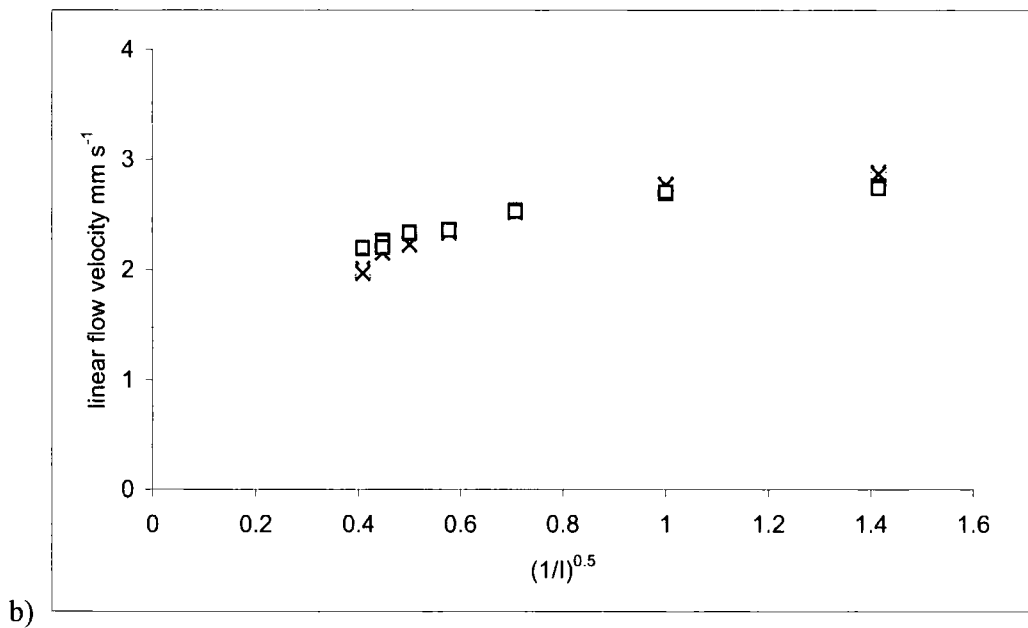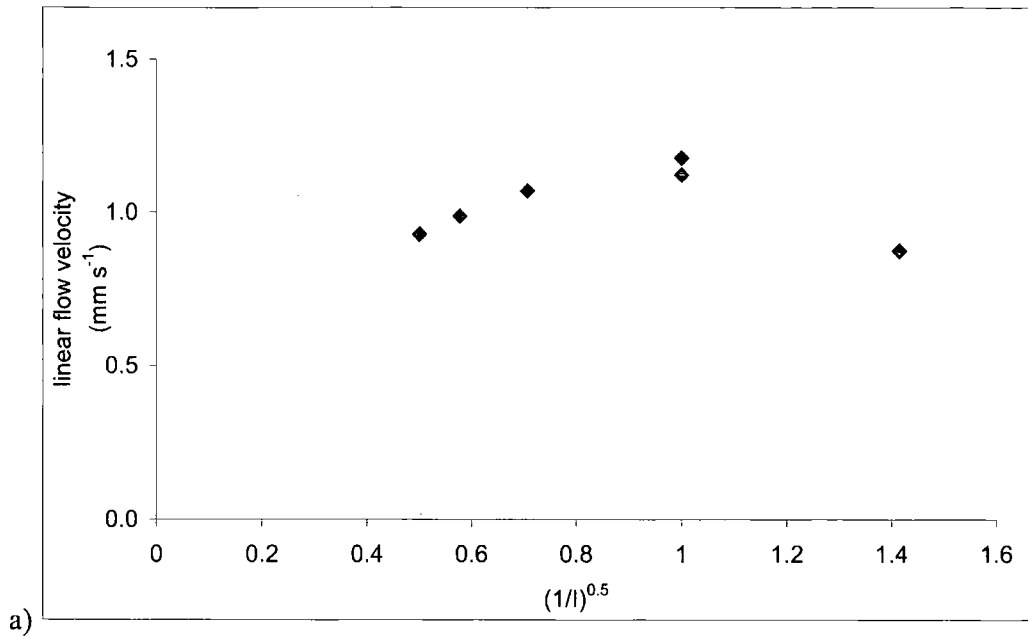
Figure 6.10 The effect of buffer ionic strength on linear velocity in a) an ODS

packed column; b) a porous monolith filled column at 50 % MeCN

v/v and × contains 0.3 wt% AMPS, □ contains 0.6 wt% AMPS.

At lower ionic strengths the linear velocity begins to reach a plateau, possibly as double layer overlap begins to occur. The Smoluchowski equation assumes the independence of packing size on linear velocity (unless double layer overlap occurs). Using traditional porous or non-porous silica a decrease in the particle size will result in an increase in surface area and an overall increase in surface functionalities. As the EOF is directly proportional to the number of surface silanol groups, any effect on linear velocity due to flow resistance is likely to be counteracted by an increase in surface charge resulting in an increased EOF.

Within the monolithic systems the surface charge of the packing is easy to alter. When the added AMPS level is doubled there is little change in the resulting linear velocity over a range of ionic strengths suggesting a larger increase in AMPS is required to significantly change the effect on the generated electrical double layer.
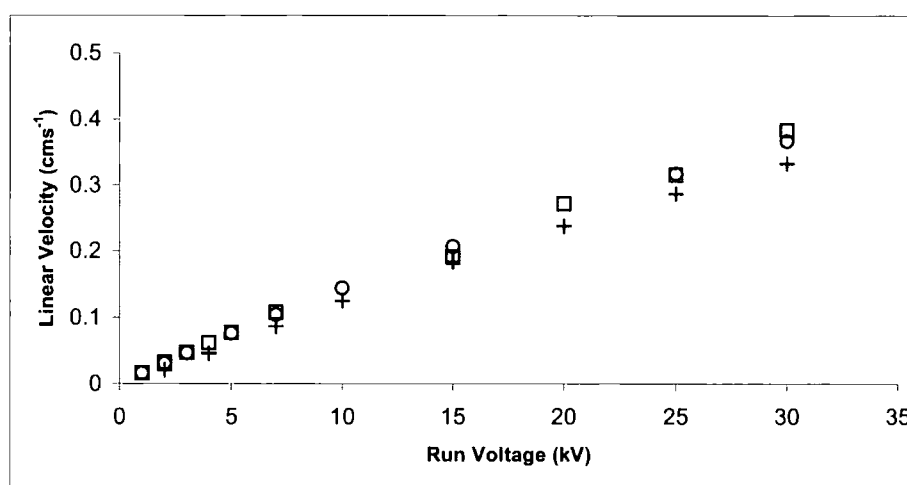
Figure 6.11 The effect of applied voltage on EOF linear velocity for monolithic columns with pore sizes of 4.9 (+), 5.3 (□) and 5.8μm (○).

6.3.3.4   Field Strength

Figure 6.11 confirms that the EOF is proportional to the electric field strength (applied voltage under standard conditions) as stated in Equation 6.3. An increase in

electric field will cause a faster migration of solvated cations in the diffuse layer towards the cathode resulting in a proportional increase in velocity.

6.3.3.5   Efficiency

Compared to the 3μm ODS packed capillary, the efficiencies of these monolithic columns are low. This could be due to a variety of reasons as yet to be established. Firstly, the surface area of the monolithic columns is significantly lower (a factor of 100 times lower) than that of the ODS beads. This low surface area reduces the number of sites available for partitioning. If this effect is significant then increasing the column length will increase the number of theoretical plates. However, in comparing the number of theoretical plates and HETP for two identical columns of different lengths, different values are obtained (Table 6.3). This suggests that there are other factors affecting the column efficiency and these are possibly dependent on column length. Columns packed using a BMA:EGDMA, 60:40 w/w mixture to prepare the stationary phase have been prepared by other groups. Efficiencies of 32,000 plates per metre have been quoted for the separation of basic pharmaceuticals [2] on columns where no porosity data was available. Peters et al. [3-5] have reported efficiencies of higher than 120,000 plates per metre for the separation of benzene derivatives. These columns have reported pore diameters in the region of 700nm therefore the higher efficiencies are expected to be due to increased surface area corresponding to the smaller pore size. However, no surface area measurements are available for these materials.

i)

ii)

iii)

iv)
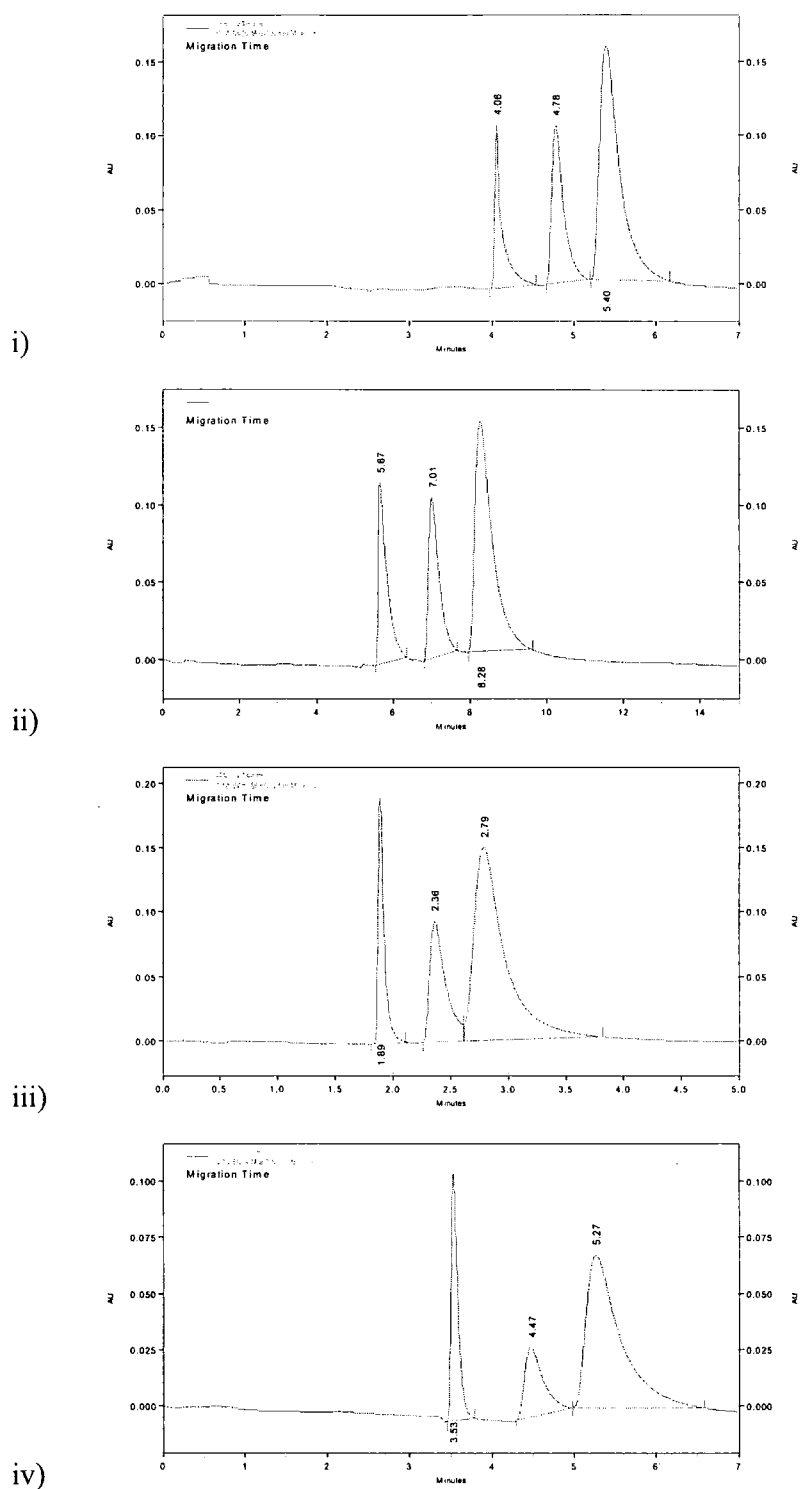
Figure 6.12 Electrochromatograms of (in order of elution) thiourea, dipropylphthalate and diphenylphthalate on (i) 30cm, 4.5μm; (ii) 40cm, 4.5μm; (iii) 20cm, 3.3μm; (iv) 30cm, 3.3μm columns. Mobile phase: phosphate containing 60% v/v acetonitrile.

154

i)

ii)

iii)
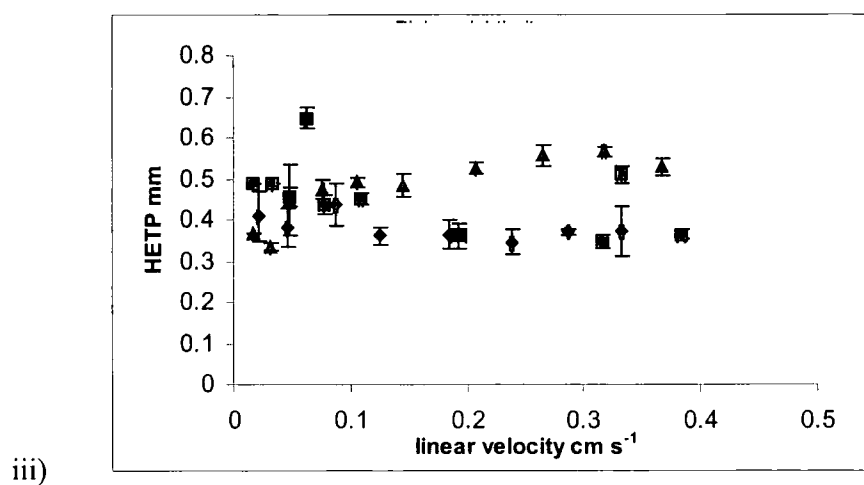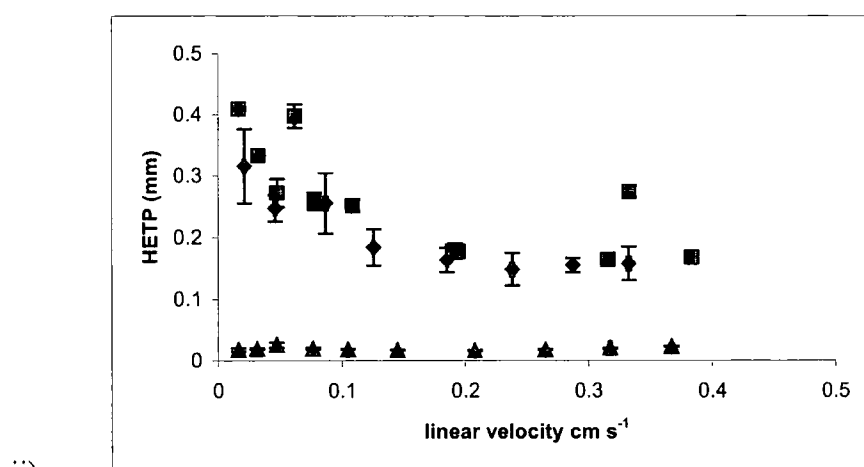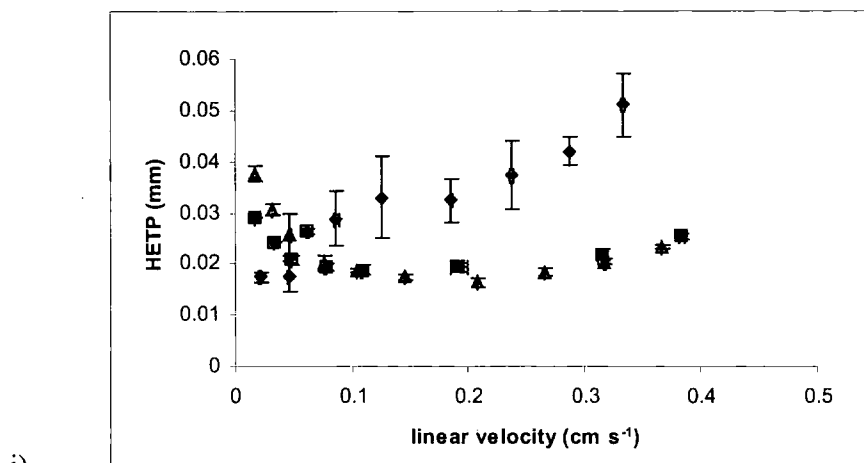
Figure 6.13 Van Deemter plots for (i) thiourea; (ii) dipropylphthalate; and (iii)

diphenylphthalate on 4.9 (◆), 5.3 (■) and 5.8 (▲) μm monoliths.

As discussed in chapter 1.2.4 there are various parameters that can affect efficiency. One of these could be due to mobile phase and analyte perfusion through the packing. A very relevant effect is that of eddy diffusion and analyte mass transfer between the mobile, stagnant mobile and stationary phases. If the porous material used for the stationary phase contains dead end pores then the analytes will take a more tortuous path along the column, increasing the time taken for a fraction of the analytes to migrate through the column. Where the right hand side 'tail' of the van Deemter plot has a shallow gradient, a negligible effect from mass transfer mechanisms is implied. In the case of thiourea for the 4.9μm column the plot does not resemble a 'usual' van Deemter plot and H appears to be proportional to the linear velocity.

Table 6.3   Efficiency data for different column lengths. Mobile phase: 1mM phosphate containing 60% v/v acetonitrile.

		3.3μm		4.5μm	
		Column Length /cm			
		20	30	30	40
Thiourea	N	8093	9424	3533	26160
	H /mm	0.0247	0.0212	0.057	0.008
	Nm^{-1}	40465	31413	17666	130798
Dipropylphthalate	N	1502	1943	2935	5792
	H /mm	0.133	0.103	0.0681	0.0345
	Nm^{-1}	7510	6477	14676	28962
Diphenylphthalate	N	675	899	1707	2773
	H /mm	0.296	0.222	0.117	0.0721
	Nm^{-1}	3375	2997	8537	13867

The shape of the plot would seem to suggest the most significant effect from mass transfer mechanisms (the C term in the van Deemter equation). As the thiourea does not interact with the stationary phase this suggests that the mechanism responsible for this decreased efficiency will be transfer between a mobile and stagnant phase. The general case observed here for these monolithic columns is that the linear velocity appears not to have a detrimental effect on efficiency, which will enable the flow rate to be altered to achieve optimum resolution without a major loss of efficiency.

6.3.3.6   AMPS level

An increased level of AMPS can be seen, in the two cases in Table 6.4, to increase the column efficiency. An increase in AMPS gives a slight decrease in the linear velocity. With a higher level of charged species along the stationary phase surface the electrical double layer produced will be slightly compressed reducing the linear velocity. A slightly slower flow rate may be responsible for the increased efficiencies by allowing more analyte – stationary phase interactions during the analyte's lifetime on the column.

Table 6.4   Theoretical plates for 20cm columns with pores of 5.6μm and 3.3 μm prepared with varying levels of AMPS.

	3.3μm		5.8μm	
	0.3wt% AMPS	0.6 wt% AMPS	0.3 wt% AMPS	0.6 wt% AMPS
Thiourea	6186	15445	7167	7822
Dipropyl-phthalate	408	802	599	744
Diphenyl-phthalate	215	450	315	349

6.3.3.7 Pore size

The linear velocity was found to be lower through columns with smaller pore sizes. Figure 6.14 shows that the efficiency of the thiourea marker is increased with decreasing pore size and vice versa for the phthalate analytes (Figure 6.15). This increase in efficiency is coupled with lower surface areas and higher linear velocities.
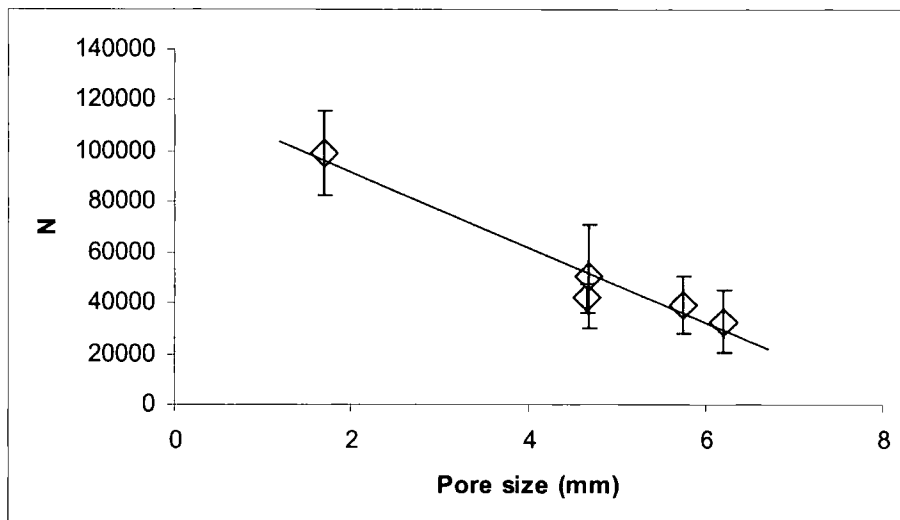
Figure 6.14 The effect of pore size on thiourea plate height.
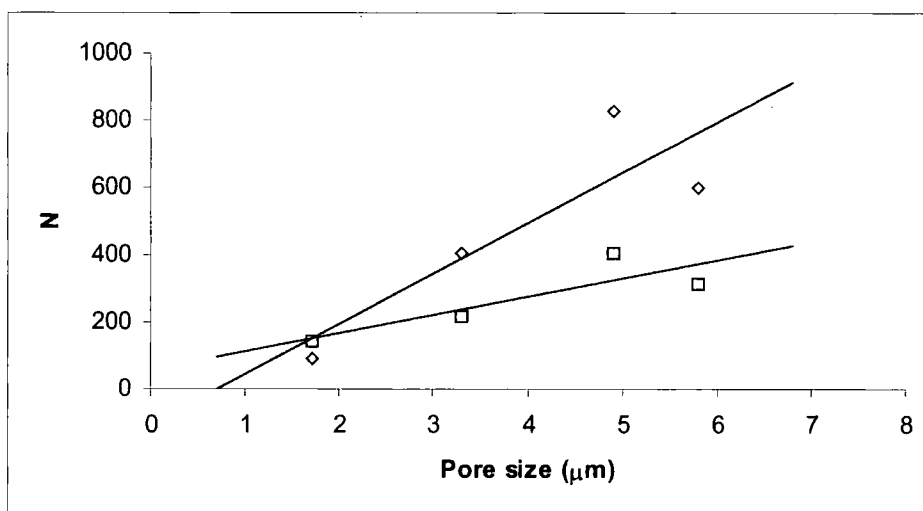
Figure 6.15 The effect of pore size on dipropylphthalate (◊) and diphenylphthalate (□) plate height at 50 % (v/v) acetonitrile content.

6.3.4   Effect of Temperature

6.3.4.1   Effect on separation

A classic description of the adsorption process is based on the Gibbs excess adsorption theory, which basically considers two similar hypothetical adsorption systems with the same volume, temperature, pressure and adsorbant surface area. The only difference is that the first system does not show any adsorption on the surface and the second one does. Linear velocity is proportional to the square root of the absolute temperature (Equation 6.3). K, the equilibrium constant, is a measure of interaction energy difference between the eluent and analyte molecules with the adsorbant surface. It is proportional to the partition ratio, k, by Equation 6.6 where β is the phase volume ratio.

$$K = \beta k$$

Equation 6.6

Using standard thermodynamics where ΔG is the standard Gibbs free energy of the system, R is the molar gas constant, ΔS is the standard entropy of the system, T is the absolute temperature and ΔH is the standard enthalpy of the system

$$\Delta G = -RT \ln K$$
$$= -RT \ln k - RT \ln \beta$$

Equation 6.7

$$\Delta G = \Delta H - T\Delta S$$

Equation 6.8

It follows that;

$$\ln k + \ln \beta = \frac{-\Delta H}{RT} + \frac{\Delta S}{R}$$

Equation 6.9

Rearrangement of Equation 6.9 enables the enthalpy of the system to be determined from the gradient of a logarithmic plot of capacity factor against the inverse temperature.

$$\ln k = \frac{-\Delta H}{RT} + \text{constant}$$

Equation 6.10

Across the different monolithic columns there is no significant difference in between the plots for dipropylphthalate and diphenylphthalate. There is no correlation between enthalpy and pore size however there is a difference when comparing equivalent columns with different AMPS levels. At 0.6 wt% AMPS the enthalpy is approximately double that at 0.3 wt% (Figure 6.16).

As can be seen from Figure 6.17 there is a lot of scatter in the data obtained using the ODS bead packed column. Due to the nature of the packing material more time is needed for the column to equilibrate to its new conditions.

Table 6.5   Gradients and calculated standard enthalpies obtained from Van't Hoff plots.

Column Reference	Dipropylphthalate		Diphenylphthalate	
	Gradient	ΔH (kJmol^{-1})	Gradient	ΔH (kJmol^{-1})
40-60-20 (0.3)	881.6	-7.33	304.9	-2.54
40-60-30 (0.3)	728.6	-6.06	802.8	-6.67
40-60-40 (0.3)	622.2	-5.17	800.5	-6.66
40-60-40 (0.6)	1160.9	-9.65	304.7	-2.53
60-40-40 (0.3)	503.4	-4.19	655	-5.45
37-63-29 (0.3)	728.6	-6.06	949.1	-7.89
Hypersil	566.4	-4.71	729	-6.06

A linear van't Hoff plot indicates that the retention mechanism under the temperature range being studied is invariant. When the plots are divergent and $\Delta(\Delta H)$ dominates over the entropy term $\Delta(\Delta S)$ it indicates that the separation is enthalpy driven, whereas a convergent plot where $\Delta(\Delta S)$ is dominant over $\Delta(\Delta H)$, an entropy driven process is indicated.

a)

b)
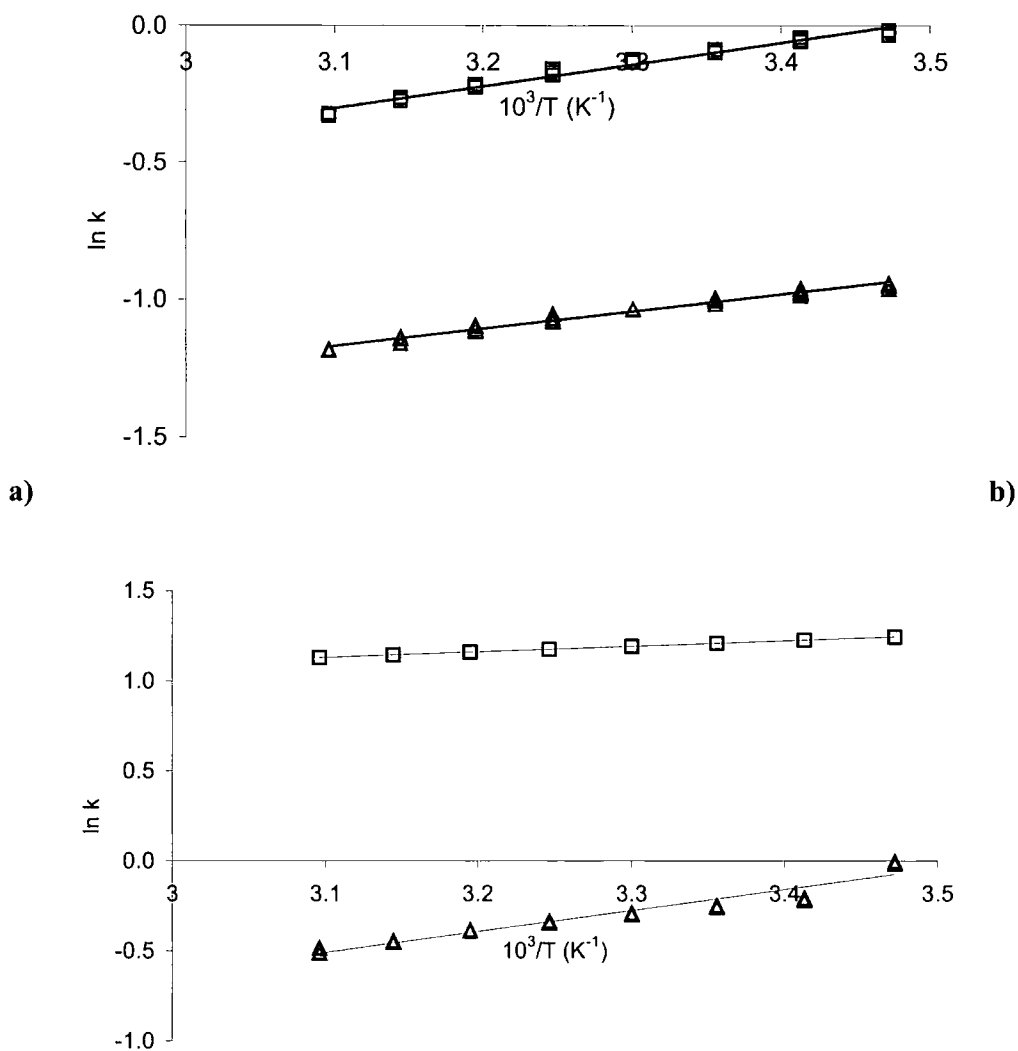
Figure 6.16 Van't Hoff plot for monolithic columns containing a) 0.3 wt% AMPS; b) 0.6 wt% AMPS for dipropylphthalate ($\triangle$) and diphenlphthalate ($\square$). Errors are smaller than the points.
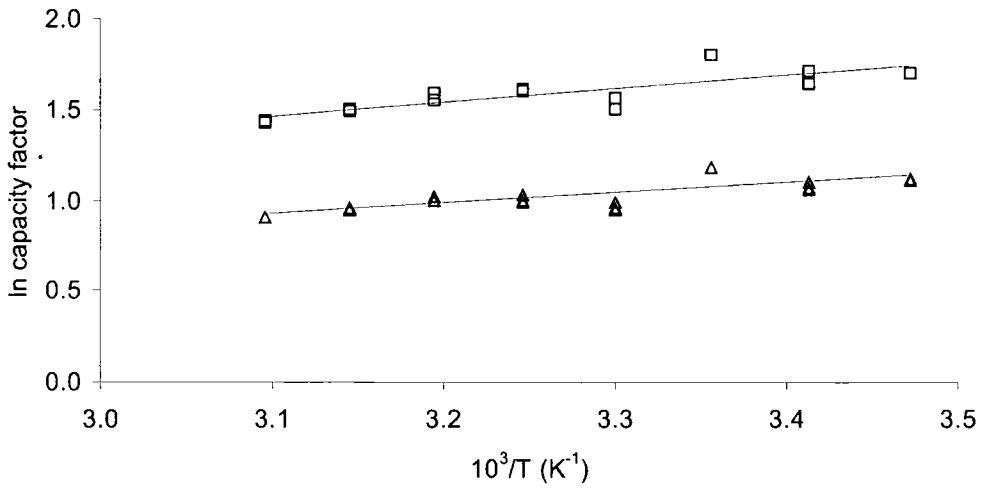
Figure 6.17 Van't Hoff plot for Hypersil ODS column for dipropylphthalate (Δ) and diphenlphthalate (□).

6.3.4.2   Effect on linear velocity
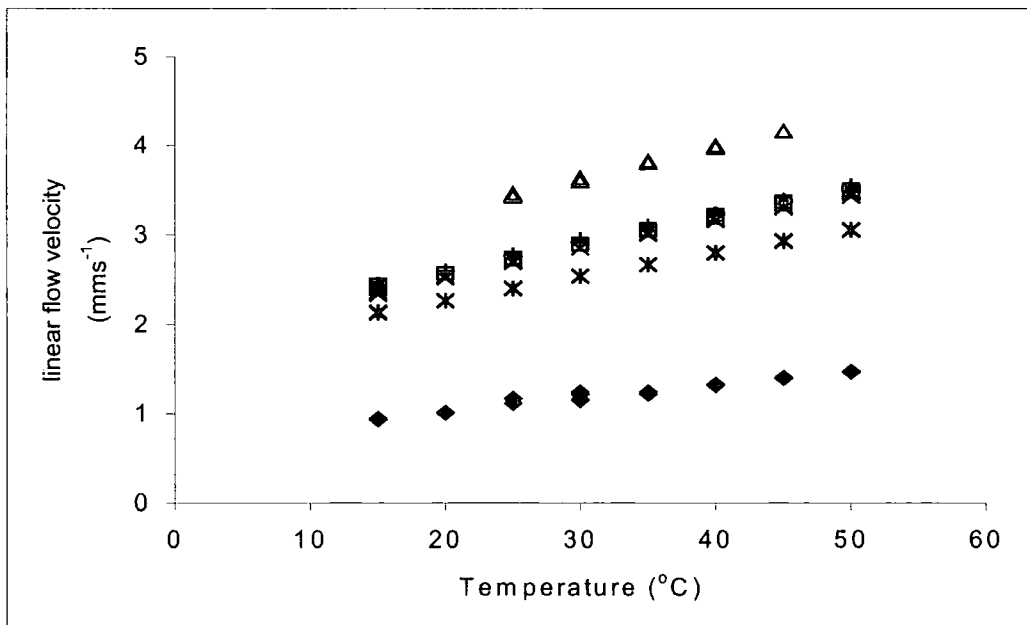
Figure 6.18 The effect of temperature on linear velocity in monolithic columns 1-4 (+, ✱, □,×) and 11 (Δ) and an ODS packed column (♦).

From Figure 6.18 it can also be seen that the increase in linear velocity is directly proportional to temperature. This is due to an exponential relationship between temperature and viscosity. As the temperature of the column increases the viscosity of the mobile phase decreases. An increase in temperature also results in an increase in current generated. As the capillary is analogous to a cylindrical conductor resistive (Joule) heat is produced on the application of a voltage when a current flows. The quantity of heat generated per volume of electrolyte, Q, can be calculated using Equation 6.11 where λ is the molar conductivity, c is the concentration of electrolyte and ε is the total porosity. The heat is dissipated by conduction through the capillary wall and surrounding air (or liquid in temperature controlled systems). The gradients of the plots in Figure 6.18 are all of similar magnitude suggesting that the heat produced in each column is easily dissipated.

$$Q = E^2 \lambda c \varepsilon$$

Equation 6.11

6.3.4.3   Effect on Efficiency

As mentioned in the previous section heat is produced on the generation of a current through the capillary. There will be a viscosity gradient across the capillary resulting from the temperature difference between the core and the capillary wall. As EOF is inversely proportional to viscosity this will cause a parabolic flow to form. An expression relating thermal effects and plate height was derived by Knox [6] where the plate height increment, H_{TH}, due to thermal effects is larger with wider capillaries, electrolyte concentrations and field strengths. D_m is the diffusion coefficient of the solute in the mobile phase.

$$H_{TH} = 10^{-8} \left(\frac{\varepsilon_0 r \delta}{D_m \eta \kappa^2} \right) E^5 dc^6 \gamma^2 c^2$$

Equation 6.12

The data shown in Figure 6.19 is in agreement with Equation 6.12, that is at increased temperatures, and viscosities efficiency is decreased.
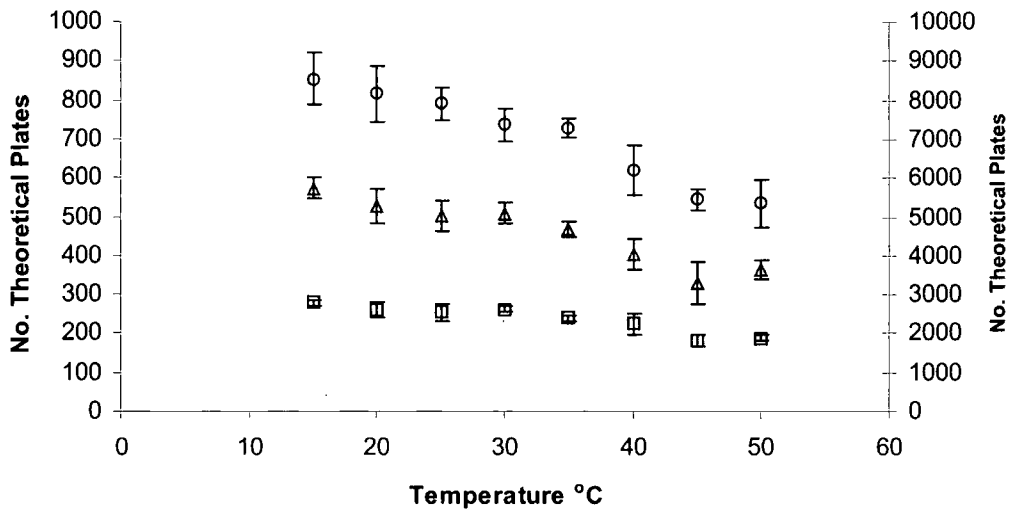
Figure 6.19 The effect of temperature on the separation efficiency of thiourea (O), plotted on right y-axis; dipropylphthlate (△) and diphentlphthalate (□) plotted on left y-axis.

6.4 Conclusions

The columns investigated in this chapter show potential as stationary phases for capillary electrochromatography. Monolithic columns show several advantages over traditional packed capillaries: their 'hands on' preparation time is short and many capillaries can be prepared simultaneously from one batch of microemulsion at one time increasing reproducibility. Also, conditioning of the columns prior to use is quick and reliable allowing rapid method development. The columns themselves

exhibit characteristics necessary for use as separation media. An alteration of the mobile phase system allows analyte capacity to be altered enabling method development with different analytes. The use of wide pore diameters allows the use of low ionic strengths without the concerns of electrical double layer overlap experienced using columns packed with ODS beads. Further development of these packing materials is required to increase efficiency and gain an understanding of the effects of channel size and distribution on this.

6.5 References

1.   Rice, C. L.; Whitehead, R. *J. Phys. Chem.* **1965**, *69*, 4017.

2.   Hindocha, D.; Smith, N. W. *Chromatographia* **2002**, *55*, 203-209.

3.   Peters, E. C.; Petro, M.; Svec, F.; Frechet, J. M. J. *Anal. Chem.* **1997**, *69*, 3646-3649.

4.   Peters, E. C.; Petro, M.; Svec, F.; Frechet, J. M. J. *Anal. Chem.* **1998**, *70*, 2288-2295.

5.   Peters, E. C.; Petro, M.; Svec, F.; Frechet, J. M. J. *Anal. Chem.* **1998**, *70*, 2296-2302.

6.   Knox, J. H. *Chromatographia* **1988**, *26*, 329.

Summary

7 Summary and Further Work

7.1 Summary

Polymerised bicontinuous microemulsions show potential as stationary phases for capillary electrochromatography. In chapter 5 it was shown that polymerised microemulsion systems containing a high proportion of surfactant were unsuitable for use as stationary phases due to the apparent production of an excess phase. Upon polymerisation these systems showed a nonporous layer which inhibited solvent flow. Lowering the surfactant level and increasing the co-surfactant level rectified this problem retaining bicontinuity toward the air surface of the microemulsion.

Capillary electrochromatography experiments showed that these materials act as effective separation media, however with efficiencies lower than would be required for commercialisation. As mentioned previously monolithic columns show several advantages over traditional packed capillaries: their 'hands on' preparation time is short and many capillaries can be prepared simultaneously from one batch of microemulsion at one time increasing reproducibility. The ability to control porous properties provides additional method development parameters towards optimum separations. Further development of these packing materials is required to increase efficiency as well as a robust method for the determination of the surface area of these materials. Monolithic columns offer further advantages over traditional bead packed columns in that conditioning prior to use is quick and reliable allowing rapid method development.

7.2 Further Work

In order to further assess the relationships between pore size chromatographic behaviour, columns should be prepared and assessed with a wider range of pore diameters. Results obtained so far suggest that materials with a large pore diameter and high surface area will be required to achieve high throughput efficient separation. This may be achieved by assessing the effect of additional non-polymerisable substances to the oil phase. Porogens in which the polymer is more soluble may increase the surface area coupled with a high water content which will aid in the creation of large channels in the resulting monolith.

Further potential materials could include stereospecific and molecular imprinted stationary phases for specific analytes.

Characterisation of the precursor microemulsions could be extended to x-ray and neutron scattering to determine domain size and cryogenic transmission electron microscopy to assess the effect of phase structure on the resulting monoliths. Further electrochromatography may link these factors together to enable effective prediction of column performance.

Appendices

8 Appendix

8.1 A – Methyl methacrylate systems

Component	Monomers			Charged species			Initiators				Surfactant		Other		Total Mass	Polymerisation Temperature	Polymerisation Duration	Extraction solvent	Capillary filled
Ref	MMA	EGDMA	HEMA	4-VP	DEAEMA	AMPS	AIBN	APS	NaPS	TMEDA	SDS	DDAB	Water	1-pentanol	(g)	°C			
1	53.9	9.1						1.0		2 drops/5g	9.1		28.0		5.0	30	6 hours	ethanol	Yes
2	58.6	2.5						0.4		2 drops/5g	3.9		35.0		5.0	30	6 hours	ethanol	Yes
3	17.6	2.5						0.3		2 drops/5g	4.1		35.1		5.0	30	6 hours	ethanol	Yes
4	10.0	15.0					1.7					65.0	8.0		10.0	70/40/RT	overnight/ 68hours/10 days	Ethanol/water	Yes
5	10.3	15.4		0.2				0.5	1.8			65.0	7.0		2.0	40	overnight	ethanol	Yes
6	10.0	15.0			0.3		0.5					67.0	7.1		2.0	70	overnight	ethanol	Yes
7	8.9	35.4			0.3		1.1					45.0	10.5		3.0	70	overnight	ethanol	Yes
8	8.5	36.0			0.5		1.0					45.6	9.4		3.0	70	overnight	ethanol	Yes
9	19.7	1.6	19.7				0.4				19.6		39.4		10.0	60	overnight	methanol/water	Yes
10	24.4	2.0	24.4				0.5				9.7		39.5		10.0	60	overnight	methanol/water	Yes
11	14.9	1.2	14.9				0.3				29.6		39.4		10.0	60	overnight	methanol/water	Yes
12	10.0	0.8	10.0				0.2				19.8		59.4		10.0	60	overnight	methanol/water	Yes
13	29.3	2.3	29.3				0.6				19.7		19.4		10.0	60	overnight	methanol/water	Yes
14	19.9	1.6					0.2				19.6		39.2	19.6	5.0	63	overnight	methanol	Yes
15	19.0	1.6					0.2				9.8		49.0	20.6	5.0	63	overnight	methanol	Yes
16	9.7	0.8					0.1				19.8		59.3	10.5	5.0	63	overnight	methanol	Yes
17	9.7	0.8					0.1				10.0		68.9	10.5	5.0	63	overnight	methanol	Yes
18	19.8	1.6	19.8				0.4				19.6		39.2		2.0	63	overnight	Methanol	Yes
19	19.7	1.6					0.2				19.5		39.4	19.7	2.0	63	overnight	Methanol	Yes
20	19.8	1.6	19.8				0.4				9.9		48.9		2.0	63	overnight	Methanol	Yes
21	19.8	1.6					0.2				9.8		49.0	19.8	2.0	63	overnight	Methanol	Yes
22	19.7	1.6	19.7			0.2	0.4				19.6		39.3		2.0	63	overnight	Methanol	Yes
23	19.6	1.6				0.2	0.2				19.5		39.7	19.6	2.0	63	overnight	Methanol	Yes
24	19.8	1.6	19.8			0.2	0.4				9.9		49.0		2.0	63	overnight	Methanol	Yes
25	19.9	1.6				0.2	0.2				9.8		48.9	19.9	2.0	63	overnight	Methanol	Yes
26	17.2	1.4	17.2			0.2	0.4				10.7		53.4		5.0	70	Overnight	Methanol	Yes

8.2 B – Butyl methacrylate systems 1

Sample No.	Total oil[1]	BMA	EGDMA	SDS	co-surfactant			water	AMPS[2]	Total (g)
					Pentanol	Butanol	Propanol			
1	57.8	57.2	0.0	10.6	21.1			10.6	none	2.0
2	24.9	24.7	0.0	12.3	24.5			38.3	none	2.0
3	22.3	22.1	0.0	10.4	20.7			46.6	none	2.0
4	22.3	22.3	0.0	10.4	20.7			46.6	2.0	2.0
5	21.9	20.8	1.1	10.4	20.8			46.8	2.0	2.0
6	21.8	19.6	2.2	10.4	20.9			46.9	2.0	2.0
7	19.0	15.2	3.8	10.8	21.6			48.6	2.0	2.0
8	70.6	67.1	3.5	7.3	14.7			7.3	none	2.0
9	66.1	62.8	3.3	6.8	13.6			13.6	none	2.0
10	48.7	46.2	2.4	8.6	17.1			25.7	none	2.0
11	30.4	28.9	1.5	9.3	18.6			41.8	none	2.0
12	50.1	47.6	2.5	12.5	25.0			12.5	2.0	4.0
13	50.1	47.6	2.5	10.0	20.0			20.0	2.0	4.0
14	25.0	23.8	1.3	18.8	37.5			18.8	0.3	4.0
15	25.0	23.8	1.3	15.0	30.0			30.0	0.3	4.0
16	20.5	19.5	1.0	13.3	26.5			39.8	0.3	4.0
17	20.4	19.4	1.0	10.6	21.2			47.8	0.3	4.0
18	24.3	23.1	1.2	7.6	15.1			53.0	0.3	4.0
19	20.0	16.0	4.0	21.3			42.7	16.0	0.3	2.0
20	30.0	24.0	6.0	18.7			37.3	14.0	0.3	2.0
21	40.0	32.0	8.0	16.0			32.0	12.0	0.3	2.0
22	50.0	40.0	10.0	13.3			26.7	10.0	0.3	2.0
23	10.0	8.0	2.0	18.0			36.0	36.0	0.3	2.0
24	20.0	16.0	4.0	16.0			32.0	32.0	0.3	2.0
25	30.0	24.0	6.0	14.0			28.0	28.0	0.3	2.0
26	40.0	32.0	8.0	12.0			24.0	24.0	0.3	2.0
27	50.0	40.0	10.0	10.0			20.0	20.0	0.3	2.0
28	60.0	48.0	12.0	8.0			16.0	16.0	0.3	2.0

[1] AIBN is dissolved in the oil phase at 1 wt% of the monomers in all compositions.
[2] The AMPS values stated are weight percent added with respect to the monomers.

Sample No.	Total oil	BMA	EGDMA	SDS	co-surfactant			water	AMPS	Total (g)
					Pentanol	Butanol	Propanol			
29	20.0	16.0	4.0	13.3			26.7	40.0	0.3	2.0
30	30.0	24.0	6.0	11.7			23.3	35.0	0.3	2.0
31	40.0	32.0	8.0	10.0			20.0	30.0	0.3	2.0
32	50.0	40.0	10.0	8.3			16.7	25.0	0.3	2.0
33	20.0	16.0	4.0	10.7			21.3	48.0	0.3	2.0
34	40.0	32.0	8.0	8.0			16.0	36.0	0.3	2.0
35	20.0	16.0	4.0	5.3			10.7	64.0	0.3	2.0
36	46.9	28.1	18.7	13.3	26.6			13.3		
37	33.2	19.9	13.3	13.4	26.7			26.2		
38	22.2	13.3	8.9	13.0	25.9			38.9	0.3	
39	46.7	28.0	18.7	14.2	28.4			10.7	0.3	
40	37.5	22.5	15.0	12.5	25.0			25.0	0.3	
41	23.3	14.0	9.3	12.8	25.6			38.3	0.3	
42	47.1	28.3	18.8	14.1	28.2			10.6	0.3	
43	40.1	24.1	16.0	12.0	24.0			24.0	0.3	
44	26.4	15.8	10.6	12.3	24.5			36.8	0.3	
45	64.5	38.7	25.8	9.2	18.4			7.8	0.3	
46	50.4	30.2	20.2	11.2	22.4			16.0	0.3	
47	36.2	21.7	14.5	12.1	24.2			27.5	0.3	
48	24.4	14.6	9.8	12.2	24.4			39.0	0.3	
49	17.6	10.6	7.0	13.7	27.4			41.3	0.3	
50	10.3	6.2	4.1	13.7	27.4			48.6	0.3	
51	63.1	37.9	25.2	9.8		19.7		7.4	0.3	
52	53.6	32.2	21.4	9.3		18.6		18.6	0.3	
53	36.8	22.1	14.7	10.5		21.1		31.6	0.3	
54	22.8	13.7	9.1	10.3		20.6		46.3	0.3	
55	13.4	8.0	5.4	8.7		17.3		60.6	0.3	
56	6.1	3.7	2.4	6.7		12.5		75.1	0.3	
57	68.5	41.1	27.4	8.4		16.8		6.3	0.3	
58	59.1	35.5	23.6	8.2		16.4		16.4	0.3	

| Sample No. | Total oil | BMA | EGDMA | SDS | co-surfactant | | | water | AMPS | Total (g) |
					Pentanol	Butanol	Propanol			
59	54.0	32.4	21.6	9.2		18.4		18.4	0.3	
60	41.2	24.7	16.5	9.8		19.6		29.4	0.3	
61	37.5	22.5	15.0	10.4		20.8		31.2	0.3	
62	59.1	35.5	23.6	8.4		16.9		15.6	0.3	
63	45.8	27.5	18.3	10.2		20.4		23.7	0.3	
64	34.5	20.7	13.8	11.5		23.0		31.0	0.3	
65	21.6	13.0	8.6	10.8		21.6		46.0	0.3	
66	10.7	6.4	4.3	8.4		16.7		64.2	0.3	
67	3.8	2.3	1.5	5.1		10.3		80.8	0.3	
68	78.7	47.2	31.5	5.7			11.3	4.3	0.3	
69	63.7	38.2	25.5	7.3			14.5	14.5	0.3	
70	42.1	25.3	16.8	9.7			19.3	29.0	0.3	
71	25.0	15.0	10.0	10.0			20.0	45.0	0.3	
72	43.2	25.9	17.3	15.2			30.3	11.4	0.3	
73	63.1	37.9	25.2	7.4			14.8	14.8	0.3	
74	60.9	36.5	24.4	7.8			15.6	15.6	0.3	
75	48.1	28.9	19.2	8.7			17.3	26.0	0.3	
76	41.3	24.8	16.5	9.8			19.6	29.4	0.3	
77	25.7	15.4	10.3	9.9			19.8	44.6	0.3	
78	24.1	14.5	9.6	10.1			20.2	45.5	0.3	
79	33.0	19.8	13.2	11.2	22.3			33.5	0.3	10.0
80	18.0	10.8	7.2	13.7	27.3			41.0	0.3	10.0
81	41.0	24.6	16.4	13.8	27.5			17.7	0.3	10.0
82	23.0	13.8	9.2	18.0	35.9			23.1	0.3	10.0
83	33.0	19.8	13.2	11.2		22.3		33.5	0.3	10.0
84	18.0	10.8	7.2	13.7		27.3		41.0	0.3	10.0
85	41.0	24.6	16.4	13.8		27.5		17.7	0.3	10.0
86	23.0	13.8	9.2	18.0		35.9		23.1	0.3	10.0
87	33.0	19.8	13.2	11.2			22.3	33.5	0.3	10.0
88	18.0	10.8	7.2	13.7			27.3	41.0	0.3	10.0
89	41.0	24.6	16.4	13.8			27.5	17.7	0.3	10.0
90	23.0	13.8	9.2	18.0			35.9	23.1	0.3	10.0

8.3   C – Butyl methacrylate systems 2

Sample No.	Total Oil / wt%	BMA / wt%	EGDMA / wt%	SDS$_{(aq)}$ / wt%	1-Propanol / wt%
1	6.1	3.7	2.4	87.8	6.1
2	52	31.2	20.8	24	24
3	38.4	23.0	15.4	38.4	23.2
4	23.0	13.8	9.2	23.1	53.9
5	18.0	10.8	7.2	41.0	41.0
6	33.0	19.8	13.2	33.5	33.5
7	41.0	24.6	16.4	17.7	41.3
8	20.0	12.0	8.0	64.0	16.0
9	30.0	18.0	12.0	56.0	14.0
10	39.9	24.0	16.0	48.0	12.1
11	50.0	30.0	20.0	40.0	10.0
12	60.0	36.0	24.0	32.0	8.0
13	20.0	12.0	8.0	56.0	24.0
14	30.0	18.0	12.0	49.0	21.0
15	40.0	24.0	16.0	41.9	18.1
16	50.0	30.0	20.0	35.0	15.0
17	60.0	36.0	24.0	28.0	12.0
18	20.1	12.1	8.0	48.0	31.9
19	29.8	17.9	11.9	42.4	27.8
20	40.6	24.4	16.2	35.6	23.8
21	49.9	30.0	20.0	30.1	20.0
22	60.0	36.0	24.0	24.0	16.0
23	20.0	12.0	8.0	40.0	40.1
24	30.0	18.0	12.0	35.0	35.0
25	39.9	24.0	16.0	30.0	30.1
26	50.0	30.0	20.0	25.0	25.0
27	59.9	36.0	24.0	20.1	20.0
28	20.0	12.0	8.0	32.0	48.0
29	30.1	18.1	12.1	28.2	42.0
30	40.0	24.0	16.0	24.0	35.9
31	50.1	30.0	20.0	21.3	30.0
32	60.0	36.0	24.0	16.0	24.1